Dissertation

Bioactive sphingolipids are critical regulators of Merkel Cell Carcinoma cell proliferation and survival

submitted by

Vishwanath BHAT KUMBLE

for the Academic Degree of

Doctor of Philosophy

(PhD)

at the

Medical University of Graz

Division of Molecular Biology and Biochemistry

Gottfried Schatz Research Center

under the Supervision of

Prof. Dr. Wolfgang SATTLER

2019

Declaration

I hereby declare that this thesis is my own original work and that I have fully acknowledged by name all of those individuals and organisations that have contributed to the research for this thesis. Due acknowledgement has been made in the text to all other material used. Throughout this thesis and in all related publications I followed the "Standards of Good Scientific Practice and Ombuds Committee at the Medical University of Graz."

Date: 8th February, 2019 *Vishwanath Bhat Kumble*

Disclosures

Parts of my dissertation have already been published and I acknowledge all the authors below who have contributed to this thesis. I confirm that all co-authors have agreed to use their data in my thesis. I have taken the permissions from Elsevier and Wiley to reproduce the publication into this thesis.

1. BHAT, V. K., BERNHART, E., PLASTIRA, I., FAN, K., TABRIZI-WIZSY, N. G., WADSACK, C., RECHBERGER, G., EICHMANN, T., ASSLABER, M., SPASSOVA, I., VERHAEGEN, M. E., MALLE, E., BECKER, J. C. & SATTLER, W. 2018a. Pharmacological inhibition of serine palmitoyl transferase and sphingosine kinase-1/-2 inhibits Merkel Cell Carcinoma cell proliferation. J Invest Dermatol, 10.1016/j.jid.2018.10.024.
2. BHAT, V. K., KRUMP, C., BERNHART, E., BECKER, J. C., SATTLER, W. & GHAFFARI-TABRIZI-WIZSY, N. 2018b. A short-term in-vivo model for Merkel Cell Carcinoma. Exp Dermatol, 27, 684-687.

Dedicated to my divine mother who is an embodiment of courage, compassion, and love

Acknowledgement

A very exciting as well as challenging PhD life is coming to an end. First of all, I would like to thank DK-Molin PhD programme, Medical University of Graz and Prof. Akos Heinemann for giving me an opportunity to do PhD. I thank Austrian Science Fund (FWF) for funding my project.

I would always be grateful to my PhD supervisor Prof. Wolfgang Sattler for taking me in his team. His guidance, support, and encouragement have made my research life much easier. Thank you, Wolfgang, for having trust in me. I would also like to thank Prof. Ernst Malle for his suggestions and guidance during my research.

The lab was like a family away from home. A big thanks to Eva, for being my mentor, guide and a friend in this PhD journey. Her valuable inputs to the project from day one deserves a special mention. A special thanks to Helga for all the help and support in the lab work whenever needed. It was a great pleasure to work with super-enthusiastic lab mates every single day. Thank you, Ioanna, Jürgen, Lisha, Anja, Chris, and Jeannine for always being there for me. A special thanks to my friend Chintan for his ever-helping nature right from the beginning. The lab would not have been so energetic and happy without you. I would like to thank Nanditha and Niroj for being the best friends away from the lab.

Further, a token of gratitude to Prof. Jürgen Becker for supervising me in this project and hosting me for six months in his lab in Essen during my research stay abroad. A humble thanks to my thesis committee members Prof. Akos Heinemann and Prof. Gunther Marsche for their guidance. I thank Prof. Nassim Ghaffari for allowing me to work in her lab and teaching me all the techniques.

This page would not be complete without thanking my better half Maya. Your support, encouragement and love has kept me going in this research life. My Acknowledgements continue to my parents, family members and friends for their love and support. Finally, I thank everyone who are directly or indirectly supported me in this PhD life.

Table of Contents

Abbreviations

ABC	ATP-binding cassette transporters
ABCA1	ATP binding cassette subfamily A member 1
ABCC1	ATP binding cassette subfamily C member 1
ABCG2	ATP binding cassette subfamily G member 2
AEC	3-amino-9-ethylcarbazole
AJCC	American Joint Committee on Cancer
AKT	Protein kinase b
ALOX15	15-lipoxygenase-1
ANOVA	Analysis of Variance
ASH1	Achaete-scute homolog 1
ASK1	Apoptosis signal-regulating kinase 1
ASMase	Acid sphingomyelinase
ATP	Adenosine triphosphate
AU	Arbitrory unit
BACE1	B-site amyloid precursor protein cleaving enzyme-1
BAX	Bcl2 associated x
BCA	Bicinchoninic acid
BCL2	B-cell lymphoma 2
CAM	Chorioallantoic membrane model
CD8+	Cluster of differentiation 8
CDC20	Cell division cycle 20
CERS	Ceramide synthase
CERT	Ceramide transfer protein
CHCl3	Chloroform
CK	Cytokeratin
CTLA-4	Cytotoxic t-lymphocyte–associated antigen 4
DAB	3,3'-diaminobenzidine
DAG	Diacylglycerol
DEGS1/DES1	Dihydroceramide desaturase
DMH	1,2-dimethylhydrazine
DMSO	Dimethyl sulfoxide
EDG	Endothelial differentiation gene

EGF	Epidermal growth factor
EGFP	Enhanced green fluorescent protein
ELISA	Enzyme-linked immunosorbent assay
EP400	E1a binding protein p400
ER	Endoplasmic reticulum
4E-BP1	Eukaryotic translation initiation factor 4e-binding protein 1
ERK	Extracellular signal-regulated kinase
FBS	Fetal bovine serum
FBXW7	F-box and wd repeat domain containing 7
FDG-PET	Fludeoxyglucose-positron-emission tomography
FFPE	Formalin-fixed paraffin-embedded
FOXP3+	Forkhead box p3
FPKM	Fragments per kilobase of exon per million reads
GEO	Gene expression omnibus
HDAC	Histone deacetylase
HDL	High-density lipoprotein
HDM2	Human double minute 2
HIF	Hypoxia-inducible factors
HIP1	Huntingtin-interacting protein 1
HIV	Human immunodeficiency virus
HNSCC	Head and neck squamous cell carcinoma
HPRT	Hypoxanthine-guanine phosphoribosyltransferase
HRAS	Harvey rat sarcoma viral oncogene homolog
HRP	Horseradish peroxidase
hTERT	Human telomerase reverse transcriptase
IARC	International agency for research on cancer
IGF	Insulin growth factor
ISTD	Internal standards
JNK	c-Jun n-terminal kinase
LSD	Long tumor antigen stabilizing domain
LT	Long tumor antigen
MAPK	Mitogen-activated protein kinase
MYC	Avian myelocytomatosis viral oncogene homolog

MAX	Myc associated factor x
MBV	Macroscopic blood vessels
MCC	Merkel cell carcinoma
MCPyV	Merkel cell polyomavirus
MHC	Major histocompatibility complex
MIC	MHC class I chain-related protein
MKRN1	Makorin ring finger protein 1
MMP	Matrix metalloproteinase
mTOR	Mammalian target of rapamycin
NCRR	Non-coding regulatory region
NF1	Neurofibromatosis type i
NF-kB	Nuclear factor kappa-light-chain-enhancer of activated b cells
NHDF	Normal human dermal fibroblast
PARP	Poly-(ADP-ribose) polymerase
PAX-5	Paired box 5
PDGF	Platelet derived growth factor
PD-1	Programmed death-1
PD-L1	Programmed death-ligand 1
PIK3CA	Phosphoinositide-3-kinase, catalytic, alpha polypeptide
PMA	Phorbol 12-myristate 13-acetate
PMSF	Phenylmethylsulfonyl fluoride
PP2A	Protein phosphatase 2 phosphatase activator
PTEN	Phosphatase and tensin homolog
RB1	Retinoblastoma transcriptional corepressor 1
RIPA	Radioimmunoprecipitation assay
RIPK1	Receptor interacting serine/threonine kinase 1
ROCK	Rho-rho kinase
RPLP0	Ribosomal protein lateral stalk subunit p0
RRM2	Ribonucleoside diphosphate reductase subunit
RTK	Receptor tyrosine kinases
SK/SPHK	Sphingosine kinase
SL	Sphingolipid
SLNB	Sentinel lymph node biopsy

SM	Sphingomyelin
SMS	Sphingomyelin synthase
SPNS2	Spinster homolog 2
SPT	Serine palmitoyltransferase
SPTLC1	Serine palmitoyltransferase long chain base subunit 1
SR-BI	Scavenger receptor class b, type 1
ST	Short tumor antigen
STAT3	Signal transducer and activator of transcription 3
TGFβ	Transforming growth factor beta
TNF-α	Tumor necrosis factor alpha
TRAF2	Tumor necrosis factor receptor-associated factor 2
TSC1	Tuberous sclerosis complex subunit 1
TTF	Thyroid transcription factor 1
VEGF	Vascular endothelial growth factor
VEGFR	Vascular endothelial growth factor receptor

Abstract (German)

Das Merkelzellkarzinom (MCC) ist ein aggressiver, metastasierender und neuroendokriner Tumor der Haut. Die Inzidenz von MCC beträgt 0,6/100.000 Personen und steigt jedes Jahr zwischen 5% und 10%. Die Sterblichkeitsrate beträgt 33% und übertrifft damit jene des Melanoms. Das Rezidivrisiko liegt zwischen 25% und 50%. Obwohl Immun-Checkpoint-Inhibitor-Antikörper von der FDA zugelassen sind, ist diese Therapie in 50% der MCC-Fälle unwirksam. MCC wird hauptsächlich durch klonal integrierte Merkelzell-Polyomaviren (MCPyV)-DNA und durch UV-vermittelte DNA-Schäden verursacht. Nahezu 80% aller MCC sind MCPyV-positiv und die viralen großen und kleinen Tumorantigene (LT bzw. sT) wurden als Onkogen nachgewiesen. Der Mechanismus der klonalen Integration und der anschließenden Transformation in MCC-Tumoren ist bisher nicht vollständig geklärt.

Bioaktive Sphingolipide gehören zu einer Gruppe von Sphingolipiden, die die Bildung, das Überleben und die Proliferation von Krebszellen regulieren. Sphingosin-1-phosphat (S1P) und Ceramide (Cer) sind die am besten untersuchten bioaktiven Sphingolipide. S1P ist ein pro-proliferatives Molekül und Cer ist meist pro-apoptotisch. Die Aufrechterhaltung des Gleichgewichts zwischen S1P und Cer ist für die normale Zellfunktion unerlässlich. Krebszellen hingegen forcieren die S1P-Synthese und hemmen die Cer-Bildung, um somit ihr Überleben und ihre Vermehrung zu fördern. Enzyme, die für die Biosynthese dieser bioaktiven Lipide von Bedeutung sind, sind in Krebszellen oftmals dysreguliert. Die Serin-Palmitoyltransferase (SPTLC1-3) ist ein Enzym, das den ersten Schritt des S1P-Synthesewegs reguliert, und Sphingosinkinase 1 und 2 (SK1/2) sind jene Enzyme, die S1P durch Phosphorylierung des Vorläufermoleküls Sphingosin synthetisieren. Es ist bekannt, dass diese beiden Enzyme in verschiedenen Krebsarten hochreguliert werden.

Wir stellten die Hypothese auf, dass das Eingreifen in das Sphingomyelin-Ceramid-S1P-Gleichgewicht eine neue Strategie in der Therapie des Merkelzellkarzinoms darstellen könnte.

Um unsere Hypothese zu testen, wurde von uns zuerst die Expression von SPTLC1-3 und SK1/2 in 21 MCC-Gewebeproben und 16 MCC-Zelllinien charakterisiert. Ferner konnten wir zeigen, dass die Transfektion von MCPyV-LTA isoliert aus MKL-1-, MKL-2- und MS1-MCC-Zellen in Fibroblasten zu einer erhöhten Transkription von SK1 und SK2 führt. Dies wurde in einer erneuten Analyse bereits veröffentlichter RNA-Sequenzierungsdaten bestätigt. In diesem Datensatz führte eine erzwungene MCPyV-sT-

Expression in Lungenfibroblasten zu einer gesteigerten Expression von SPTLC1/2- und SK1/2. Darüber hinaus erbrachte die Analyse weiterer GEO-Datensätze eine gesteigerte Expression von SK1 in MCC im Vergleich zu normalem Hautgewebe.

Für in-vitro-Studien eignen sich die gut charakterisierten MKL-1- und WaGa-MCC-Zelllinien sowie nicht transformierte humane dermale Fibroblasten (NHDF) als Kontrollzellen. Um die Bedeutung der S1P-Synthese für das Überleben und die Proliferation von MCC zu testen, wurde die Aktivität der Serin-Palmitoyltransferase mit Myriocin, sowie die SK1/2-Aktivität mit SKI-II und ABC294640 pharmakologisch inhibiert. Von diesen Inhibitoren hemmt SKI-II beide SK-Isoformen, während ABC294640 spezifisch für SK2 ist. Darüber hinaus setzten wir das von der FDA zugelassene Medikament FTY720/Fingolimod für MCC-Proliferationsversuche ein. Myriocin verringerte die zellulären Cer-, Sphingomyelin (SM)- und S1P-Konzentrationen in MKL-1- und WaGa-MCC-Zellen, während SKI-II die S1P- und SM-Konzentrationen verringerte, die Cer-Konzentration jedoch erhöhte. Die Zellviabilität wurde von Myriocin, SKI-II, ABC294640 und FTY720 reduziert, Apoptose und Nekrose hingegen gesteigert. Von Bedeutung ist, dass die Viabilität von nicht-transformierten NHDF-Zellen durch die Behandlung mit Myriocin, SKI-II und ABC294640 nicht beeinträchtigt wurde, während FTY720 Apoptose induzierte. Mit S1P angereichertes „high density lipoprotein“ (HDL) erhöhte die Lebensfähigkeit von MKL1- und WaGa-Zellen im Vergleich zu nativem HDL. Darüber hinaus verringerte die Hemmung von SPTLC1-3 und SKI-II durch Myriocin bzw. SKI-II die Phosphorylierung von AKT und erhöhte die Caspase3- und PARP-Aktivität in MKL-1- und WaGa-Zellen. Präklinisch noch relevanter, reduzierten Myriocin und SKI-II das Wachstum und die Proliferation von MKL-1- und WaGa- Xenotransplantaten im ex-ovo-Chorioallantoismembran-Tumormodell.

Mit dieser Arbeit konnte gezeigt werden, dass der S1P-Signalweg für das Überleben von MCC-Zellen in-vitro und im ex-ovo-Modell essentiell ist, und dass ein Eingreifen in das SM-Cer-S1P-Gleichgewicht einen vielversprechenden Therapieansatz zur Behandlung von MCC-Tumoren darstellt.

Abstract (English)

Merkel cell carcinoma (MCC) is an aggressive metastatic neuroendocrine tumor of the skin. The incidence of MCC is 0.6 in 100,000 persons and is rising 5%-10% every year. The mortality rate is 33% which exceeds melanoma. The recurrence risk ranges from 25%-50%. Though immune checkpoint inhibitor antibodies are approved by the FDA, the drug is ineffective in 50% of MCC cases. MCC is mainly driven by clonally integrated Merkel cell polyomavirus (MCPyV) DNA, and UV mediated DNA damage. Nearly 80% of MCC cases are $MCPyV^{+,}$ and the viral large and small tumor antigens (LT and sT, respectively) were shown to be oncogenic. The mechanism of clonal integration and subsequent transformation into MCC tumors is not fully understood. To be able to develop mechanism-based targeted therapies it is essential to gain detailed insight into pathways that drive MCC.

Bioactive Sphingolipids are an indispensable class of sphingolipids that regulate cancer cell formation, survival, and proliferation. Sphingosine 1-phosphate (S1P) and ceramide (Cer) are the most studied bioactive sphingolipids. S1P is a pro-proliferative molecule, and Cer is mostly pro-apoptotic. Maintaining the rheostat between S1P and Cer is vital for normal cell function. In contrast, cancer cells upregulate S1P synthesis and inhibit Cer formation to survive and proliferate. Enzymes that synthesize these bioactive lipids are dysregulated in cancer cells. Serine palmitoyltransferase (SPTLC1-3) is an enzyme that regulates the first step of S1P synthesis pathway, and sphingosine kinase 1 and 2 (SK1/2) are the enzymes that synthesize S1P by phosphorylating its precursor sphingosine. Both of these enzymes where shown to be upregulated in various cancer entities.

We hypothesized that targeting the sphingomyelin-ceramide-S1P rheostat could represent a novel anticancer strategy in MCC.

To test our hypothesis, we first characterized the expression of SPTLC1-3 and SK1/2 in 21 MCC tissue samples and 16 MCC cell lines. Further, transfection of MCPyV-LTA derived from MKL-1, MKL-2, and MS1 MCC cells into lung fibroblasts upregulated SK1 and SK2 transcription. Additionally, analysis of published microarray GEO datasets revealed upregulation of SK1 in MCC as compared to healthy skin tissue. Also, reanalysis of published RNA sequencing data showed that forced MCPyV-sT expression upregulates SPTLC1/2 and SK1/2 expression in lung fibroblasts.

For in-vitro studies, we used the well-characterized MKL-1 and WaGa MCC cell lines and non-transformed human dermal fibroblasts (NHDF) as control cells. To test the importance of S1P synthesis for MCC survival and proliferation, we pharmacologically targeted SPT with myriocin and SK1/2 activity with SKI-II and ABC294640. Of these, SKI-II inhibits both kinases, while ABC294640 is SK2 specific. In addition, we also used the FDA approved drug FTY720/fingolimod during MCC proliferation experiments. Myriocin treatment decreased cellular ceramide, sphingomyelin (SM), and S1P concentrations while SKI-II treatment decreased S1P and SM but increased ceramide in MKL-1 and WaGa MCC cells. Myriocin, SKI-II, ABC294640, and FTY720 reduced cell viability and increased apoptosis and necrosis. Of importance, non-transformed NHDF cell viability was not affected by myriocin, SKI-II, and ABC294640 treatment while FTY720 induced apoptosis. S1P-enriched high-density lipoprotein (HDL) increased the viability of MKL1 and WaGa cells in comparison to native HDL. Furthermore, inhibition of SPTLC1-3 and SKI-II with myriocin and SKI-II decreased phosphorylation of AKT and increased caspase3 and PARP activity in MKL-1 and WaGa cells. In a pre-clinically more relevant setting we could demonstrate that myriocin and SKI-II treatment reduced MKL-1 and WaGa tumor xenograft growth and proliferation in the ex-ovo chorioallantoic membrane tumor model.

In conclusion, we show that the S1P pathway is critical for MCC survival in in-vitro and ex-ovo condition and targeting the SM-Cer-S1P rheostat holds promise to interfere with MCC tumor growth and proliferation.

1. Introduction

1.1 Merkel cell carcinoma

Merkel cell (MC) carcinoma (MCC) is an aggressive, deadly metastatic non-melanoma skin cancer (Bhat et al., 2018a). This neuroendocrine tumor was identified by Cyril Toker in 1972 and was termed as 'trabecular carcinoma of the skin' (Toker, 1972). Later, it was described as MCC due to its characteristic features resembling MC (Becker et al., 2017b) that are present in the basal layer of the epidermis. In the epidermis, they mainly present around the hair follicles and work as mechanoreceptors mediating the light touch sensation. (**Figure 1**) (Maricich et al., 2009). These cells express neuroendocrine markers such as cytokeratin 20, chromogranin-A and synaptophysin which are also the main characteristic features of MCC cells (Mauzo et al., 2016). Age >50 years, immune deficiency, clonally integrated Merkel cell polyomavirus (MCPyV) or chronic ultraviolet (UV) radiation are the known causes of MCC pathogenesis (Hughes et al., 2014).

MCC is an aggressive cutaneous neoplasm. The fatality rate of MCC is higher (>30%) than that of melanoma (Lemos and Nghiem, 2007). More than one-third of affected patients die of this carcinoma (Schadendorf et al., 2017). MCC is not tractable to surgery and radiotherapy. The recent FDA approved immuno-modulating drugs have shown promising treatment outcome yet nearly 50% of the patients remain unresponsive for the current treatment regimen (Colunga et al., 2018).

1.2 Epidemiology

1.2.1 Incidence

The incidence of MCC was 0.6 in 100,000 people per year (2009) in the United States of America (USA) (Hughes et al., 2014) and in Sweden, an incidence rate of 0.19 per 100,000 people was reported for 2012 (Zaar et al., 2016). With 1.6 per 100,000 people, the incidence is much higher in Queensland, Australia (from 2006-2010) (Youlden et al., 2014). The epidemiologic data of the European Union (EU) shows that there 2500 new MCC cases have been registered every year (Becker et al., 2018). During the observational period 2005 to 2008 the Netherlands, Sweden and USA showed an increased incidence rate whereas the incidence in Scandinavian countries like Denmark, Finland, Iceland, and Norway remained stable since 1995 (Becker et al., 2017b). Thus, one can say that though the mortality rate of MCC patients is higher than that of melanoma the incidence rate is 50

times lower. The average age of MCC diagnosis is 75-80 years. An analysis from the American joint committee on Cancer (AJCC) documented that only 12% of the patients were below 60 years and the remaining patients were at a median age of 76 years out of >9,000 patients (Harms et al., 2016a). The larger national database showed that the 5-year relative survival rate of patients was ~60% in the USA (1973-1999) and ~40% in Australia (2006-2010) (Youlden et al., 2014).

1.2.2 Risk factors

The MCPyV was shown to be clonally integrated into 80% of MCC cases. The remaining 20% are MCPyV negative (MCPyV$^-$) MCC tumors showing signatures of UV associated mutations (**Figure 1**). The incidence of MCPyV$^-$ MCC is 76% in Australia and 20% in USA/Europe (Colunga et al., 2018). The MCC occurrence was frequent in the elderly and white population, especially in sun-exposed regions. Notably, the risk is lower for Asians and Africans. Weak immune system could be one reason for the high rate of MCC in the older generation. Moreover, prolonged exposure to UV radiation could damage the immune cells in the skin, which may render the development of cancer cells (Becker et al., 2017b).

Immunodeficiency is also a significant risk factor for MCC tumor burden. Immune suppression due to UVA photochemotherapy has shown to increase the incidence of MCC. Further, HIV infection or immune suppression in organ transplanted patients have increased MCC pathogenesis (Schrama et al., 2012). MCC was shown to be associated with various other cancers such as melanoma, basal cell carcinoma, squamous cell carcinoma, leukemia and lymphoma (Suarez et al., 2015, Wang et al., 2011, Becker et al., 2017b). It is also reported that MCC is associated with chronic inflammatory disorders e.g., rheumatoid arthritis (Engels et al., 2002, Sahi et al., 2017).

1.2.3 Origin of MCC

The origin of MCC is still ambiguous. MCC cells are thought to originate from dermal stem cells, pro/pre-B cells, or dermal fibroblasts (**Figure 1**) (Sunshine et al., 2018). In earlier years it was thought that MCs are the precursors of MCC due to the expressions of the same neuroendocrine markers. Conversely, MCs are terminally differentiating cells, and MCCs grow in a distantly MC-free micro-anatomic compartment of the skin suggesting MCs may not be the cell of origin of MCC. Dermal stem cells differentiating to

epidermal skin cells were thought to be the next candidate for the origin of MCC (Sunshine et al., 2018).

MCCs also express paired box 5 (PAX-5), terminal deoxynucleotidyl transferase (TdT) and various immunoglobulins, including monoclonal IgH (Immunoglobulin gamma heavy chain) and Igk (Immunoglobulin kappa light chain) which are the characteristic features of pro/pre-B cells (Sauer et al., 2017). The expression of B cell markers strengthened the view that MCC could originate from early B cells. Till date, MCPyV expression failed to transform the cells mentioned above under in-vitro conditions (Becker et al., 2017b). Interestingly, dermal fibroblasts were shown to promote infection and normal viral life cycle of MCPyV (Liu et al., 2016b) and MCPyV-T antigens were shown to encourage the growth of human and mice embryonic fibroblast in-vitro (Cheng et al., 2013). It is essential to gain insight into the origin of MCC to understand the pathogenicity via MCPyV driven tumorigenesis and to locate potential susceptibility factors.

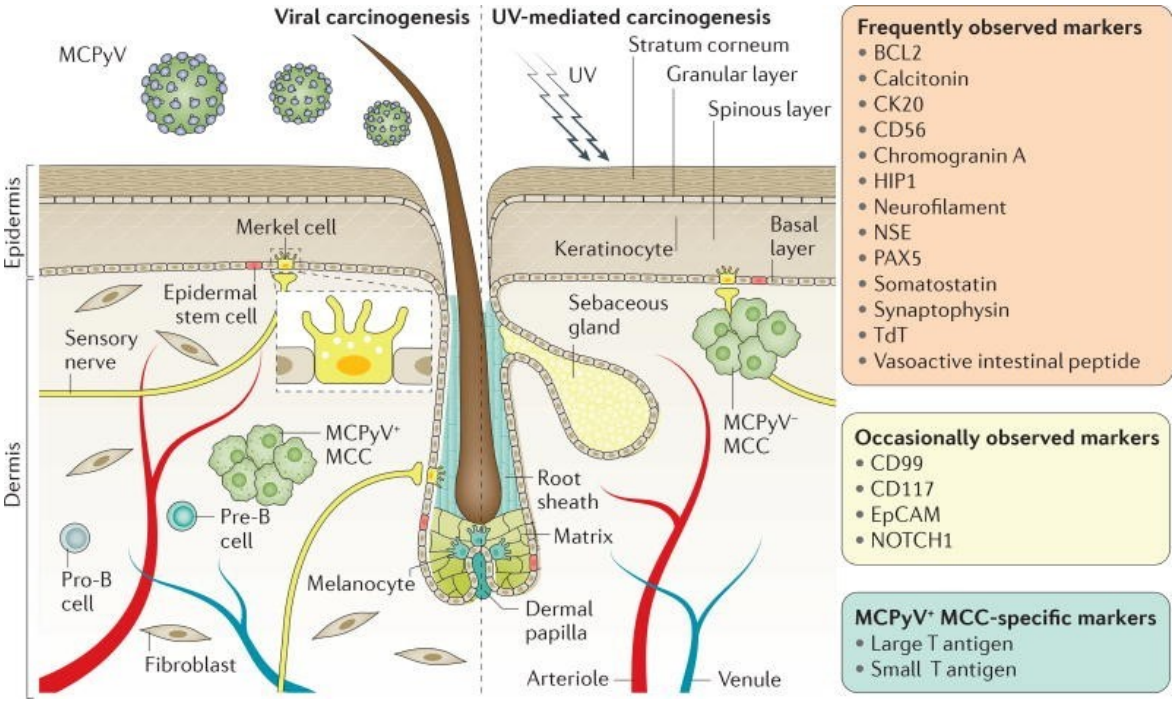

Figure 1: Graphical representation of MCPyV^{+} and MCPyV^{-} MCC tumor cells, their markers, and the potential precursor cells.

The graph depicts the epidermal and dermal region of the skin. MCC development in response to MCPyV infection or UV exposure is shown. Epidermal stem cell, pre/pro-B cells, keratinocytes, and dermal fibroblast are the primary candidates for the cell of origin of MCC. MCs functions as mechanoreceptor previously thought to be the origin of MCC. Markers used to characterize MCC cells are also shown. The figure displayed above is from Becker and colleagues (Becker et al., 2017b) and reproduced here with prior permission from Springer Nature (License number 4514370872208)

1.3 Pathophysiology

UV radiation and MCPyV are the main drivers of MCC pathogenesis. Approximately 20% of the MCC cases are MCPyV$^-$ mainly originated due to the UV related DNA damage. Apart from this, UV exposure can also play a role in local immune suppression. Chronic UV exposure can damage DNA directly by pyrimidine dimer formation or indirectly by reactive oxygen species (ROS) generation. This can then impact cytokine secretion and antigen-presenting dendritic cell function, which in turn results in impaired immunosurveillance. Immune suppression due to UV can also amplify the development of MCPyV mediated MCC tumorigenesis.

1.3.1 Merkel cell polyomavirus

MCPyV was discovered in 2008 by Feng and colleagues (Feng et al., 2008). This polyomavirus was initially identified in MCC samples hence named as MCPyV. Feng and colleagues used digital transcriptome subtraction (DTS) technique to identify the viral genome in MCC cells. The sequencing revealed a ≈5.4-kilobase circular double-stranded viral DNA (**Figure 2**). Initially using PCR, they found 8 out of 10 MCC tumor samples (80%) positive for MCPyV(Feng et al., 2008). Later, the presence of MCPyV in 80% of MCC patients was confirmed by several groups (Rodig et al., 2012, Kassem et al., 2008, Becker et al., 2009, Sastre-Garau et al., 2009). The MCPyV antibody titer was much higher even in MCPyV$^-$ MCC patients in comparison to control patients. It was also shown that MCPyV is clonally integrated into the genome of MCC tumors. Interestingly, MCC-derived metastases share the same integration pattern as the primary infected tumor. All the above evidence pointed towards a decisive role of MCPyV during tumor initiation. Out of the eleven known human polyomaviruses, MCPyV is the only family member known to be carcinogenic which is supported by robust scientific evidence (Spurgeon and Lambert, 2013, Houben et al., 2009, Verhaegen et al., 2015).

MCPyV belongs to the family of polyomaviridae. The MCPyV genome is identical to that of other human polyomaviruses, which mainly contain the non-coding regulatory region (NCRR) and bidirectional early and late gene regions. The NCRR of MCPyV codes for the origin of replication. Early region expresses tumor antigens also called T-antigens, that include large T antigen (LT), small T antigen (sT) and 57kT antigen (57kT). Finally, the late region expresses structural proteins, major capsid viral protein 1 (VP1) and the minor capsid proteins 2 and 3 (VP2 and VP3) (**Figure 2**) (Spurgeon and Lambert, 2013, Liu et

al., 2016b). MCPyV was shown to be a part of normal skin microbial flora. Furthermore, MCPyV is generally detected in the skin of children's and young population. Liu and colleagues showed that human dermal fibroblasts are the natural host for MCPyV and the virus actively replicates in fibroblasts and follows the normal viral life cycle (Liu et al., 2016b). Currently, the reason for truncating mutation in the C-terminal region of LT-antigen and subsequent clonal integration of the viral genome is unknown. Several groups have reported that both LT-antigen, as well as an sT antigen, play a crucial role in the transformation, proliferation, and survival of the MCC cells by regulating various pathways (Shuda et al., 2008, Shuda et al., 2011, Houben et al., 2010).

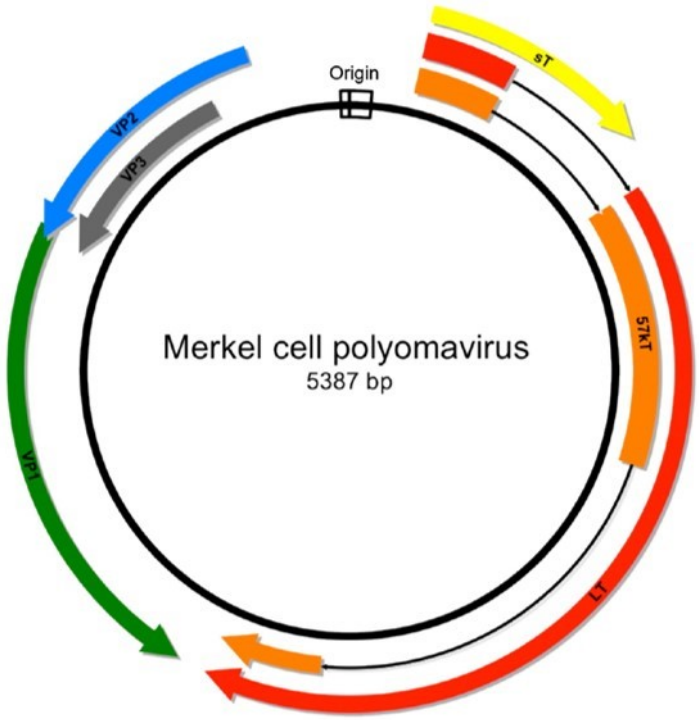

Figure 2: Genome of Merkel cell polyomavirus.

Schematic map of the 5.4-kilobase MCPyV genome. The image shows bidirectional replication of origin, early region coding LT-antigen (red), sT-antigen (yellow) and 57kT (orange), and late region viral capsid proteins VP1 (green), VP2 (blue), and VP3 (gray). The figure is from Spurgeon and colleagues (Spurgeon and Lambert, 2013) and reproduced here with prior permission from Elsevier (License number 4514370607843)

1.3.2 MCPyV tumor antigens

The MCPyV T antigen expression is preserved in the primary as well as metastatic tumor cells but not in the normal surrounding tissues (Shuda et al., 2009). Houben and colleagues showed that knockdown of MCPyV T antigens (LT and sT) leads to the growth arrest and

ultimately to death of MCC cells in-vitro (Houben et al., 2010). In all the MCPyV positive ($MCPyV^+$) tumor samples C-terminal truncating mutations have been reported, but these mutations were not observed in viral particles from the healthy population. This mutation renders the virus non-replicative, but it conserves the CR1, DnaJ, MUR, NLS, and pRB-binding motifs (**Figure 3**) (Shuda et al., 2008). Hesbacher and colleagues showed that MCPyV-LT antigen binds to RB1 (Retinoblastoma Transcriptional Corepressor 1) and renders it inactive. This was necessary to abolish inhibition of E2F transcription factor mediated by RB1 which regulates G1 to S-phase transition thus supporting the growth of $MCPyV^+$ MCC cells (Hesbacher et al., 2016). It is reported that the expression of LT-antigen alone is not sufficient to induce transformation in normal cells (Spurgeon and Lambert, 2013).

MCPyV-sT was shown to collaborate with the truncated LT in the transformation of rat and human fibroblast cells. Furthermore, in some MCC cases, only MCPyV-sT expression was reported (Berrios et al., 2016). In a very interesting study, Verhaegen and colleagues showed that genetically engineered embryonic mice expressing MCPyV-sT and Atoh1 (a transcription factor promoting ectopic MC development) in keratinocytes induce MCC-like tumors. This transformation was independent of LT antigen (Verhaegen et al., 2017). This is the first study demonstrating MCC-like tumor cells in a genetically engineered mouse model. All this shows the importance of sT antigen in the transformation and survival of MCC. Hence, both of the antigens are referred to as oncogenic viral proteins in MCC (Houben et al., 2009). The MCPyV-sT antigen is expressed from a spliced intact mRNA and contains an N-terminal J domain, a PP2A (Protein phosphatase 2 phosphatase activator) binding region, and a unique region containing the LT stabilizing domain (LSD) (**Figure 3**). PP2A binding may not be required for viral-mediated transformation of cells, but LSD has been reported to bind CDC20 and E3 ubiquitin ligase FBXW7 and to stabilize LT expression (Shuda et al., 2015, Kwun et al., 2013). Furthermore, MCPyV-sT increases cap-dependent translation through hyperphosphorylation of 4E-BP1 (Eukaryotic translation initiation factor 4E-binding protein 1) (Shuda et al., 2011). Recently, sT-antigen was also linked to the expression of 15-lipoxygenase-1 (ALOX15) that is potentially linked to lymphatic vessel density (Fochtmann-Frana et al., 2018). Together, all these functions mostly contribute to sustaining oncogenesis in MCC.

How MCPyV-sT contributes to oncogenic transformation is not fully understood. An increase in aerobic respiration is a hallmark of cancer (the Warburg effect), and expression of MCPyV-sT was shown to increase glycolytic genes in fibroblast (Berrios et al., 2016). Cheng and colleagues showed that MCPyV-sT could particularly recruit MYC (Avian myelocytomatosis viral oncogene homolog) and MAX (MYC Associated Factor X) towards the EP400 complex and together this complex transactivates several gene expression and boost oncogenesis (Cheng et al., 2017). Due to these reasons the International Agency for Research on Cancer (IARC) of WHO has classified MCPyV as a group 2A carcinogen (Bouvard et al., 2012).

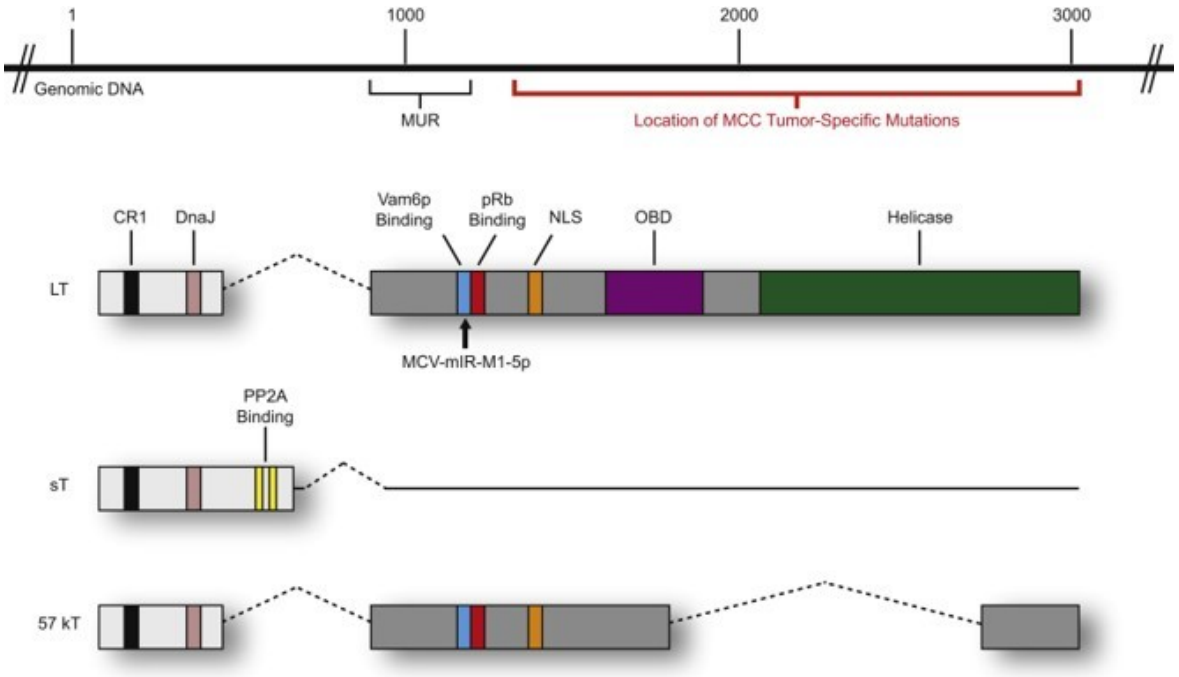

Figure 3: Genome of Merkel cell polyomavirus early region and encoded T antigen.

The early region of MCPyV encodes three spliced variants LT, sT, and 57kT antigens. LT-antigen is showing specific protein binding regions such as CR1 (in Black), DnaJ (pink), Vam6p (blue), pRb binding site (red), nuclear localization signal (orange), origin-binding domain (purple) and Helicase binding domain (green). LT also show MCPyV-unique region and microRNA binding site (MCPyV-mIR-M1-5p). Apart from CR1 and DnaJ, sT antigen also shows PP2A binding domain. 57kT identical to LT but without the origin of replication and helicase domain. The above showed figure is from Spurgeon and colleagues (Spurgeon and Lambert, 2013) and reproduced here with prior permission from Elsevier (License number 4514370607843)

1.3.3 Mutational burden

The mutational analysis of MCC by next-generation sequencing identified two MCC subtypes. One with clonally integrated MCPyV$^+$, rare somatic and UV related mutations, and the second group of MCPyV$^-$ UV associated DNA mutations in key pathways. Nevertheless, both subtypes ultimately followed two different mechanisms to regulate one similar pathway to maintain MCC pathogenesis (Becker et al., 2018). As shown above, in MCPyV$^+$ MCC cells the viral antigen directly inhibits active RB1 protein, whereas in MCPyV$^-$ cells UV-induced mutations render RB1 inactive (Cimino et al., 2014). Similarly, in the case of P53, MCPyV$^+$ MCC's show less active P53 without any mutations but in MCPyV$^-$ cases inactivating or deletion mutations were reported (Houben et al., 2013). Thus, in both MCC subtypes inactivation and/or less active RB1 and P53 is observed (Gonzalez-Vela et al., 2017). The reason for partial P53 inactivation in MCPyV$^+$ MCC is not understood clearly, but Houben and colleagues showed that knockdown of T-antigen did not activate P53 but inhibiting ubiquitin ligase HDM2 (human double minute 2) resulting in an increase in P53 activation and ultimately induced P53 mediated apoptosis in MCPyV$^+$ MCC. This suggests that inactivation of P53 activity is independent of oncogenic viral antigens (Houben et al., 2013).

In MCPyV$^-$ MCC studies have reported a loss of function mutation in NOTCH1 and NOTCH2 thereby inhibiting the Notch pathway (Harms et al., 2015, Goh et al., 2016). Several studies have shown mutations that activate receptor tyrosine kinases (RTKs) and the PI3K/AKT/mTOR (phosphatidylinositol-3-kinase/protein kinase B/mammalian target of rapamycin) signaling pathway. Further, a gain of function was reported in HRAS (Harvey rat sarcoma viral oncogene homolog), PIK3CA, AKT1, and loss of function in PTEN (Phosphatase and tensin homolog), NF1 (neurofibromatosis type I), and TSC1 (Tuberous Sclerosis Complex subunit 1) (Harms et al., 2015, Goh et al., 2016, Becker et al., 2017b). These mutations were observed both in MCPyV$^+$ and MCPyV$^-$ MCCs.

1.3.4 Immune status

High CD8$^+$ T cell response was reported to be associated with better prognosis in MCC. A 100% recovery was reported in some MCC cases with high tumor-infiltrating CD8$^+$ T cell

counts (Paulson et al., 2011). The $CD8^+$ T cells recognize and target the epitopes derived from viral antigens in $MCPyV^+$ MCC, or they target neoantigens produced due to UV associated high mutations (Schadendorf et al., 2017). Unfortunately, this type of MCC cases was observed in less than 20% of tumors (Paulson et al., 2011). Expression of programmed death-1 (PD-1) and programmed death-ligand 1 (PD-L1) were observed in $CD8^+$ T cells in MCCs suggesting tumor recognition by immune cells. Accordingly, tumor cells find different immune escape strategies either by PD-1/PD-L1 pathway or loss of expression of MHC class I chain-related protein (MIC) A and B (Becker et al., 2018).

1.4 Prognostic factors

1.4.1 Clinical features

MCC is mostly observed in sun-exposed regions like the head and neck. In some cases, it was also observed in extremities and buttocks. MCC is cutaneous or subcutaneous, and tumors show rapid growth in the region (Schadendorf et al., 2017). The lesions are present in red to violet nodules which do not show any symptoms. This might be misdiagnosed as cysts or inflammatory lesions. Due to challenging clinical diagnosis, histopathological diagnosis is suggested to confirm the MCC cases (Heath et al., 2008).

Sentinel lymph node biopsy (SLNB) meaning excision and examination of sentinel lymph nodes, is an important criterion to diagnose the stage of MCC in patients (Lemos et al., 2010). The most recent AJCC system suggested four clinical stages of MCC prognosis. Stage 0 represents in-situ. Stage I represents localized disease and primary lesion ≤2 cm. Stage II represents localized disease, but primary lesion is >2 cm. Stage III represents the spread of the tumor to a regional lymph node. Stage IV represents distant metastasis beyond regional lymph nodes (Harms et al., 2016a). The survival rate decreases with late diagnosis. Depending on the stage of MCC tumor the five-year overall survival rate is 62.8% for stage I MCC cases, 34.8% to 54.6% for stage II, 26.8% to 40.3% in stage III and 13.5% in stage IV (Schadendorf et al., 2017). MCC tumors were found to metastasize into distant nodes, liver, lungs, bones, and brain.

1.4.2 Histopathology of tumor

Studying histopathology of MCC tumor biopsies are essential to confirm the disease. Histology sections showed three main types of MCCs, namely the small cell, trabecular

and intermediate cell type (Schadendorf et al., 2017). Microscopic evaluation of hematoxylin-eosin (HE) stained MCC tumor sections revealed small blue round tumor cells present in dermal or subcutaneous nodules or sheets of monomorphic round to oval cells. The MCC cells show sparse cytoplasm, abundant mitotic activity with multiple nucleoli (Bichakjian et al., 2018). Isolated tumor cells, intralymphatic invasion, and epidermotropism are some observation in the histopathology of MCC tumors (Becker et al., 2017b, Calder and Smoller, 2010). HE stained MCC cells show a pattern similar to other tumors like neuroblastoma, small cell or amelanotic melanoma, small cell lung cancer [SCLC], and lymphomas to name a few (Bichakjian et al., 2018, Kolhe et al., 2013). Diagnosis is reported to be most difficult between primary MCC and metastatic SCLC (Busam et al., 2009).

1.4.3 Immunohistological markers

Immunohistochemistry (IHC) has proven to be most beneficial in differentiating MCC from other small round cell tumors. MCC cells express several types of cytokeratins (CK). CK20 expression in IHC analysis of the biopsies are the main characteristic features of MCC diagnosis. Apart from this CK8, CK18 and CK19 expression were also observed during IHC analysis (Andres et al., 2011, Bechert et al., 2013). In the majority of cases, $MCPyV^{+}$ MCC express both the oncogenic viral antigens which can be used as a diagnostic marker. Staining for LT or sT antigen is also a characterizing feature of $MCPyV^{+}$ MCC. Further, MCC also express neuroendocrine markers such as chromogranin, synaptophysin, microtubule-associated protein-2, CD56, and neuron-specific enolase (NSE) (Koljonen et al., 2005) (**Figure 1**). Along with CK20, chromogranin and synaptophysin expression were widely used to confirm diagnosis of MCC by IHC technique (Bichakjian et al., 2018) (**Figure 1**). Apart from this staining for tumor protein 63 (p63) has been observed in approximately 30% of the cases and associated with worse prognosis (Fleming et al., 2014). MCC also stained positive for huntingtin-interacting protein 1 (HIP1) in the majority of cases (Ames et al., 2011). Less than 10% of MCC cases were also reported to be negative for CK20. These CK20 negative MCC cases are generally $MCPyV^{-}$ MCC and show high UV related mutations (Harms et al., 2016b). The majority of MCC cases stains negative for CK7 and thyroid transcription factor 1 (TTF1). Achaete-scute homolog 1 (ASH1), S100B, vimentin (Becker et al., 2017b, Busam et al., 2009). CK20 (highly expressed) and TTF1 (no expression) in MCC

were used in differentiating MCC tumors form SCLC (Busam et al., 2009). Recently, Fan and colleagues proved that circulating miR-375 can be used as a surrogate marker for MCC tumor burden (Fan et al., 2018).

Apart from histopathological diagnosis, MCC patients were also scanned for the presence of extracutaneous tumors by X-ray, CT, ultrasound, MRI and FDG-PET/CT (Bichakjian et al., 2018, Eftekhari et al., 1996, Kouzmina et al., 2017, Peloschek et al., 2010). FDG-PET/CT was found to be more useful in the majority of cases for staging and management of MCC. If the whole body FDG-PET/CT is not available then CT or MRI was used to identify the primary or metastatic MCC tumors (Peloschek et al., 2010, Bichakjian et al., 2018). Ultrasound is commonly used to scan for lymph nodes in MCC patients (Llombart et al., 2017).

1.5 Management of MCC

1.5.1 Surgery

Surgery is the first line of treatment for stage I/II MCC cases. Incision of primary tumor lesions up to 1-2 cm clinically free area is recommended in MCC patients (Schadendorf et al., 2017). In case of finding positive tumors even after surgery re-excision is followed. Mohs microsurgery is used in the case of surgery involved with risky areas of tissue to reduce further complications (Schadendorf et al., 2017, O'Connor et al., 1997).

Further, SLNB is widely recommended in cases where the MCC has infected locoregional lymph nodes. Along with complete removal of the nodal region, adjuvant radiotherapy is also recommended in controlling disease (Schadendorf et al., 2017, Bichakjian et al., 2018). In any case, histopathological studies are necessary to confirm that the region is clinically free of MCC.

1.5.2 Radiotherapy

Radiotherapy (RT) is found to be essential as adjuvant therapy in all stages of the disease. It was highly recommended in cases of stage I/II MCC or in-operable conditions like poor health or substantial tumor burden (Mortier et al., 2003, Veness et al., 2010). In several cases and one randomized clinical trial adjuvant RT reduced the recurrence risk MCC in comparison to surgery alone. In some trials, it was also shown that adjuvant RT was associated with better results than adjuvant chemotherapy (Schadendorf et al., 2017).

Surgery and RT may be beneficial in stage I/II cases but MCC recurrence is also possible. In advanced cases of MCC, even though not beneficial regarding overall survival, RT helps in reducing tumor burden and other symptoms such as pain, bleeding, secondary infection and ulceration (Schadendorf et al., 2017, Bichakjian et al., 2018). There are only a few data to support the notion that adjuvant RT is beneficial in a specific stage of MCC (Bichakjian et al., 2018).

1.5.3 Chemotherapy

The most common treatment for metastatic MCC was chemotherapy before the introduction of immunotherapies. Chemotherapy including various antineoplastic drugs alone or in combination was tried in advanced MCC cases. The drugs used in the trials are etoposide, cyclophosphamide, 5-FU (5-Fluorouracil), topotecan, gemcitabine, irinotecan and several other varieties (Becker et al., 2017a, Bichakjian et al., 2018). The overall outcome of these trials was not favorable towards MCC cases. The response rate of chemotherapy in MCC cases was temporary with a median range of 2-9 months, and toxicity related death was 3% to 10% (Fenig et al., 1997, Tai et al., 2000, Bichakjian et al., 2018). The overall response rate in these studies ranged from 20% to 61%. The response rate was higher in the first line chemotherapy (53% to 61%) in comparison to the second line (23% to 45%). The overall median survival rate is 9.5 months (Bichakjian et al., 2018, Becker et al., 2017b). Currently, the mTOR kinase inhibitor MLN0128 is in Phase I/II (NCT02514824) clinical trial in recurrent/metastatic MCC.

1.5.4 Immunotherapy

In 2018 the Nobel's prize was awarded for the development of immune checkpoint therapies in cancer. These immunotherapies include antibodies targeting PD-1, PD-L1, or CTLA-4 (Cytotoxic T-lymphocyte–associated antigen 4) used alone or in combination (Seidel et al., 2018). MCC is mainly an immunogenic tumor entity. IHC study in 49 MCC patients revealed expression of PD-L1 in 49% of the cases, and it is found to be associated with viral positivity. This finding also suggested that an endogenous immune response also promotes PD-L1 expression in MCC (Lipson et al., 2013). PD-L1 expression was observed to be higher in $MCPyV^{+}$ MCC in comparison to $MCPyV^{-}$ MCC (Uchi, 2018).

Till date, avelumab, nivolumab and pembrolizumab are the three therapeutic antibodies used to inhibit the PD-1/PD-L1 immune checkpoint pathway in MCC clinical trials.

Avelumab targets PD-L1 and, nivolumab and pembrolizumab target PD-1 (Bichakjian et al., 2018). Clinical trials of avelumab in chemotherapeutically treated advanced MCC cases showed a progression-free survival rate of 30% and an overall survival rate of 50% in one year follow up studies (Kaufman et al., 2018). This led to US FDA approval of avelumab for MCC. Avelumab (NCT02155647), pembrolizumab (NCT02267603), and nivolumab (NCT02978625) are currently in a Phase II trial and a new therapeutic monoclonal antibody, MGA012, targeting PD-1 is also in Phase II (NCT0251482) patient recruitment stage. Previous trials involving avelumab, nivolumab, and pembrolizumab showed that treatment-related adverse events occurred in 68% to 77% MCC patients. Immune-related adverse events were observed in patients administered avelumab (Kaufman et al., 2016). Despite all these new developments, nearly 50% of the cases remain unresponsive to immune-checkpoint blockade (Colunga et al., 2018).

Several clinical trials have reported that in MCC the recurrence rate is in the range of 25% to 50%. Apart from the newly invented immune checkpoint inhibitors, there is currently no other mechanism-based clinical therapy available. As stated earlier the durability of immune checkpoint inhibitors is 50%. Research in MCC has unraveled several pathways that may be useful in MCC pathogenesis. Nevertheless, viral or UV mediated MCC transformation, survival, and growth have not been understood completely. Further studies are necessary to understand the mechanisms used by the cancer cells for its oncogenicity. This will further enhance the development and translation of mechanism-based targeted therapy.

1.6 Sphingolipids

Sphingolipids (SLs) are an important class of lipid molecules that play a crucial role in normal cell function. In the past decades, research in SLs has thrown a lot of light on the structure, function and overall mechanism of action in different cell types. Generally, sphingolipid structure constitutes a long chain 18 carbon amino-alcohol as sphingoid base attached to a fatty acid (Sedic et al., 2019, Futerman and Riezman, 2005). SLs are not only present inside cells but also circulating in the blood. SLs play a major role in plasma membrane integrity. Few important classes of SLs work as secondary messengers controlling basic cell functions like cell survival and proliferation, neuronal development, cardiovascular function and immunity hence also referred to as bioactive SLs (Hannun and Obeid, 2018). Recently, a wealth of studies have reported a significant role for bioactive SLs in diabetes, cardiovascular disease, inflammation, neurodegeneration, and cancer (Hannun and Obeid, 2018, Proia and Hla, 2015).

1.7 Sphingolipid synthesis, metabolism, and compartmentalization

Ceramide (Cer), an important class of SLs, form precursor molecules for various other classes of SLs such as glycosphingolipids, galactosylceramide, sphingomyelins, ceramide 1-phosphate and sphingosine 1-phosphate (S1P) (Gault et al., 2010, Ogretmen, 2018) (**Figure 4**). Cer is synthesized by de-novo synthesis in the endoplasmic reticulum (ER) or via the salvage pathway in acidic compartments such as lysosomes (Kitatani et al., 2008). In the ER, condensation of serine and palmitoyl-CoA by serine palmitoyltransferase (SPT) leads to 3-ketosphinganine which is then converted to sphinganine, then to dihydroceramide ultimately leading to Cer formation by the enzymes 3-ketosphinganine reductase, ceramide synthases (CERS1–6), and dihydroceramide desaturase (DEGS1/DES1), respectively (Gault et al., 2010, Ogretmen, 2018). Cer is then converted to galactosylceramide in the ER (Sedic et al., 2019) (**Figure 4** and **5**).

From the ER, Cer is transported to the Golgi complex by Cer transfer protein (CERT) (Hanada, 2010). In trans-Golgi, Cer is converted to ceramide-1-phosphate (C1P) and sphingomyelin (SM) by ceramide kinase or sphingomyelin synthase (SMS) respectively. In the cis-Golgi, glucosylceramide (GC) is formed from Cer by the action of glucosylceramide synthase (GCS) (Hanada, 2010). Glucosylceramide is then converted to glycosphingolipids (GSLs) in distal Golgi compartments (Ogretmen, 2018). Apart from

this, glucosylceramide, galactosylceramide, SM and C1P can also be converted back to Cer by the enzymes glucosylceramidase, galactosylceramidase, or sphingomyelinases (Bartke and Hannun, 2009) (**Figure 4**). SM, C1P, and GSLs form part of the plasma membrane and GSLs beside receptor function in the plasma membrane, also provides a basis for virus attachment and internalization (Taube et al., 2010) (**Figure 5**).

Finally, Cer can be hydrolyzed by ceramidases (CDases) to form sphingosine and other free fatty acids in the lysosome from then it can enter the Salvage pathway (Kitatani et al., 2008). In the Salvage pathway sphingosine and other free fatty acids are utilized by CERS1–6 to synthesize Cer. Sphingosine is then phosphorylated by sphingosine kinase 1 or 2 (SK1 and SK2) to form bioactive S1P (Chi, 2011, Bhat et al., 2018a). In a backward reaction, S1P can be converted to sphingosine and then back to Cer by S1P phosphatases and CERS1–6 respectively (Bartke and Hannun, 2009). S1P is synthesized in the plasma membrane by SK1 and in the nucleus and mitochondria by SK2. Further, S1P is irreversibly degraded by the enzyme S1P lyase to form hexadecenal and phosphoethanolamine (Bartke and Hannun, 2009) (**Figure 4** and **5**).

Cer is a pro-apoptotic molecule, and S1P promotes cell survival and proliferation. Cer and S1P both have several intracellular targets, and extracellularly S1P also shows autocrine and paracrine function through its specific receptors (**Figure 6**). Maintaining sphingolipid homeostasis for normal functioning of cells is essential. Enzymes play a crucial role in keeping this rheostat in balance and dysregulation by various stimuli can lead to abnormal function of cells which can further lead to cancer (Sedic et al., 2019).

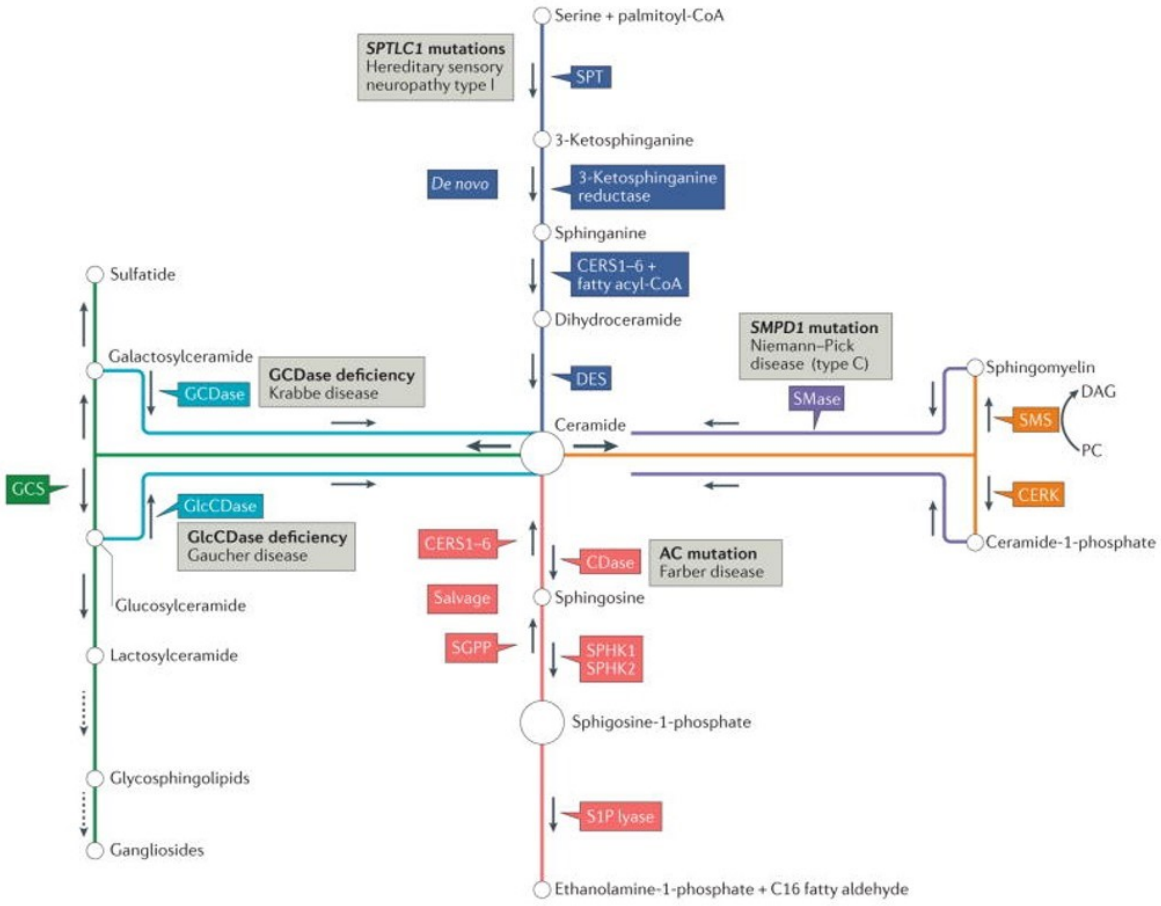

Figure 4: De-novo synthesis pathway of sphingolipids

The graph shows de-novo synthesis pathways of Cer, S1P, SM, C1P, GSLs and galactosylceramide by the respective enzymes. The pathway initiates from the condensation of serine and palmitoyl-CoA by enzyme serine palmitoyltransferase and leads to the synthesis of bioactive SLs. The graph is from Ogretmen (Ogretmen, 2018) and reproduced here with prior permission from Springer Nature (License number 4514441425255).

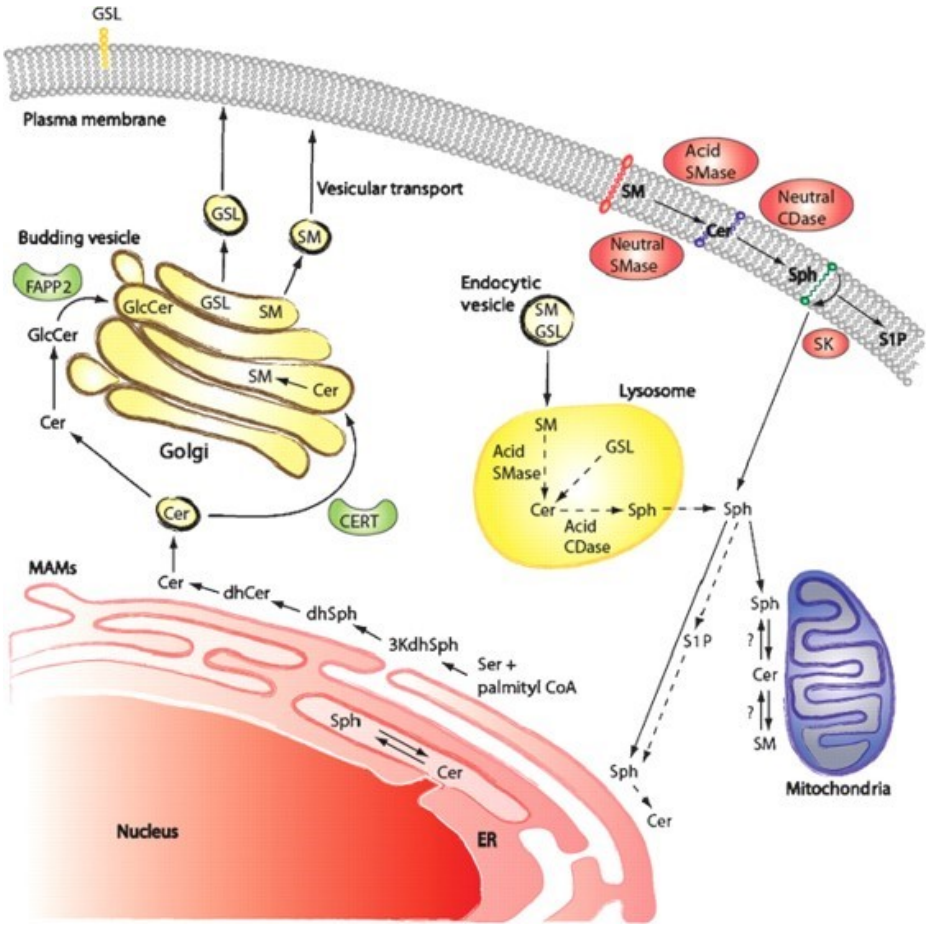

Figure 5: Compartmentalization of sphingolipid synthesis

Graphical image showing synthesis and translocation of SLs in different cell organelles. Sphingosine 1-phosphate (S1P), Ceramide (Cer), Sphingosine (Sph), Sphingomyelin (SM), Glycosphingolipids (GSLs). The figure is from Bartke and colleagues (Bartke and Hannun, 2009) and reproduced here with prior permission from the American Society for Biochemistry and Molecular Biology (License number 4516171152124).

1.8 Bioactive sphingolipids and their role in cancer

1.9 Sphingomyelins in cancer

SM is an integral part of plasma membrane performing a distinct role in cell proliferation, migration, microdomain formation, membrane trafficking, cell signaling and apoptosis (Taniguchi and Okazaki, 2014). SM is the most abundant sphingolipid formed by the action of SM-synthases (SMS) (Sedic et al., 2019). SM is synthesized from its precursor Cer by two enzymes SMS1 and 2. SMS1 is present in the Golgi complex and SMS2 present in the Golgi as well as plasma membrane (Taniguchi and Okazaki, 2014). SM is also hydrolyzed to Cer by sphingomyelinases (SMase). SM forms part of extracellular and intracellular vesicles, lipid rafts thereby regulating cellular signaling pathways. Along with

SM synthesis, SMSs also synthesize diacylglycerol (DAG) an activator of PKC (Villani et al., 2008).

SM mainly promotes tumor cell growth, proliferation, migration, invasion, and angiogenesis (Taniguchi and Okazaki, 2014, Hannun and Obeid, 2018, Kim et al., 2002). Reduction in SM content was observed to reduce cell growth of HeLa cells after siRNA mediated knockdown of SMSs (Tafesse et al., 2007). Further, a decrease in SM content in microdomains was shown to reduce the proliferation rates of HEK293, Huh7, and CHO cell lines (Taniguchi and Okazaki, 2014). Induction of SM synthesis through SMS1 expression promoted SM deficient-lymphoma cell proliferation. Besides, restoration of SM increased endocytosis of transferrin thereby promoting iron uptake and cell proliferation (Shakor et al., 2011). High SMS activity was observed in chemo-resistant HL-60 leukemia cells suppressing pro-apoptotic Cer level (Itoh et al., 2003). Studies have also shown that SM isolated from EMVTCs (extracellular membrane vesicles from tumor cells) promotes migration and angiogenesis in endothelial cells (Kim et al., 2002). In contrast to the studies described above, exogenous addition of dietary SM in addition to gemcitabine-induced cell death via Cer generation in pancreatic cancer cells (Ryland et al., 2011, Modrak et al., 2004). In addition, it was shown that dietary SM decreases 1,2-dimethylhydrazine (DMH)-induced colon cancer in CF1 mice (Ryland et al., 2011, Dillehay et al., 1994). These data indicate that SM can promote cancer cell proliferation, however, if degraded, the newly formed Cer species might promote apoptosis.

1.10 Ceramide and its role in cell death

Cer is a pro-apoptotic molecule and is composed of sphingosine long-chain base and 14 to 26 carbons long amide-linked fatty acyl chain (Sedic et al., 2019). In de-novo pathway several species of Cer differing in fatty acid chain length are generated by CERS1-6 enzymes. C14–16 Cer species are generated by CERS5 and CERS6, C18–20 Cer species are generated by CERS1 and CERS4, CERS2 selectively generates C22–24 ceramides, and CERS3 generated very long chain C28–32 Cer species (Ogretmen, 2018). These ceramides are then interacting with various intracellular targets ultimately determining cell fate.

Ceramides can facilitate mitochondrial-mediated apoptosis, necroptosis, and autophagy. In lung cancer cells, it was shown that direct binding of Cer to PP2A inhibitor I2PP2A activates PP2A leading to RIPK1 (serine/threonine-protein kinase 1) mediated necroptosis

(Saddoughi et al., 2013). Cer-mediated activation of PP2A, a tumor suppressor gene, was shown to inhibit oncogenic protein AKT (Zhou et al., 1998). Besides, PP2A catalytic subunit PP2Ac inhibit anti-apoptotic protein BCL-2 (B-cell lymphoma 2) and promotes P53/BCL2 complex leading to apoptosis (Deng et al., 2009). Additionally, Cer-mediated activation of PKCζ regulates membrane potential, inhibits AKT, and activates the pro-apoptotic pathway in stem cells. Similarly, ASK1 (apoptosis signal-regulating kinase 1) is activated by the action of Cer, which activates p38 and JNK signaling. JNK and p38 activated mitochondrial pro-apoptotic protein BAX leads to activation of the intrinsic apoptotic pathway (Bourbon et al., 2002). In cancer cells, it was observed that chemotherapy-induced stress response could increase the concentrations of C18 Cer species. The activated C18 ceramides then translocate to the mitochondrial outer membrane and bind to LC3B-II (a lipidated form of microtubule-associated protein 1 light chain 3β) which then engage with autophagosomes to mediate lethal mitophagy (Sentelle et al., 2012). Radiation therapy induced Cer accumulation in mitochondria was also reported to induce caspase 3 activation and then apoptosis through BAX (Chipuk et al., 2012).

Conflicting to the findings described above, in HNSCC (head and neck squamous cell carcinoma) studies have shown that C16 Cer species produced by CERS6 promotes tumor cell proliferation (Saddoughi and Ogretmen, 2013). In addition, research in breast and colon cancer cells have shown that upregulation of CERS2 induced tumor cell proliferation but production of C16, C18, and C20 Cer species-induced apoptosis (Hartmann et al., 2012). This suggests that the majority of Cer species induce apoptosis, but in cancer cells, some Cer species also play an important pro-survival function.

1.11 Sphingosine 1-phosphate signaling, transport, and receptors

S1P is reported to regulate diverse cell function by intracellular and extracellular signaling circuits. S1P is a potent effector of proliferation, survival, differentiation, angiogenesis, and migration (Ksiazek et al., 2015) and is also associated with several diseases such as autoimmunity, myocardial infarction, osteoporosis, atherosclerosis, and cancer (Ksiazek et al., 2015, Maceyka et al., 2012). S1P is synthesized by SK1 or SK2 through sphingosine phosphorylation. Although both enzymes synthesize the same molecule, they display different subcellular distribution, catalytic properties and may possess unique function (Ksiazek et al., 2015). SK1 is mainly present in the cytoplasm but when activated

translocates to the plasma membrane for S1P synthesis. Interestingly, S1P was also identified in the extracellular microenvironment and extracellular vesicles. It was reported that approximately 8% of activated SK1 is released into the extracellular environment (Ancellin et al., 2002). In contrast, SK2 was found to synthesize S1P inside the cell nucleus and within mitochondria. Intracellularly, S1P act as secondary messenger and extracellularly it behaves as ligand molecule to its five specific G-protein coupled receptors, sphingosine 1-phosphate receptor 1 to 5 (S1PR 1-5).

1.11.1 Intracellular S1P

Intracellular S1P regulates the TNF-α/NF-kB signaling pathway, epigenetic mechanisms, and mitochondrial respiration (Nagahashi et al., 2014). Intracellular S1P binds and acts as a cofactor to E3 ubiquitin ligase activity of tumor necrosis factor receptor-associated factor 2 (TRAF2) in the TNF-α/NF-kB signaling pathway and regulates various cell functions (Alvarez et al., 2010). SK2-derived S1P in the nucleus exclusively binds and inhibited HDAC1 and HDAC2 activity thereby epigenetically regulating expression of various genes (Hait et al., 2009). In cancer cells, S1P promotes telomerase activity and thus survival and proliferation. Nuclear S1P binds to hTERT (human telomerase reverse transcriptase) and allosterically mimics phosphorylation thereby maintaining telomerase stability and maintenance, and tumor growth and survival (Panneer Selvam et al., 2015). Furthermore, S1P produced by SK2 in mitochondria was reported to interact with prohibitin 2, a chaperone protein in mitochondria that plays a role in mitochondrial respiration (Strub et al., 2011). In Alzheimer's disease, it was observed that SK2 is upregulated in the brain of affected patients. In addition, S1P modulates the activity of BACE1 (β-site APP cleaving enzyme-1), the enzyme responsible for the generation of amyloid-beta peptides by binding and mimicking activating phosphorylation of the enzyme (Takasugi et al., 2011).

1.11.2 S1P transporters

In various cell types, several members of the ABC (ATP-binding cassette transporters) family and SPNS2 (spinster homolog 2) were identified as active transporters of S1P (Pyne and Pyne, 2010, Nagahashi et al., 2014). In SPNS2 null mice, plasma levels of S1P were unchanged, but in lymph, S1P content was significantly decreased (Mendoza et al., 2012). In addition, in-vitro ABCA1, ABCG2, and ABCC1 which are the ATP dependent transporters were identified to facilitate cellular S1P efflux (Ksiazek et al., 2015). In

RBCs, ABCC1 was reported as an S1P efflux facilitator. However, Abcc1/Mrp1, Abca1, and Abca7 null mice did not show any changes in plasma S1P levels indicating that these ABC transporters are of minor importance in-vivo (Lee et al., 2007).

1.11.3 Extracellular S1P and its receptors

Red blood cells are the primary source of S1P in plasma. Additionally, non-hematopoietic cells such as vascular endothelial cells and activated macrophages, mast cells, platelets are also contributing to the S1P pool (Venkataraman et al., 2006, Hanel et al., 2007, Yatomi et al., 1997, Olivera et al., 2007). In the thymus, neural crest-derived pericytes are the sources of S1P, and for lymph, it is lymphatic endothelial cells (Pham et al., 2010, Zachariah and Cyster, 2010). The concentration of S1P in interstitial fluid and blood varies significantly. It was observed that in tissue, the S1P level ranges from 0.5 to 75 pmol/mg, in plasma, S1P concentrations are in the range of 0.2 to 0.9 μM and in serum, levels are ranging from 0.4 to 1.1 μM (Takabe et al., 2008). In plasma, HDL (high density lipoprotein) is the primary physiological carrier of S1P (50% to 60%), and the remaining fraction is transported in association with albumin (≈30%) and other lipoproteins (≈10%) (Ksiazek et al., 2015).

Extracellular S1P function as an autocrine and paracrine signaling ligand (Ogretmen, 2018). S1P regulates biological and pathological functions of the cell through S1PR 1-5 residing on the membrane (**Figure 6**). Each of these receptors can regulate a variety of functions such as angiogenesis, lymphocyte trafficking, and cancer hallmarks (Strub et al., 2010). Expression levels of these receptors vary between tissue types and are to the extracellular stimuli. Therefore, it is essential to study the expressions of the individual receptor isoforms in the context of specific cell types to understand the behavior of the cells in response to S1P stimulation (Young and Van Brocklyn, 2006, Blaho and Hla, 2014). S1PR1-5 receptors function in combination with G-proteins. These receptors form complexes with G_i, G_q, G_{12} and G_{13} heterotrimeric G proteins (Young and Van Brocklyn, 2006) (**Figure 6**). S1P stimulation leads to S1P receptor coupling to their G proteins and then regulates various downstream pathways such as PI3K/AKT pathway, p38/JNK/MAPK pathway, Rho-Rho kinase (ROCK) pathways, and Ras-mitogen-activated protein kinase pathway (Okamoto et al., 2011) (**Figure 6**).

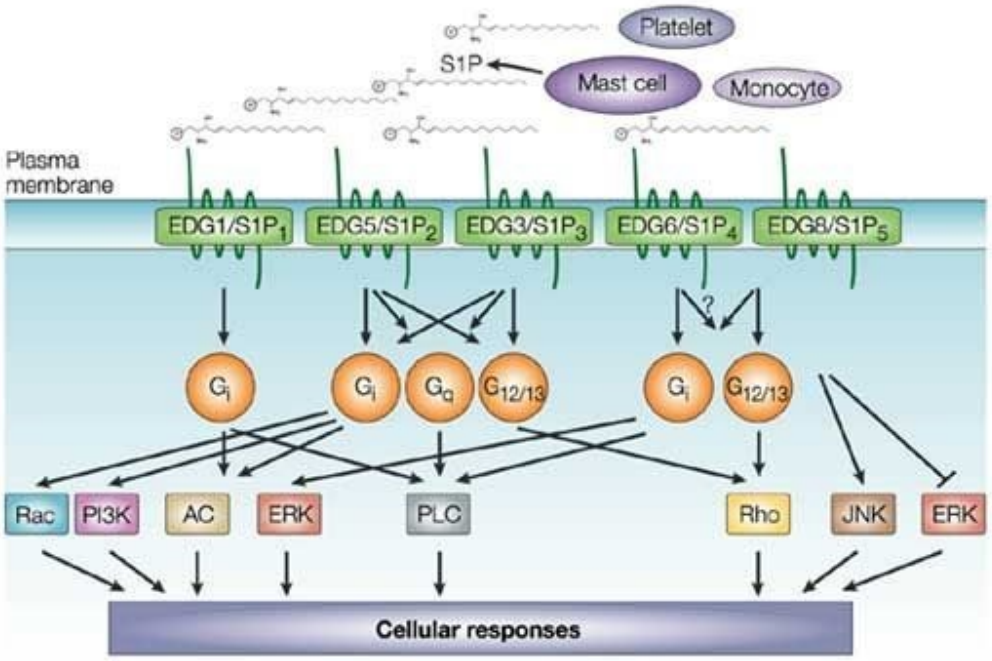

Figure 6: Extracellular S1P signaling pathways mediated by S1PR1-5

Graphical image representing extracellular S1P release from platelets, mast cells and monocytes and subsequent binding and activation of its specific G-protein coupled receptors. Activated S1PR1-5 stimulates downstream signaling and regulate various cell function. S1P receptors are also known as EDG (endothelial differentiation gene) receptors. The graph is from Spiegel and colleagues (Spiegel and Milstien, 2003) and reproduced here with prior permission from Springer Nature (License number 4514431386765).

S1P receptors are known to be mediators of several physiological functions, for example, S1PR1 expression is essential for normal development of the mouse embryonic cardiovascular system. Further, both in-vitro and in-vivo studies have demonstrated the importance of S1PR1 expression in vascular endothelial cells morphogenesis, development, and maintenance of vascular barrier through adherence junction formation (Blaho and Hla, 2014, Young and Van Brocklyn, 2006). Further, S1PR1 expression in the lymphocyte has been shown to be a major factor in the S1P mediated lymphocyte egress from lymphoid organs to the blood. The FDA approved drug FTY720/fingolimod in the treatment of Multiple sclerosis (MS) has shown to decrease S1PR1 activity and lymphocyte egress in patients (Brinkmann et al., 2010). On the other hand, S1PR2 mediates microvascular constriction leading to reduced blood flow to the cochlea (Maceyka et al., 2012). Further, S1PR2 has also been shown to regulate vascular activation and permeability, and lymph vessels contractility (Blaho and Hla, 2014).

In-vitro, S1PR3 was reported to be involved in the migration of B cells. Additionally, S1PR1 and S1PR3 promote migration of macrophages and dendritic cells (Blaho and Hla, 2014). S1PR4 expression was reported to be profuse in immune cells and shown to promote rearrangement of cytoskeleton and cell shape (Olesch et al., 2017). On the other hand, S1PR5 expressed in brain endothelial cells promotes optimal barrier formation and reduces immune trafficking (van Doorn et al., 2012). Further, S1PR5 also regulates NK (natural killer) cell egress from bone marrow to blood (Olesch et al., 2017).

1.12 Sphingosine 1-phosphate in cancer

S1P is a pro-proliferative molecule. As mentioned above, it acts not only via intracellular targets but also via binding to extracellular specific receptors. Several studies in cancer biology revealed that S1P promotes cancer cell survival, proliferation, migration, metastasis, and angiogenesis (Kunkel et al., 2013). S1P can exert pro-tumorigenic functions in an S1PR-dependent or independent manner. Specific receptor exerts specific function depending on the cancer cell type and context (Kunkel et al., 2013, Ogretmen, 2018).

In lung cancer cells S1P promoted tumor cell survival and growth by binding hTERT and mimicking activating phosphorylation. This prevented the binding of hTERT to U3 ubiquitin ligase MKRN1 (Makorin ring finger protein 1) and ultimately its degradation and increased pro-tumorigenic telomerase activity (Panneer Selvam et al., 2015). Recent study identified that S1PR1 is a key component in the persistent activation of STAT3 in tumor cells. STAT3 is a transcription factor for S1PR1 hence, activated STAT3 increased the expression of S1PR1. Thus, S1P binding to S1PR1 leads to an autocrine activation loop of STAT3 activation in in-vitro and in-vivo tumor studies. STAT3 activation was also essential to upregulate IL-6 expression which is crucial for the activation of STAT3 to induce tumor cell transformation and progression (Lee et al., 2010). This is one mechanism which cancer cells use persistently to maintain oncogenicity. Upregulated S1PR1 and S1PR3 is correlated with poor prognosis for estrogen receptor (ER)-positive breast cancer patients. Further, S1PR4 expression is associated with ER-negative breast cancer (Mukhopadhyay et al., 2015). In breast cancer cells it was shown that S1P is exported through ABCC1 and ABCG2 to promote autocrine cell survival and proliferation (Takabe et al., 2010). SPNS2 is a transporter of S1P in mice. In $SPNS2^{-/-}$ mice a reduction in lung metastasis and improved T cells and NK cell infiltration suggested a role of

SPNS2/S1P in tumor metastasis (van der Weyden et al., 2017). All the above studies indicate the importance of S1P and its receptors in tumorigenesis.

1.12.1 Dysregulated S1P pathway in cancer

S1P is synthesized by the condensation of serine and palmitoyl CoA as described above. Several reports are suggesting that this pathway is dysregulated in cancer cells (Hannun and Obeid, 2018, Ryland et al., 2011, Hisano and Hla, 2019). Several enzymes are maintaining this pathway and are used by cancer cells to transform and proliferate. These enzymes can affect S1P-Cer homeostasis to promote pro-proliferative S1P synthesis and inhibit pro-apoptotic Cer formation (Ksiazek et al., 2015). Out of several enzymes that regulate the sphingolipid pathway, SK1 and SK2 are the most intensely studied enzymes in cancer biology. In particular, SK1 has been shown to promote oncogenesis in skin, breast, lung, stomach, colon, ovarian, uterine, kidney, and brain (Shida et al., 2008).

1.12.2 SK1 in cancer

Sphingosine Kinase 1 (SK1) is mainly present in the cytosol and translocates to the plasma membrane when activated leading to S1P formation (Shida et al., 2008). Various growth factors and chemoattractants such as EGF (epidermal growth factor), IGF (insulin growth factor), PDGF (platelet derived growth factor), and TGFβ (transforming growth factor beta) have been shown to activate SK1 (Shida et al., 2008). A number of studies demonstrated that ERK1/2 (Extracellular signal-regulated kinase 1/2) activates SK1 by phosphorylation at Ser^{225} and promotes subsequent translocation to the plasma membrane (Pitson et al., 2003). Also, SK1 mRNA is upregulated by TGF-β, EGF, PMA, prolactin, 1,25-dihydroxy vitamin D3, and histamine (Shida et al., 2008, Yamanaka et al., 2004). Upregulation of SK1 increases S1P synthesis and thereby promotes cell proliferation.

In NIH3T3 fibroblasts, overexpression of SK1 and subsequent increase in S1P levels demonstrated the transformation of these cells and when injected into immuno-compromised mice gave rise to the formation of fibrosarcomas (Xia et al., 2000). This led to the classification of SphK1 as an oncogenic lipid kinase. Upregulation of SK1 expression has been reported in many tumor entities such as melanoma, squamous cell carcinoma, advanced stage cervical cancer, bladder cancer, head and neck cancer, glioblastoma and leukemia (Pyne and Pyne, 2010, Shida et al., 2008). A meta-analysis study of various tumor tissues (n=4,673 patients) in comparison to its normal unaffected tissues showed upregulated SK1 on mRNA and protein level. Additionally, the high

expression of SPHK1 was correlated with poor prognosis and decreased survival (Zhang et al., 2014). In prostate cancer, it was shown that siRNA mediated knockdown of SK1 increased the Cer/S1P ratio and promoted apoptosis. In contrast, SK1 overexpression induced resistance against chemotherapy and promoted oncogenesis in leukemia, prostate and pancreatic cells (Guillermet-Guibert et al., 2009, Pchejetski et al., 2005, Baran et al., 2007, Sobue et al., 2008). These data suggest a predominant role of SK1 in oncogenesis and resistance to chemotherapy in tumor cells. Therefore, inhibiting activity of SK1 might be an attractive strategy to overcome carcinogenesis.

1.12.3 SK2 in cancer

SK2 is mainly present in the nucleus or ER (Pyne and Pyne, 2010). In response to phosphorylation by PKD (protein kinase D) SK2 translocates from the nucleus to the cytosol (Ding et al., 2007). Unlike SK1, various studies have shown dual roles for SK2. Contrary to SK1, nuclear localization of SK2 induce cell cycle arrest apparently leading to cell death in tumor cells (Liu et al., 2003). Unlike SK1, overexpression of SK2 in NIH3T3 cells led to apoptosis (Maceyka et al., 2005). SK2 contains a BCL-xL BH3 binding domain, which inhibits anti-apoptotic BCL-xL and promotes apoptosis (Liu et al., 2003, Maceyka et al., 2005).

Nevertheless, other studies also indicated a survival function for SK2. For example, the impact of SK2 knockdown on the reduction of glioblastoma proliferation was more pronounced when compared to SK1 knockdown (Van Brocklyn et al., 2005). In breast and colon cancer, SK2 knockdown in combination with doxorubicin treatment induced P53 independent G2/M cell cycle arrest (Sankala et al., 2007). Moreover, in MDA-MB-453 breast cancer cells, EGF-induced activation of SK2 (phosphorylation at Ser^{351} and Thr^{578}) through ERK1 and promote tumor cell migration (Hait et al., 2007). Similar to SK1, high expression of SK2 in NSCLC tissue was observed. Furthermore, high expression of SK2 in patients correlated with resistance to gefitinib and lower overall survival (Wang et al., 2014). Thus, these studies underline anti-apoptotic and pro-proliferative activity of SK2 and suggest that SK2 could be an important target to reduce tumor burden.

1.12.4 S1P in cell migration, invasion, and metastasis

The mechanism of cancer cell migration is mediated by Rho and Rac GTPase subfamilies and involves reorganization of actin cytoskeleton. Rho regulates stress fiber formation and focal adhesion while Ras promotes lamellipodia formation (Ridley, 2015). Additionally,

activation of plasminogen activators is essential for the degradation of the extracellular matrix. Plasminogen activators convert inactive plasminogen to plasmin (serine protease) which degrades several extracellular matrix constituents (Andreasen et al., 2000). Degradation of extracellular matrixes further promotes cancer cell migration subsequently inducing invasion and metastasis induced by various stimulus in cancer cells.

S1P stimulated upregulated S1PR1 and S1PR3 expression and induced Rho and Rac dependent cell migration of B16 melanoma cells while overexpression of S1PR2 abrogated cell migration (Arikawa et al., 2003). Similarly, S1PR3 overexpression in MKN1 and HGC-27 human gastric cancer cells induced S1P dependent migration, but higher expression of S1PR2 in comparison to S1PR3 abrogated cell migration in AZ-521 and MK74 cell gastric cells (Hisano and Hla, 2019). In contrast, S1P binding to S1PR2 was shown to promote invasion and metastasis by activating matriptase (serine protease) (Hisano and Hla, 2019). Additionally, S1PR2 knockdown abolished plasminogen activation in glioblastoma cells (Hisano and Hla, 2019, Bryan et al., 2008). Through its receptors, S1P was shown to promote expression of the plasminogen activator system and MMP2 and MMP9 (Matrix metalloproteinase) (Bryan et al., 2008, Devine et al., 2008). This suggests the importance of S1PR2 during cancer cell invasion and metastasis. Taken together these data suggest an essential role for S1P/S1PR-mediated signaling events during cancer cell migration, invasion, and metastasis.

1.12.5 S1P in angiogenesis

For survival and metastasis cancer cells modify its tumor microenvironment and stimulate angiogenesis to sustain nutrient and oxygen supply (Martin et al., 2016). S1P is one of the key players in the development of the vasculature. One of the important findings in S1P signaling shows that S1PR1 null mice do not develop a well-defined vasculature and die at early stages of the development (Liu et al., 2000). Also, S1PR1-3 triple knockout mice showed more severe phenotype suggesting the importance of S1pr1-3 and S1P signaling during angiogenesis and development (Hisano and Hla, 2019). Importantly, S1PR1 promotes barrier function and thereby increases vascular stability (Blaho and Hla, 2014).

VEGF (vascular endothelial growth factor) is an important mediator of angiogenesis and vasculogenesis (Hisano and Hla, 2019). VEGF regulates functions in endothelial cells by binding to its receptor VEGFR receptor tyrosine kinases. Stimulation of VEGFR2 through VEGF plays a critical role in early development of angiogenesis in endothelial cells, and

later S1PR1/S1P signaling stabilizes the newly formed vasculature (Hisano and Hla, 2019). Chae and colleagues demonstrated high expression of S1PR1 in the tumor vasculature and subsequent knockdown of S1PR1 by siRNA abrogated angiogenesis and tumor growth in a Lewis lung carcinoma cell xenograft nude mouse model (Chae et al., 2004). Moreover, IL-8 is a chemokine known to be upregulated in many cancer types and to induce tumor angiogenesis (Shi and Wei, 2016). In breast cancer and ovarian cancer cell lines it was shown that S1P induces upregulation of pro-angiogenic IL-8 expression and secretion (Boucharaba et al., 2009, Schwartz et al., 2001).

Angiogenesis in cancer is promoted by hypoxia and regulated by HIFs (hypoxia-inducible factors). In glioma cells, it was shown that HIF-2α directly bind to the promoter of SK1 and induces upregulation of S1P synthesis (Anelli et al., 2008). Contrarily, in A549 adenocarcinoma cells, SK2 induces S1P synthesis under hypoxic conditions (Schnitzer et al., 2009). This evidence indicates that the SK/S1P/S1PR signaling axis is vital in tumor-induced angiogenesis.

1.13 Role of sphingolipids in virus binding and endocytosis

Recent studies have revealed the role of SLs in the lifecycle of pathogenic viruses. Apart from playing a critical role in the translocation, replication, and budding SLs also support viral attachment to the cell membrane and subsequent uptake into the cells (Schneider-Schaulies and Schneider-Schaulies, 2015).

GSLs present in the outer layer of the plasma membrane serve as receptors for viral attachment and subsequent initiation of viral endocytosis (Schneider-Schaulies and Schneider-Schaulies, 2015). As mentioned above, GSLs are synthesized in the de-novo sphingolipid synthesis pathway in distal Golgi complex. GSLs are synthesized from hydrophobic ceramides and hydrophilic carbohydrates molecules (Taube et al., 2010). Based on their net charge, GSLs are classified into neutral, basic or acidic GSLs and, based on main structures are classified into lacto-, neolacto-, ganglio- and globo-GSLs (Hakomori, 2003). It was reported that GSLs such as Gb3 and galactosylceramide mediate HIV entry into immune cells by binding to the V3 loop of HIV envelope protein gp120 (Nehete et al., 2002). Apart from HIV, other pathogenic human viruses such as SV40 (Simian Virus 40), Parvovirus B19, Rotavirus, and Norovirus were shown to interact with GSLs (Taube et al., 2010). Additionally, and of relevance for the present thesis project

Merkel cell polyoma viral capsid VP1 was shown to interact with the ganglioside GT1b carbohydrate chain (Erickson et al., 2009). Using a lung cancer cell line, it was shown that MCPyV needs glycosaminoglycans such as HS (heparan sulfate) for initial attachment to the cell membrane (Schowalter et al., 2011). Further, the virus capsid VP1 contains sialic acid binding site through which it binds to sialylated GT1b thereby facilitating the entry of its virions into the host cells. These data indicate that MCPyV uses glycosaminoglycans as a primary receptor for its attachment and sialylated GSL as a secondary receptor for the gene transduction (Neu et al., 2012, Schowalter et al., 2011).

Further, Cer-enriched membranes are shown to be necessary for virus entry by endocytotic mechanisms. Human rhinovirus (RV) was shown to promote Cer-enrichment at plasma membrane domains by activating ASMase (acid sphingomyelinase) (Grassme et al., 2005, Schneider-Schaulies and Schneider-Schaulies, 2015). All the above data suggests that SLs serve as critical structural platforms during virus uptake.

1.13 Targeting the S1P pathway in cancer

Cancer cells use S1P synthesis pathway to transform, survive and proliferate hence, targeting S1P signaling is a promising anticancer strategy. A pharmacological inhibitor of SPHK2 and DES1, ABC294640, is currently in clinical trials in several cancer entities. In hepatocellular carcinoma, it is under Phase II clinical trial (NCT02939807), in Multiple Myeloma under Phase Ib and II (NCT02757326), in cholangiocarcinoma under Phase IIa (NCT03377179), and pancreatic cancer Phase I clinical trial is completed but results not disclosed (NCT01488513). ABC294640 inhibited lung tumors by inducing telomerase instability (Panneer Selvam et al., 2015). Further, in pancreatic cells inhibition of SK2 by ABC294640 resulted in a reduction of tumor growth via suppression of c-Myc and RRM2 (ribonucleoside-diphosphate reductase subunit) (Lewis et al., 2016).

FTY720 is an FDA approved drug for relapsing multiple sclerosis (MS). In glioma, FTY720 phase I clinical trial (NCT02490930) is completed, but results have not been disclosed. FTY720 is a sphingosine analog and was shown to inhibit S1PR1 in relapsing MS. FTY720 is phosphorylated by SK2, this step generates p-FTY720 that behaves as S1P analog and induces degradation of S1PR1. In-vitro and in-vivo studies in colon and lung cancer demonstrated that FTY720 inhibits tumor growth through S1PR1-dependent and -independent pathways, respectively (Saddoughi et al., 2013, Liang et al., 2013). In patient-

derived ovarian cancer xenografts, FTY720 enhanced antitumor activity in combination with carboplatin or tamoxifen and induced the formation of proapoptotic Cer species (Kreitzburg et al., 2018).

Furthermore, SK1-I a specific inhibitor of SK1 was shown to suppress glioblastoma (Kapitonov et al., 2009) and melanoma (Madhunapantula et al., 2012) growth and proliferation in-vitro and in-vivo. Similarly, SKI-II an inhibitor of SK1 and DES1 activity was also shown to inhibit cancer cell growth in melanoma (Madhunapantula et al., 2012), acute myelogenous leukemia (Yang et al., 2015), and HNSCC (head and neck squamous cell cancer) (Sinha et al., 2011) in-vitro and in-vivo in mouse models. Furthermore, PF-543 a potent SK1 inhibitor is effective against triple-negative breast and colorectal cancer in-vitro and in-vivo (Ogretmen, 2018). Additionally, VPC03090, an inhibitor of S1PR1 and 3 (Kennedy et al., 2011) and AB1, an S1PR2 inhibitor (Li et al., 2015) will enter clinical trials as potential anticancer drugs.

2. Hypothesis and Objectives

We hypothesize that the bioactive sphingolipid pathway regulates MCC survival and proliferation. We further propose that driving the SM-Cer-S1P rheostat towards a pro-apoptotic phenotype might be a promising anti-cancer strategy in MCC

To achieve the above hypothesis the following objectives were outlined:

- To characterize the expression of serine palmitoyltransferase (SPTLC1-3) and sphingosine kinase 1 and 2 (SPHK1/2) in MCC cell lines and tissues.
- To check the effect of MCPyV large T and small T antigens on mRNA level of SPTLC1-3 and SPHK1/2 in human lung fibroblasts.
- To study the outcome of pharmacological inhibition of SPTLC1-3 by myriocin and SPHK1/2 by SKI-II on intracellular S1P, Cer and SM synthesis.
- To elucidate the effect of SPTLC1-3 and SPHK1/2 inhibitors on MCC cell proliferation and survival.
- To assess the effect of SPTLC1-3 and SPHK1/2 inhibitor on cell viability of non-transformed normal dermal fibroblasts (NHDF).
- To analyze the mechanism of cell death upon inhibitor treatment by Flow cytometry and Western blot analysis.
- To study the effect of myriocin and SKI-II inhibition in MCC chicken chorioallantoic membrane model.

3. Materials and methods

Most of the methods described here in this section are reproduced from my published paper (Bhat et al., 2018a).

3.1 Tumor tissue samples from patients

Formalin-fixed and paraffin-embedded (FFPE) tumor samples of MCC (n=21) and nine non-MCC [Basal cell carcinoma (n=5) and melanoma samples (n=4)] samples were used to identify mRNA expression of SPTLC1-3 and SPHK1/-2. The patient's tumor samples were collected at the University Hospital Essen (Germany). All details related to the patient cohorts are published (Fan et al., 2018, Bhat et al., 2018a).

3.2 Cell lines and culture conditions

The $MCPyV^+$ MCC cell lines MKL-1, WaGa, MKL-2, LoKe, BroLi, MS-1, and PeTa were cultured in RPMI1640 media containing 10% fetal bovine serum (FBS) and 1% penicillin/streptomycin at 37°C and supplied with 5% CO_2 as described (Houben et al., 2013). Already established $MCPyV^+$ MCC cell lines UM13, UM29, UM52, UM565, and the $MCPyV^-$ MCC cell lines UM9, UM31, UM32, UM34, UM623, UM624 (Verhaegen et al., 2014) were cultured in neural crest stem cell self-renewal medium supplemented with 15% chick embryo extract. Primary human skin fibroblasts were cultured in DMEM supplemented with 15% FBS at 37°C and 5% CO_2. Normal human dermal fibroblasts (NHDF) were purchased from Lonza (Walkersville, MD, USA) and cultured in FGM™-2 BulletKit™ supplemented with 2% FCS at 37°C and 5% CO_2. MRC-5 cells (human lung fibroblasts) were cultured in MEM Eagle media containing 10% FBS at 37°C and 5% CO_2 (Bhat et al., 2018a).

3.3 Lentiviral transduction of human lung fibroblasts (MRC-5 cells)

MKL-1, MKL-2, and MS-1 derived truncated MCPyV-LT antigens were cloned into pLJM1-EGFP plasmids. HEK293T cells were used to produce lentiviral particles by co-transfecting pLJM1-EGFP-LTAs or pLJM1-EGFP plasmids with helper plasmids (pHCMV-G, pRSV rev and pMDLg/pRRE). Post 48 h of transfection viral particles were harvested by filtering through 0.45 µm filters. For transduction, 200 µl of virus supernatant and 4 µg/ml polybrene were added to the MRC-5 fibroblasts and incubated overnight; then

cells were washed twice with culture medium Eagle's Minimum Essential Medium. Puromycin 1 µg/ml was added to establish stably transduced cells (Bhat et al., 2018a).

3.4 RT-qPCR

Total RNA was isolated utilizing the RNA Kit purchased from PeqGOLD. Two-hundred ng of isolated RNA was transcribed into cDNA using Transcriptor First Strand cDNA Synthesis Kit. LuminoCt SYBR Green qPCR ReadyMix (Sigma, St. Louis, MO) was added to the cDNA with primers. The qRT-PCR analysis was performed on a CFX384 Touch™ Real-Time PCR machine. QuantiTect primers were purchased for SPTLC1-3 and SPHK1/2 (Qiagen, Hilden, Germany). The 60S acidic ribosomal protein-P0 (RPLP0) was used as housekeeping gene and detected with LuminoCt qPCR ReadyMix (Sigma, St. Louis, MO), Details of all the primers and probe used is given in **Table 1** (Bhat et al., 2018a).

3.5 RT-qPCR of S1PR1-5

Expression of S1PR1-5mRNA was measured in MKL-1, MKL-2, WaGa, BroLi, LoKe, and PeTa MCC cell lines; total RNA was extracted from the cell lines mentioned above using the RNeasy Plus Kit (Qiagen, Hilden, Germany). cDNA was synthesized using high-capacity cDNA reverse transcription kit (Applied Biosystems, Applied Biosystems, Foster City, CA). RT-qPCR was performed in an Applied Biosystems 7900HT Fast Real-Time PCR machine using QuantiFast SYBR Green PCR kit (QIAGEN, Hilden, Germany) and QuantiTect primers S1PR1-5 (QIAGEN, Hilden, Germany). The obtained Ct values were then normalized to housekeeping gene HPRT. The expression was calculated using $2^{-\Delta\Delta Ct}$ method relative to S1PR1. Information about the primers is given in **Table 1** (Bhat et al., 2018a).

3.6 Re-analysis of GEO datasets

Microarray data from the GEO database (GSE39612) was used to re-analyze mRNA expression of SPTLC1-3 and SPHK1/2 in renormalized 64 normal skin tissues and 30 MCC tumor tissues (Harms et al., 2013). The data were re-analyzed using ExAtlas, an online gene expression meta-analysis tool (Sharov et al., 2015). RNA sequencing data (GSE79968) was downloaded from GEO datasets (Berrios et al., 2016). The FPKM (Fragments per kilobase of exon per million reads) values for SPTLC1-3 and SPHK1/-2

were obtained from datasets deposited for GFP transfected or MCPyV-sT transfected IMR90 cells (Bhat et al., 2018a).

3.7 LC-MS/MS analysis

Approximately 750,000 MKL-1 and WaGa MCC cells were seeded in 12 well plates supplemented with RPMI1640 media and 0.5% FBS (Fetal bovine serum) and left overnight. Then the cells were treated either with DMSO (Dimethyl sulfoxide 0.1% as a vehicle) or myriocin (10 mM in DMSO) or SKI-II (30 mM in DMSO). After 24 h of treatment, MKL-1 and WaGa cells were harvested in a 1ml tube and lysed by sonication in cold phosphate buffered saline (PBS; pH 7.4). The sonicated MKL-1 and WaGa samples were then mixed with three volumes of chloroform/methanol solution (2:1; v/v) and subsequently CerC17:0 and SMC17:0 was added as internal standards (ISTD) (Avanti Polar Lipids, Alabaster, USA). To analyze SLs, mild alkaline hydrolysis was done by adding 400 µl 1 M NaOH in methanol/$CHCl_3$/H_2O (16:16:5, v/v/v) to lipid extracts and incubated for 45 min at room temperature. The samples were then neutralized using 150 µl 1 M acetic acid and 400 µl 0.5 M EDTA Then, 1 ml $CHCl_3$ was added, samples were vortexed, centrifuged, and the upper aqueous layer was removed. Once again, the samples were washed with 700 µl H_2O, vortexed, centrifuged and the aqueous phase was removed. The organic layer was dried under N_2. Lipids were separated on a UPLC-column analyzed using a QTOF-MS system as described (Knittelfelder et al., 2014). Data analysis was performed using the Lipid Data Analyzer Software (Hartler et al., 2011). Data were normalized to recovery, extraction, and ionization efficacy by calculating analyte/ISTD ratio. Further, the ratio obtained was normalized to protein content (arbitrary units/mg protein) (Bhat et al., 2018a).

3.8 S1P measurement

Intracellular S1P in MCC cells was quantitated using the S1P ELISA kit from Echelon (Echelon Biosciences, UT, US). To analyze S1P concentration, MKL-1 and WaGa cells were seeded in 21 cm^2 petri dishes and cultured in the absence or presence of DMSO (0.1% as a vehicle) or myriocin (10 mM in DMSO) or SKI-II (30 mM in DMSO). S1P-ELISA assay was performed post 24 h of treatment as suggested in the manufacturer's protocol. A nonlinear regression model was used to quantitate S1P levels as suggested by

the manufacturer. Data obtained were normalized to cell protein content (Bhat et al., 2018a).

3.9 Inhibitor treatment and cell viability assay

CellTiter-Glo 3D cell viability assay was used to measure cell viability in MKL1, WaGa, and NHDF cells. Briefly, MKL1 and WaGa cells ($2x10^4$) were seeded in 96 well plates supplemented with RPMI1640 media and 0.5% FBS. Then the cells were treated with myriocin, SKI-II, Triciribine, ABC294640 or FTY720 at increasing concentrations. DMSO was used as (0.1%) a vehicle. After 48 h of inhibitor treatment cell viability was measured using CellTiter-Glo 3D cell viability assay kit as described in the manufacturer's protocol. Untreated MKL-1 and WaGa cells were used as a control. To measure cell viability in NHDF cells, ≈ $2x10^3$ cells per well were seeded in 96 well plates containing media with 0.5% FCS and allowed to attain 80% confluence before inhibitor treatment was performed as mentioned above. Viability assay was carried out using CellTiter-Glo 3D cell viability assay kit (Bhat et al., 2018a).

3.10 S1P enrichment of high-density lipoprotein (HDL)

The HDL was isolated from healthy human volunteers as described (Sattler et al., 1994). S1P enrichment in HDL was achieved by incubating isolated HDL (4 mg protein/ml) with S1P (50 µg) on a rotating wheel for 4 h at 37°C. S1P-ELISA assay was performed to measure S1P concentration in native HDL, and S1P enriched HDL (HDL-S1P) as described (Bernhart et al., 2015, Bhat et al., 2018a).

3.11 Native HDL, HDL-S1P, and S1P lyase treated HDL in MCC cell viability assay

HDL and HDL-S1P were prepared as stated above. MKL-1 and WaGa cells were then treated with either HDL or HDL-S1P at increasing concentrations and left for 48 h. Cell viability was measured using CellTiter-Glo 3D cell viability assay kit.

Native HDL (200µl of 4 mg protein/ml) was incubated with S1P lyase (3 µg) for one hour. Then MKL-1 and WaGa cells were treated with native HDL (20 µg/ml), or S1Plyase treated HDL (20 µg/ml). S1P lyase was used as a control. 48 h after treatment cell viability was measured using CellTiter-Glo 3D cell viability assay kit.

3.12 VPC23019 treatment and cell viability assay

MKL-1 and WaGa cells were initially incubated with VPC23019 (1 μM or 5 μM) for one hour. Then native HDL (20 μg/ml) or HDL-S1P (20 μg/ml) was added for 48 h. Cell viability was measured using CellTiter-Glo 3D cell viability assay kit.

3.13 Annexin V/propidium iodide staining

MKL-1, WaGa and NHDF cells ($3x10^5$) were seeded in 12 well plates supplemented with RPMI1640 media containing 0.5% FBS and treated with myriocin, SKI-II, Triciribine, ABC294640, or FTY720 as indicated. DMSO was used as a vehicle (0.1% v/v). After 48 h of inhibitor treatment MKL-1, WaGa and NHDF cells were harvested and stained using the FITC Annexin V Apoptosis Detection Kit 1 (BD Biosciences) according to the manufacturer's protocol. Flow cytometric analyses were performed using a Guava EasyCyte8 flow cytometry machine (Millipore, Billerica, MA, USA) and analyzed using software InCyte 3.1 (Millipore) (Bhat et al., 2018a).

3.14 Caspase-3 activity assay

MKL-1 and WaGa cells ($7.5x10^5$) were seeded in 12 well plates supplemented with RPMI1640 media containing 0.5% FBS. The cells were then treated with myriocin (15 μM) or SKI-II (15 μM) or DMSO (vehicle) or left untreated for 24 and 48 h. Later, cells were harvested, and the caspase-3 activity assay was performed using EnzChek Caspase-3 Assay Kit #2 Invitrogen (Waltham, MA) as described by the manufacturer (Bhat et al., 2018a).

3.15 Western blot analysis

For Western blotting, $1x10^6$ cells were seeded in 6-well plates supplemented with RPMI1640 media containing 0.5% FBS. The cells either were treated with myriocin (10 μM and 15 μM) or SKI-II (10 μM and 15 μM) or DMSO (vehicle) or left untreated as indicated. After 36 h the cells were lysed in RIPA buffer (50 mM Tris-HCl pH 7.4, 1 % NP-40, 150 mM NaCl, 1 mM Na_3VO_4, 1 mM NaF, 1 mM EDTA) containing protease inhibitors and 10 μM PMSF. BCA kit was used to measure protein concentration of cell lysates as described by the manufacturer (Thermo Scientific). Equal concentration of protein aliquots was loaded (50 μg/lane) into 10% SDS-PAGE gel, and then the protein was separated based on their size on SDS-PAGE under reducing conditions. After

separation, proteins were transferred to PVDF (polyvinylidene difluoride) membranes. Initially, membranes were blocked in 5% milk prepared in TBST (Tris-buffered saline containing Tween 20) buffer for 2 h to reduce non-specific binding of antibodies. Next, membranes were incubated with specific primary antibodies (dilution1:1000) for overnight at 4^0C (list of all the antibodies given in **Table 2**). Then membranes were washed in TBST buffer and further incubated with corresponding HRP-conjugated secondary antibodies for 2 h. Immunoreactive bands were visualized using ECL reagents. Membranes were stripped and re-probed for β-actin (1:5000) as a loading control. Densitometric analysis was done using ImageJ software, and immunoreactive bands were normalized to corresponding actin and control lanes. Each experiment was repeated at least three times. (Bhat et al., 2018a).

3.16 MCC-CAM tumor xenograft model

The MCC-CAM tumor xenograft model was implemented as reported (Bhat et al., 2018b). The ex-ovo CAM assay was performed as described (Deryugina and Quigley, 2008). Schematic workflow of MCC-CAM is shown (**Figure 28**). In brief, fertilized eggs of white leghorn chicken were from a local commercial hatchery. The fertilized egg was considered as day 0 of the embryo. The fertilized eggs were then incubated for 3 days (37.6°C, 50 % humidity) lying horizontally with continuous rotation. On day 3 of the embryo, before cracking the egg, the plastic dishes were sterilized by 70% ethanol and UV-radiation. The eggshells were then cracked by using a mechanical fret saw. Then egg content was placed carefully into the sterilized plastic container and incubated for additional 7 days. Next, on day 10 of the embryo, silicone rings (5 mm diameter) were placed on vascular branches of the CAM. MKL-1 and WaGa MCC cells were then mixed with Matrigel (BD MatrigelTM Basement Membrane Mix) in a 1:3 ratio and from the mixture 20 µl (containing $2x10^6$ cells/onplant) was applied into the silicone rings and left a day to allow the cells to interact with CAM. On day 11 of the embryo, DMSO or myriocin (15 µM) or SKI-II (15 µM) treatment was started and continued for once in every 24 h. Progression of MKL-1 and WaGa tumor xenografts was monitored by photo-documentation using Olympus SZX16 throughout the incubation period. On day 15 of the embryo, the tumors were photo-documented, and tumor area was quantified using Image J software (Bhat et al., 2018b, Azoitei et al., 2011). The CAM with the attached xenografts of MKL-1 and WaGa was then removed by a square cut, and the host chick embryo was killed by decapitation.

Samples were then washed and fixed with 4 % (v/v) paraformaldehyde for 16 h at room temperature followed by FFPE-tissue embedding (Bhat et al., 2018a).

3.17 Histology

Sectioning of the paraffin-embedded MKL-1 and WaGa tumor xenografts was performed using microtome tissue sectioning machine. Five µm sections were prepared from the above samples. Then the sections were stained with Haematoxylin and eosin or analyzed immunohistochemically according to manufacturer's protocol (mouse and rabbit specific HRP/DAB Detection IHC Kit, Abcam). In brief, the sections were incubated with primary antibodies (list of all the antibodies given in **Table 2**) for 60 min at 37^0C after de-paraffinization, rehydration and blocking procedure. Then the sections were washed and subjected to incubation with polyclonal secondary antibodies. The detection of target antigens was performed via streptavidin-peroxidase-mediated reaction of AEC or DAB. Anti-cytokeratin-20 (CK-20; Dako, 1:200) staining was performed manually, Ki-67 (Dako) antibody staining was performed on an automated staining system (Dako-Autostainer). Ki-67 index was calculated by identifying Ki-67-positive tumor area using ImageJ as described (Peulen et al., 2013). Images were taken on an Olympus BX53 (Bhat et al., 2018a).

3.18 Statistical analyses

Data were presented here as mean ± SD. Unpaired Student`s t-test, Mann-Whitney U test or one-way ANOVA was used for analysis of statistical significance (using the Graph Pad Prism6 package). All values of $p < 0.05$ were considered significant (Bhat et al., 2018a).

4. Results

4.1 Characterization of *SPTLC1-3* and *SPHK1/2* expressions in MCC skin tumor samples

Initially, we characterized mRNA expression of *SPTLC1-3* (coding for the three catalytic subunits of SPT) and *SPHK1/2* (coding for SK1/2; the two enzymes that phosphorylate sphingosine to S1P) in nine non-MCC skin tumor samples (consisting of 5 basal cell carcinomas and 4 melanomas) and 21 MCC tumor samples by qRT-PCR. The comparison of non-MCC tumor samples to MCC tumor samples revealed significantly higher expression of *SPTLC1* in MCC tumors (**Figure 7A**). *SPTLC2/3* and *SPHK1/2* showed a clear trend towards higher expression though the difference was statistically not significant (**Figure 7A** and **7B**).

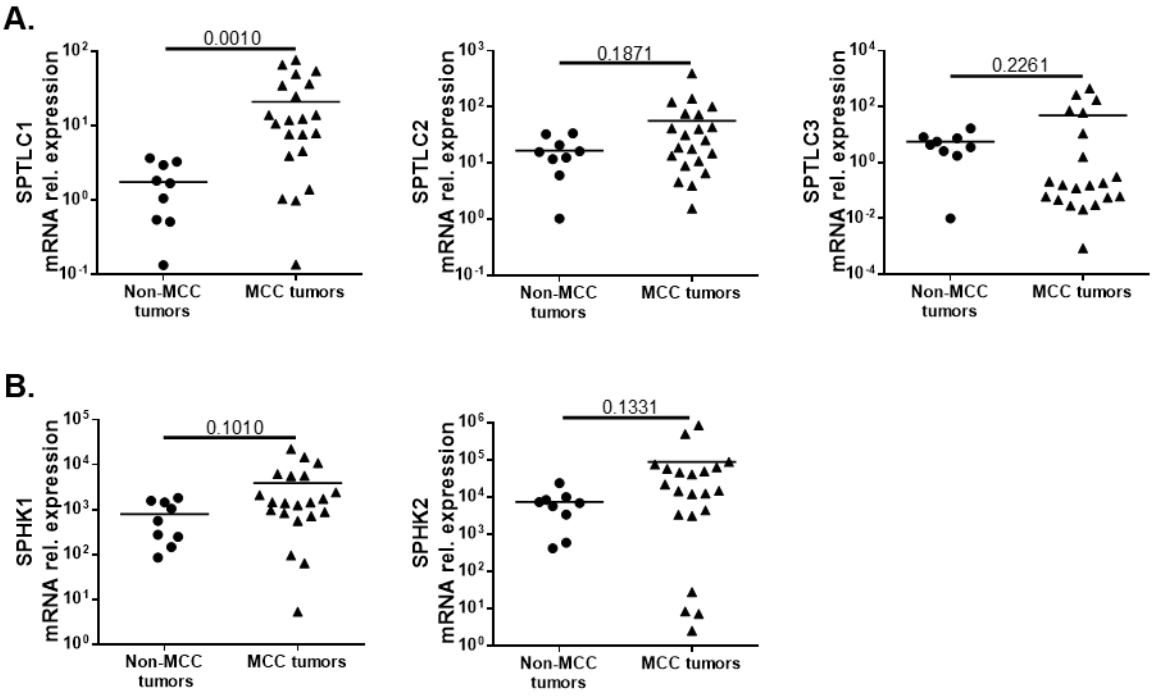

Figure 7: *SPTLC1-3* and *SK1/2* mRNA expression in MCC tumor samples.

RNA was isolated, and cDNA was prepared from nine non-MCC (5 basal cell carcinomas and 4 melanomas) and 21 MCC tumor samples. (**A** and **B**) The obtained Ct-values were normalized to *RPLP0* and *SPTLC1-3* and *SPHK1/2* expression was analyzed using the method $2^{-\Delta\Delta Ct}$ relative to skin fibroblasts. Statistical analysis was done between non-MCC and MCC tumor samples using the Mann-Whitney test (p-value < 0.05 was considered significant). The data shown above are from my published article (Bhat et al., 2018a) and reproduced here with the permission from Elsevier.

4.2 Characterization of *SPTLC1-3* and *SPHK 1/2* expression in MCPyV-positive and MCPyV-negative MCC cell lines

After investigating the expression in MCC tumor samples, we quantitated mRNA expression of *SPTLC1-3* and *SPHK1/2* in 10 $MCPyV^+$ and 6 $MCPyV^-$ MCC cell lines. Non-transformed NHDF cells (normal human dermal fibroblast) were used as relative control. qRT-PCR results are shown relative to the expression in NHDF cells. The expression of *SPTLC1* was higher in 13/16 cell lines. *SPTLC2* expression was higher in 16/16 cell lines, and *SPTLC3* expression showed higher expression in 8/16 cell lines (**Figure 8A**). In *SPHK's*, 3/16 MCC cells showed higher expression of *SPHK1* and, *SPHK2* expression was lower in all MCC cell lines when compared to NHDF (**Figure 8A**). Further, we compared *SPTLC1-3* and *SPHK1/2* expressions between 10 $MCPyV^+$ and 6 $MCPyV^-$ MCC cell lines. Interestingly, *SPHK1* and *2* expression levels were significantly higher in $MCPyV^+$ in comparison to $MCPyV^-$ cells, but there was no significant difference in *SPTLC1-3* levels (**Figure 8B**).

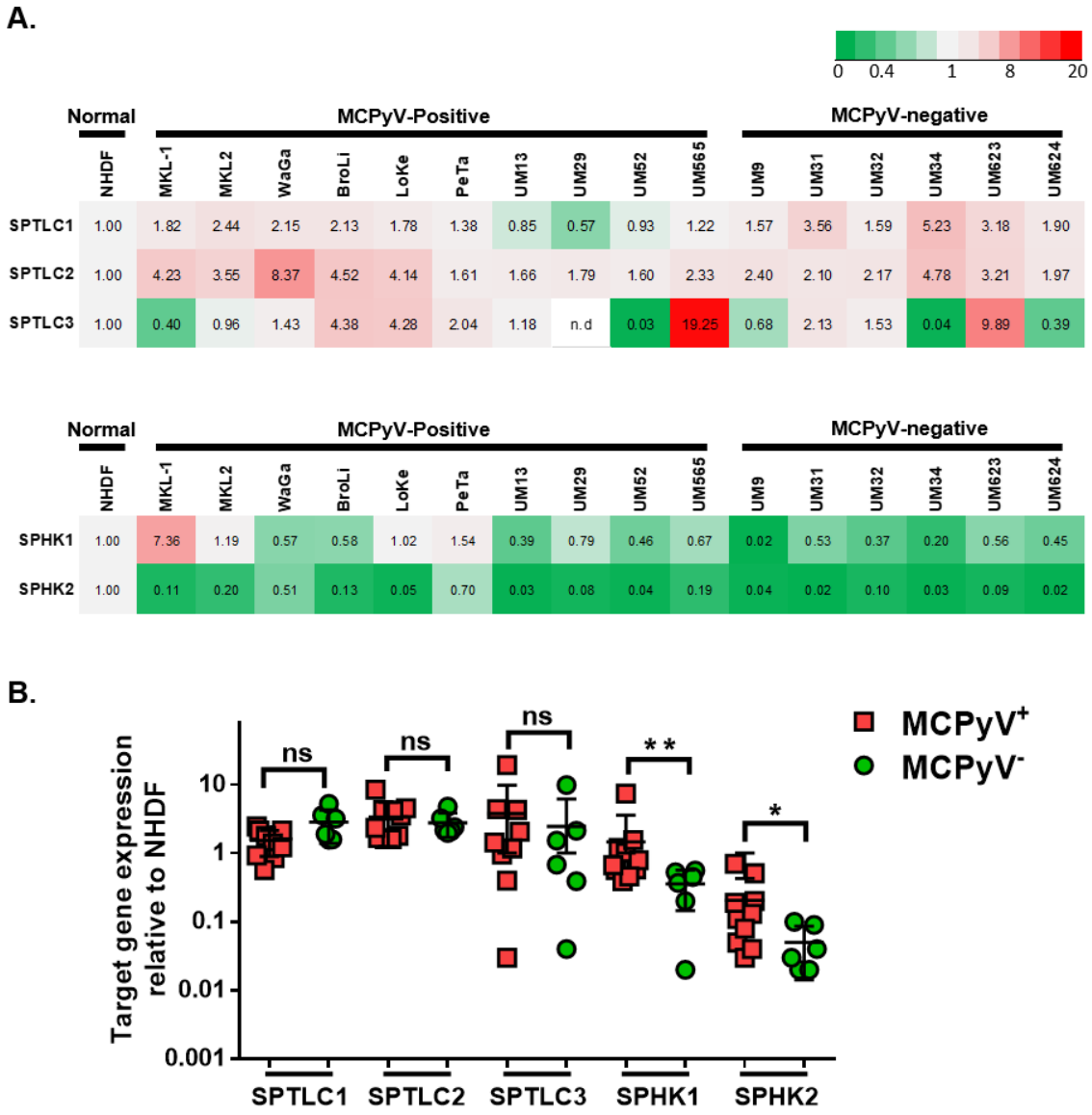

Figure 8: *SPTLC1-3* and *SK1/2* mRNA expression in MCPyV$^+$ and MCPyV$^-$ MCC cell lines.

(**A**) Normal human dermal fibroblast (NHDF) cells, 10 MCPyV$^+$, and 6 MCPyV$^-$ MCC cell lines were used to check the mRNA expression of *SPTLC1-3* and *SK1/2*. The heat map was generated after mRNA expressions were calculated using the $2^{-\Delta\Delta Ct}$ method. Ct-values were normalized to *RPLP0* and are shown relative to NHDF. The experiment was performed in triplicates. (**B**) mRNA expression of *SPTLC1-3* and *SK1/2* was analyzed in 10 MCPyV$^+$ and 6 MCPyV$^-$ MCC cell lines and statistical analysis was performed by Mann-Whitney test. (mean ± SD, *p ≤ 0.05, **p ≤ 0.01, ns., not significant, n.d., not detected). The data shown above are from my published article (Bhat et al., 2018a) and reproduced here with the permission from Elsevier.

4.3 MCPyV-LTA expression in fibroblasts upregulates SPTLC1-3 and SPHK1-2 mRNA

To investigate whether MCPyV-LTA induction in the human lung fibroblast MRC-5 cell line affects *SPTLC1-3* and *SPHK1/2* mRNA levels, we transduced MCPyV-LTA in MRC-5 cells. First, MCPyV-LTA was isolated from the MKL-1, MKL-2, and MS1 cell lines and cloned in a lentiviral expression vector and separately transduced in MRC-5 cells. EGFP expressing cells were used as negative control. MCPyV-LTA expression was confirmed by qRT-PCR (**Figure 9A**). Surprisingly, MCPyV-LTA expression led to the formation of two kinds of cell populations one growing exclusively adhesive (a natural state in culture flask) and the other floating. *SPTLC1-3* and *SPHK1/2* mRNA expression were checked in both cell populations (**Figure 9B** and **9C**). In comparison to EGFP (Enhanced green fluorescent protein)-expressing cells, *SPHK1* showed a significant upregulation in the MKL-1_LTA, and MKL-2_LTA expressing adherent MRC-5 cell populations and in the MKL-1_LTA expressing floating cells (**Figure 9C**). *SPHK2* was upregulated in nonadherent cells but not in the adherent cell population (**Figure 9C**). Conversely, *SPTLC1* and *2* did not show any change in expression while *SPTLC3* was consistently downregulated under all conditions (**Figure 9B**).

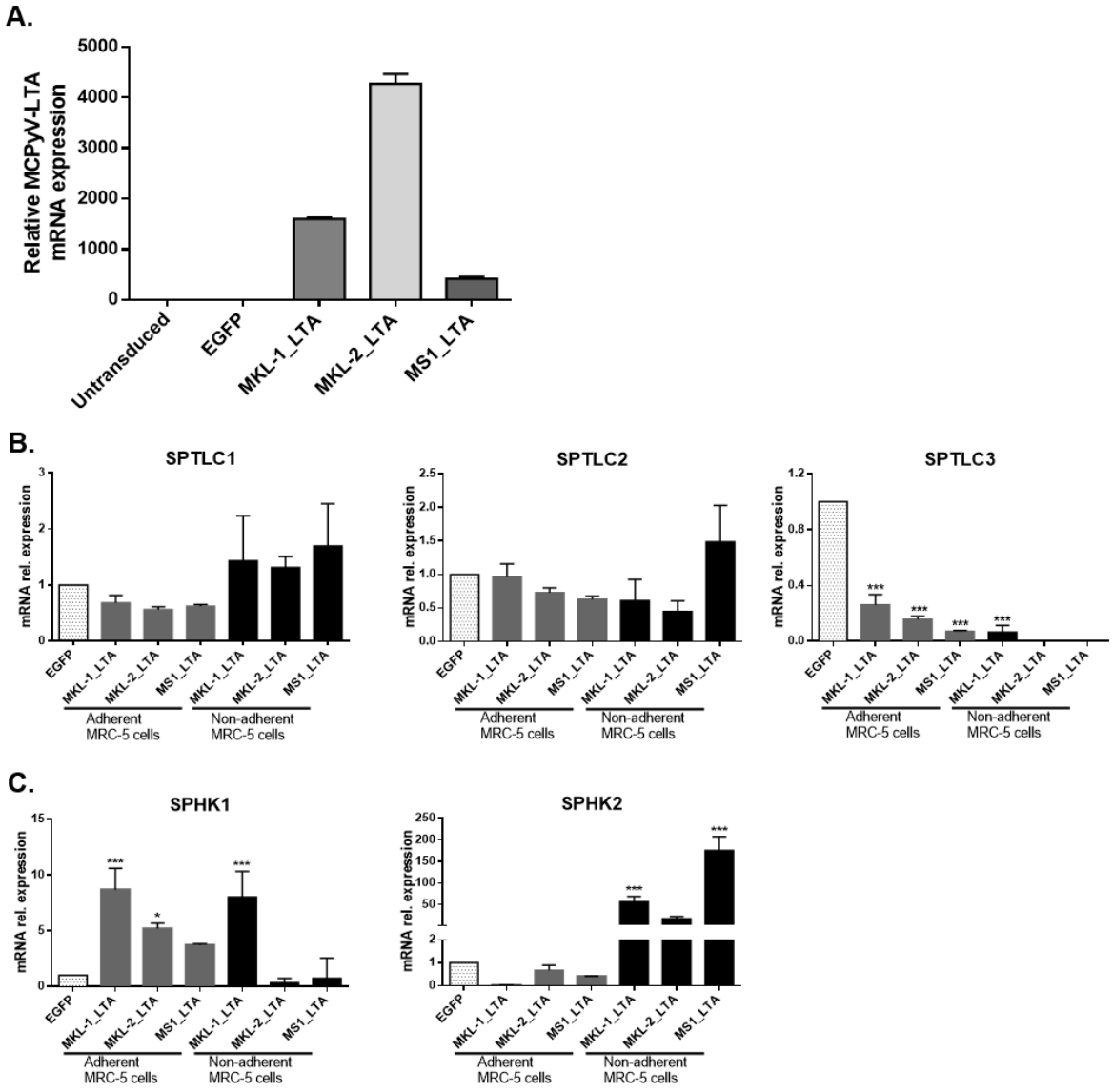

Figure 9: Forced expression of MCPyV-LTA in MRC-5 cells upregulates *SPHK1* and *SPHK2* mRNA.
The MCPyV-LTA of MKL-1, MKL-2, or MS1 cells were cloned into a lentiviral expression system and transduced into the MRC-5 cell line. (**A**) The mRNA expression of MKL-1_LTA, MKL-2_LTA, and MS1_LTA was shown using MCPyV-LTA specific primers. Non-transduced and EGFP expressing clones were used as negative control. (**B**) Two different cell populations (adherent and non-adherent) were obtained after transduction. These cell populations were collected separately, and mRNA expression of *SPTLC1-3* and *SPHK1/2* were analyzed using the $2^{-\Delta\Delta Ct}$ method relative to EGFP expressed cells. Statistical analysis was done using one-way ANOVA (n=3, mean ± SD, *p ≤ 0.05, **p ≤ 0.01, ***p ≤ 0.001). The data shown above are from my published article (Bhat et al., 2018a) and reproduced here with permission from Elsevier.

4.4 Reanalysis of MCC data from published GEO data set GSE39612 and GSE79968

We next reanalyzed two GEO dataset (Edgar et al., 2002) from two different published articles. From the GSE39612 microarray dataset (Harms et al., 2013) I compared SPHK1/2 mRNA expression in normal skin (n=64) and MCC tissues (n=30). The statistical analysis of the data revealed significantly higher expression of SPHK1 and 2 in MCC tumor samples in comparison to unaffected normal skin (**Figure 10A**). We did not observe differences in SPTLC1-3 expression (data not shown).

The second data set GSE79968 (Berrios et al., 2016) was obtained by RNA-Seq of MCPyV-sT expressing human lung fibroblasts (the IMR90 cell line). The authors used GFP-overexpressing cells as controls. Cells were harvested at the time points indicated and subjected to whole transcriptome RNA sequencing. The obtained FPKM values of SPTLC1-3 and SPHK1/2 from RNA sequencing data were retrieved from the raw data set and are compared between MCPyV-sT- and GFP-expressing cells. The statistical analysis disclosed upregulation of both SPTLC1-3 and SPHK1/2 in response to MCPyV-sT transduction (**Figure 10B**).

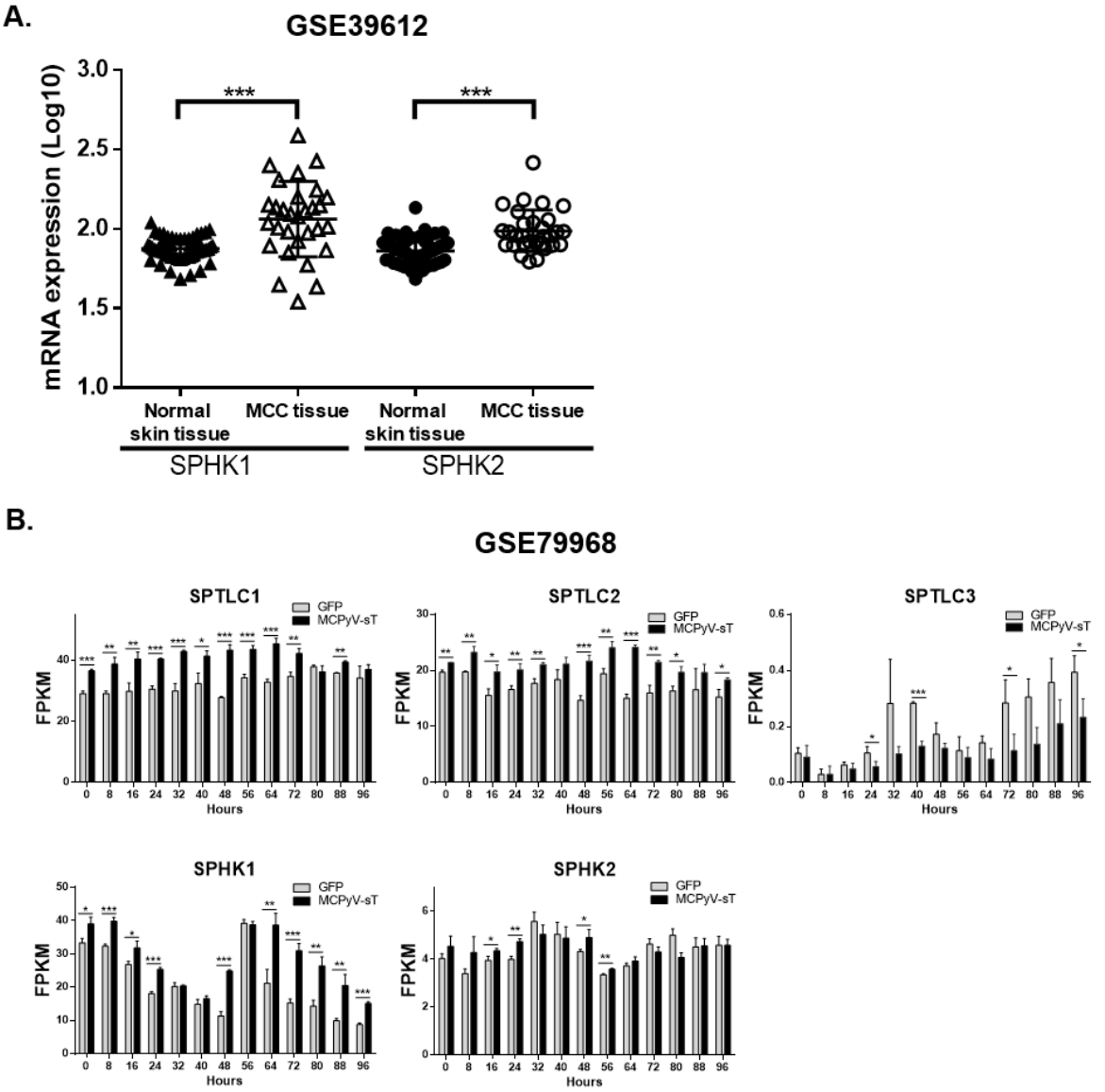

Figure 10: Retrieval and re-analysis of GEO datasets GSE39612 and GSE79968 show upregulation of SPHK1 and 2 in MCC tumor samples and upregulation of SPTLC1/2 and SPHK1/2 in MCPyV-sT expressing IMR90 cells.

The online meta gene-expression analysis tool ExAtlas (Sharov et al., 2015) was used to re-analyze the GSE39612 microarray data set (Harms et al., 2013). SPHK1/2 mRNA expressions were obtained and compared between normal skin (n=64) and MCC tissues (n=30). Mann-Whitney test was used to statistically evaluate the data (mean ±SD, *** $p \leq 0.001$). (**B**) GSE79968 RNA sequencing data (Berrios et al., 2016) were obtained from the GEO database. FPKM values of SPTLC1/2 and SPHK1/2 were retrieved for GFP or MCPyV-sT expressing IMR90 cells. Doxycycline was used to induce the expression of GFP or MCPyV-sT at different time points as shown. The FPKM values were compared between GFP vs. MCPyV-sT expressed IMR90 cell lines. Unpaired Student`s t-test was used for statistical analysis of the data (n=3, mean ±SD, *$p \leq 0.05$, ** $p \leq 0.01$, *** $p \leq 0.001$). The data shown above are from my published article (Bhat et al., 2018a) and reproduced here with permission from Elsevier.

4.5 Myriocin and SKI-II affect intracellular ceramide, sphingomyelin, and S1P homeostasis

Transcriptome analysis revealed that the $MCPyV^+$ MKL-1 and WaGa cell lines more closely resemble global MCC tumor samples in comparison to other MCC cell lines (Daily et al., 2015). Therefore, the two well-characterized $MCPyV^+$ MCC cell lines MKL-1 and WaGa were used for our in-vitro studies.

After verifying SPTLC1-3 and SK1/2 expression at mRNA level, SPTLC1-3 and SK1/2 were targeted by their respective pharmacological inhibitors myriocin and SKI-II. In order to determine the impact of myriocin and SKI-II on intracellular Cer, SM, and S1P homeostasis LC-MS analysis and S1P-ELISA were performed (**Figure 11** and **12**). LC-MS analysis revealed that the total Cer and SM content is approximately 1.3 to 1.5-fold higher in MKL-1 in comparison to WaGa (**Figure 11**). The total SM concentration is 10-fold higher in both cell lines when compared to the total Cer content (**Figure 11**). Myriocin treatment significantly decreased the total Cer content in MKL-1 but not in Waga cells when compared to the corresponding vehicle controls (**Figure 11A**). Total SM content was only affected in WaGa cells (**Figure 11D**). Conversely, SKI-II treatment significantly increased Cer concentration (**Figure 11E** and **11G**) and decreased SM content (**Figure 11F** and **11H**) in both the cell lines in comparison to vehicle (DMSO) treatment.

In comparison to DMSO, myriocin treatment significantly decreased pro-apoptotic Cer species C18:0, 20:0, 22:0, 24:0, 24:1 in MKL-1 (**Figure 12A**) and C20:0, 22:0, 24:0 in WaGa cells (**Figure 12D**). Further, all the SM species (SMC16:0, 18:1, 20:0, 20:1, 22:0, 22:1, 24:0, 24:1) were decreased in in MKL-1 and WaGa cells (**Figure 12B** and **12E**). In addition, myriocin reduced intracellular S1P levels in both MCC cell lines (**Figure 12C** and **12F**). In contrast, SKI-II treatment increased all Cer species except in C24:0, C24:1 in MKL-1 and C14:0 in WaGa (**Figure 12G** and **12J**). For sphingomyelins, SMC16:0, C24:0 and C24:1 was reduced in MKL-1 and SMC16:0, C20:1 species were reduced in WaGa cells (**Figure 12H** and **12K**). Moreover, S1P-ELISA showed a significant decrease in S1P level in both cell lines in response to SKI-II treatment (**Figure 12I** and **12L**).

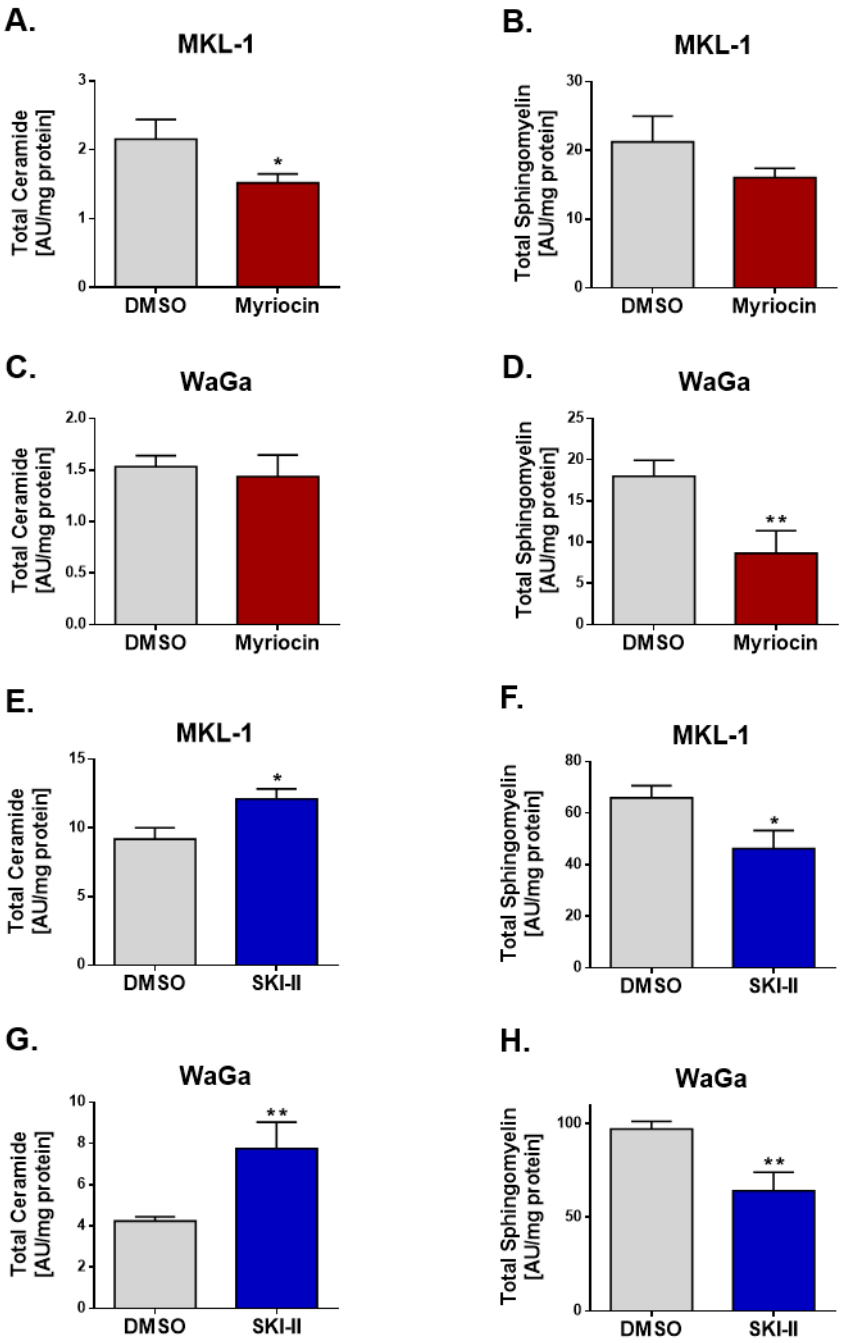

Figure 11: Total ceramide and sphingomyelin concentration were altered by myriocin and SKI-II treatment of MCC cell lines.

MKL-1 and WaGa cells were treated with either (**A, B, C,** and **D**) DMSO (vehicle, grey) and myriocin (15µM, red) or (**E, F, G,** and **H**) DMSO (0.1% v/v) and SKI-II (15µM, blue). The total Cer and total SM concentration were obtained by LC-MS analyses after 24 h of treatment. Statistical analysis was done between DMSO and inhibitor-treated samples using unpaired Student`s t-test (n=3, mean±SD, *p ≤ 0.05, **p ≤ 0.01). The data shown above are from my published article (Bhat et al., 2018a) and reproduced here with permission from Elsevier.

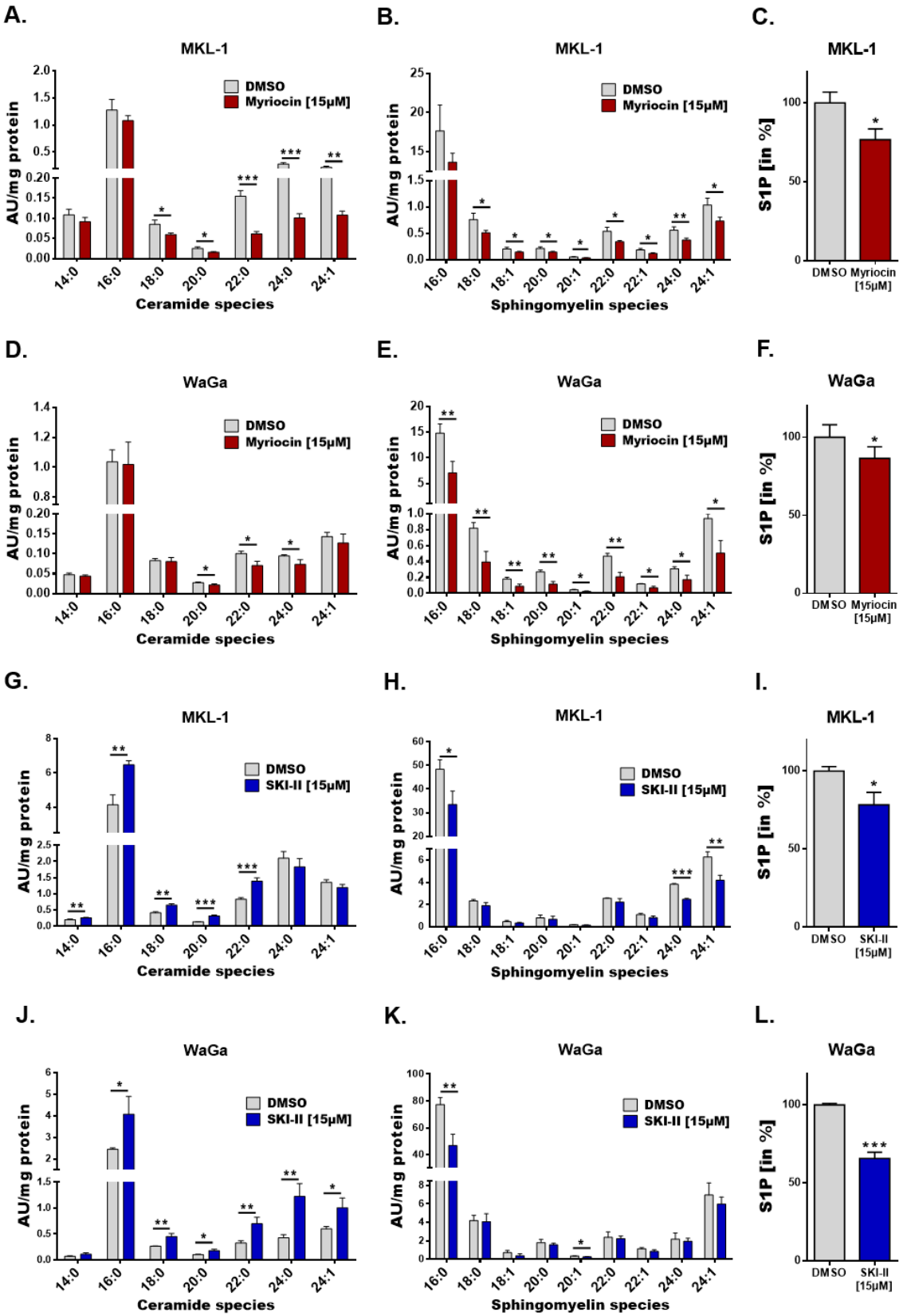

Figure 12: Myriocin and SKI-II impact ceramide, sphingomyelin and S1P content and composition in MCPyV$^+$ MCC cells.

(**Figure 12:** continued in the next page)

MKL-1 and WaGa MCC cells were treated with DMSO (vehicle, grey), myriocin (red) or SKI-II (blue; both 15 µM) in RPMI1640 media containing 0.5% FCS. After 24 h lipids were extracted, then separated on a C-18 UPLC-column, and Cer and SM species were identified by LC-MS. The data obtained were analyzed using Lipid Data Analyzer software. Ion intensities were then normalized to the ISTD and then to total cellular protein (arbitrary units (AU)/mg cell protein). S1P concentration was analyzed by S1P-ELISA.
(**A-C** and **D-F**) Cer, SM, S1P profiles of myriocin treated MKL-1 and WaGa cells. (**G-I** and **J-L**) Cer, SM, S1P profiles of SKI-II treated MKL-1 and WaGa cells. Statistical analysis was performed using unpaired Student`s t-test (n=3, mean ± SD, *p ≤ 0.05, **p ≤ 0.01, ***p ≤ 0.001 in comparison to DMSO). The data shown above are from my published article (Bhat et al., 2018a) and reproduced here with permission from Elsevier.

4.6 Myriocin and SKI-II abrogate proliferation, and extracellular S1P promote proliferation in MCC cells

4.6.1 SPTLC1-3 and SK1/2 inhibitors abrogate MCC cell viability

Having verified the impact of myriocin and SKI-II on SL homeostasis we wanted to analyze the inhibitors' impact on MCC cell viability. Upon myriocin treatment, we observed a dose-dependent decrease in MKL-1 and WaGa cell viability analyzed with the CellTiter-Glo 3D Cell viability assay (**Figure 13A** and **13B**). Myriocin (15 µM) induced a reduction of cell viability (MKL-1 and WaGa) by approximately 50 % (**Figure 13A** and **13B**). Notably, the inhibitor did not show any effect on NHDF viability (**Figure 13C**). Under control conditions, MKL-1 cells grow in irregular spheroids. The microscopic images of MKL-1 cells show that myriocin decreases the spheroid size and increases the disintegrated cell population when compared to DMSO or untreated cells (**Figure 13D**).

SKI-II was incubated with MKL-1 and WaGa MCC cells and, NHDF cells. SKI-II significantly decreased the cell viability in CellTiter-Glo 3D Cell viability assays in a dose-dependent manner in both MKL-1 and WaGa cells (**Figure 13E** and **13F**). MKL-1 and WaGa cell viability was reduced by more than 90% at SKI-II concentration of 15 µM (**Figure 13E** and **13F**), indicating the importance of SPHK function in MCC cell survival. On the other hand, the viability of NHDF cells was unaffected by SKI-II treatment (**Figure 13G**). The spheroid size was decreased, and cells were seen to be disintegrated in SKI-II-treated MKL-1 cells (**Figure 13H**).

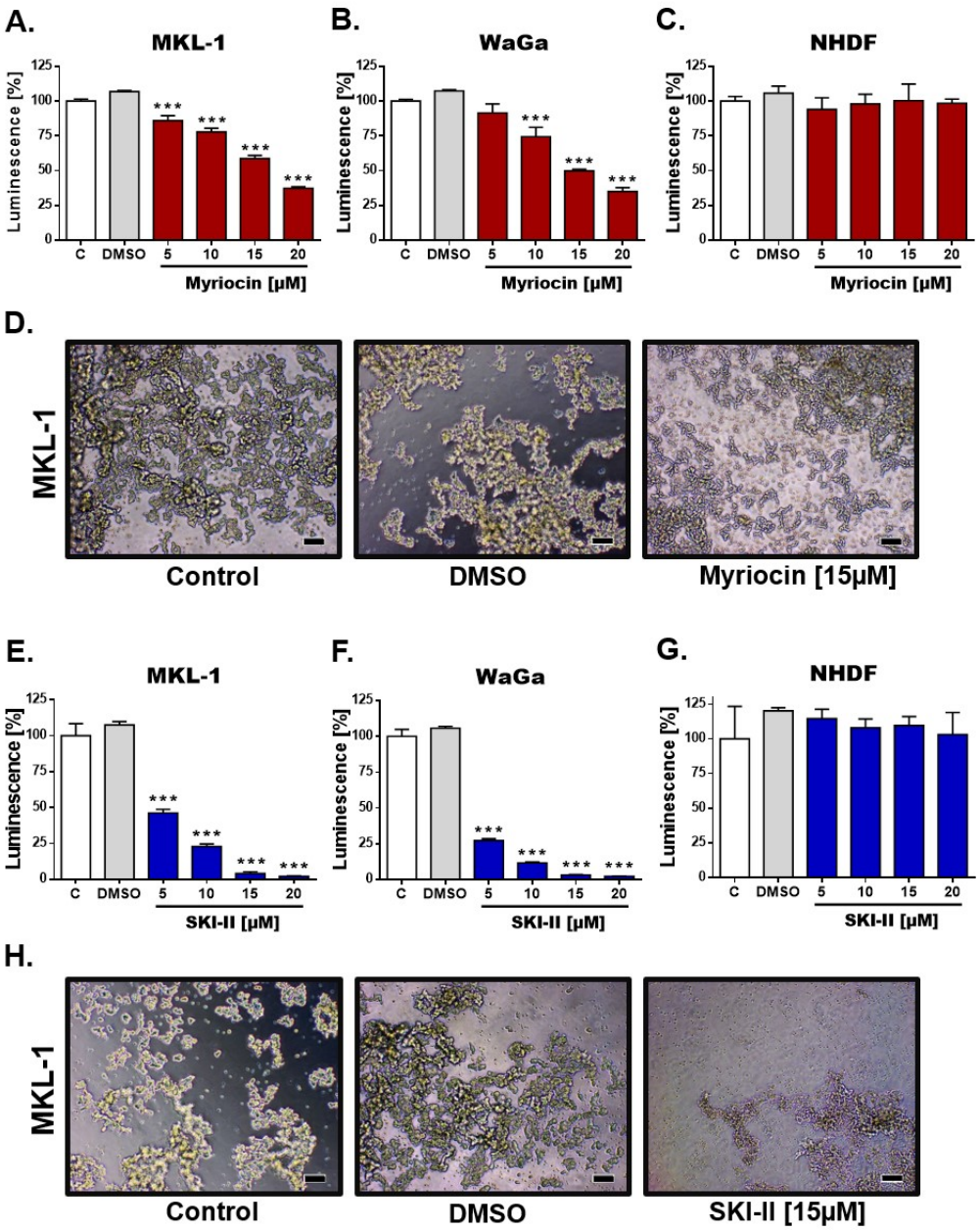

Figure 13: Pharmacological interference with SL homeostasis decreases cell viability of MCPyV$^+$ cells without affecting non-transformed NHDF cells.

MKL-1, WaGa, and non-transformed NHDF cells were treated with DMSO (vehicle, grey), myriocin (red) and SKI-II (blue) at the indicated concentrations. After 48 h of treatment cell viability was analyzed using CellTiter-Glo 3D Cell viability assay. (**A-C**) Cell viability of untreated ('C', control), vehicle (DMSO), and myriocin-treated MKL-1, WaGa and NHDF cells. (**D**) Light microscopic images of untreated, DMSO, and myriocin-treated MKL-1 cells (scale bar = 100µm). (**E-G**) Cell viability of untreated ('C', control), DMSO and SKI-II treated MKL-1, WaGa, and NHDF cells. (**H**) Light microscopic images of untreated, DMSO and SKI-II treated MKL-1 cells (scale bar = 100µm). Results were normalized to untreated controls (100 %) and represent mean±SD from triplicate experiments. Statistical analysis was done using one-way ANOVA with Bonferroni's multiple comparison tests. ***$p \leq 0.001$ compared to untreated controls.

The data shown above are from my published article (Bhat et al., 2018a) and reproduced here with permission from Elsevier.

4.6.2 Extracellular S1P promotes MCC cell proliferation

Extracellular S1P is known to regulate cell function via five specific receptors termed S1PR1-5 (Ogretmen, 2018). We first followed expression of *S1PR1-5* at mRNA level in 6 MCPyV$^+$ cell lines by qRT-PCR. All receptors were expressed in 6 MCPyV$^+$ cell lines (**Figure 14**). Relative to *S1PR1* mRNA, the highest expression was observed for *S1PR2* and/or *S1PR3* in all the cell lines (**Figure 14**).

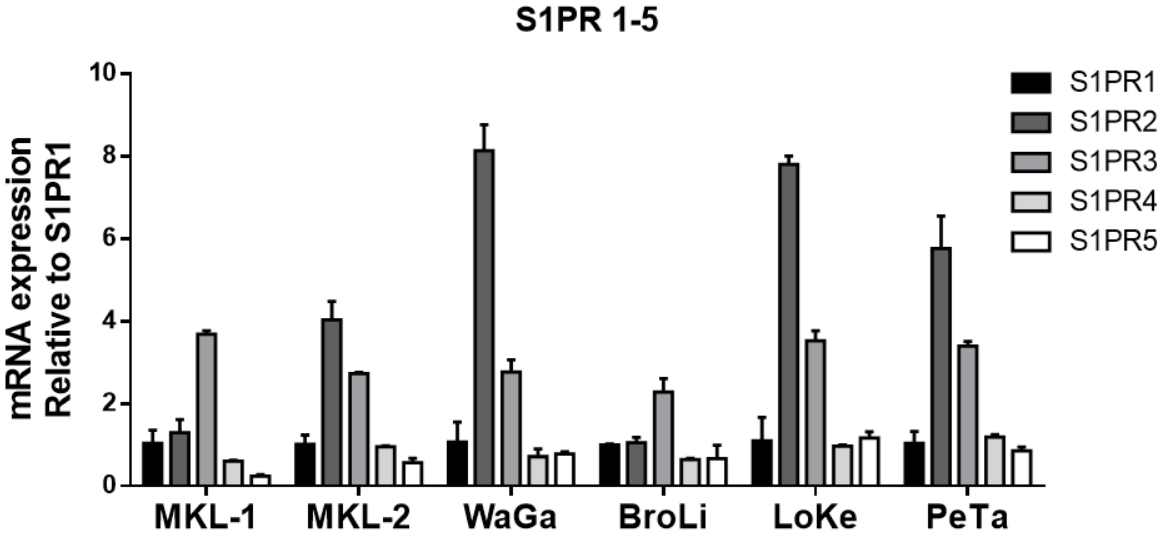

Figure 14: Characterizing the mRNA expression of S1P receptors in MCPyV$^+$ MCC cell lines.
S1P receptor expression (S1PR 1-5) of 6 MCPyV$^+$ cell lines was analyzed at mRNA level. The RNA was isolated, and cDNA was prepared. qRT-PCR was done to obtain the Ct-values. The $2^{-\Delta\Delta Ct}$ method was used to calculate RNA expression. The results were normalized to HPRT and are shown relative to S1PR1 (set to 1). The experiment was done in triplicates, mean±SD was plotted. The data shown above are from my published article (Bhat et al., 2018a) and reproduced here with permission from Elsevier.

Having shown expressions of all five S1P receptors, we then measured the impact of endogenously added S1P on MCC cell proliferation. We treated MKL-1 and WaGa cells with HDL (a major physiological carrier of S1P in the circulation; (Maceyka et al., 2012)) and S1P-enriched HDL (HDL-S1P). HDL-S1P showed significantly higher proliferation rates as compared to native HDL in both MCC cell lines (**Figure 15A**). To further confirm that the pro-proliferative effect is mediated by HDL-associated S1P (and not another constituent), we incubated HDL with S1P lyase. S1P lyase is an enzyme, which irreversibly degrades S1P to phosphoethanolamine and hexadecanol. After incubation, S1P lyase treated and untreated HDL was added to MKL-1 and WaGa cultures. Although S1P lyase treatment of HDL decreased cell proliferation the relevance of these findings is

currently unclear. This is because the addition of S1P lyase alone also induced a significant reduction in cell viability (**Figure 15B**).

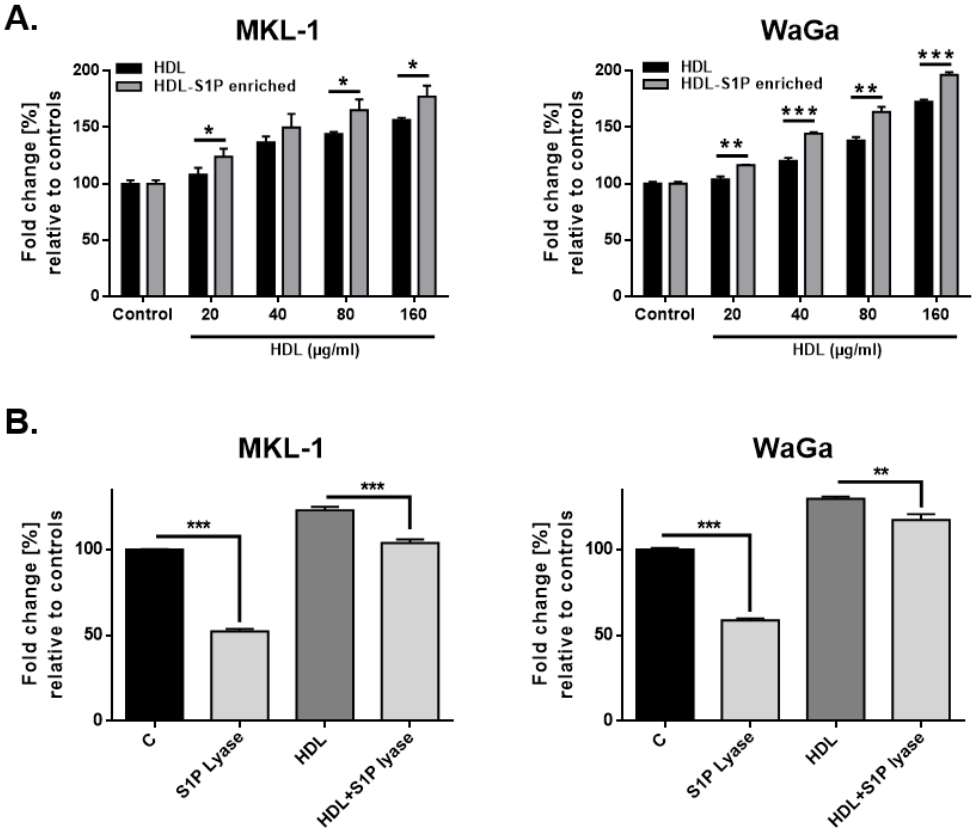

Figure 15: S1P-enriched HDL increases proliferation of MCPyV$^+$ MCC cells.

(**A**) MKL-1 and WaGa cells were treated with native HDL and S1P-enriched HDL as indicated. Post 48 h of the treatment cell viability was analyzed using CellTiter-Glo 3D Cell viability assay. Untreated cells were taken as controls. Statistical comparison was performed between cells cultured in the presence of native HDL or S1P-enriched HDL. (**B**) Cells were incubated in the presence of S1P lyase (3 µg), native HDL (20ug/ml), and S1P lyase treated HDL (20ug/ml). Cell viability was assessed using the CellTiter-Glo 3D Cell viability assay. S1P lyase treated cells were compared to control and native HDL compared to S1P lyase treated HDL. Statistical analysis was done using unpaired Student`s t-test (n=3, mean ±SD, * $p \leq 0.05$, **$p \leq 0.01$, ***$p \leq 0.001$). The data shown above are from my published article (Bhat et al., 2018a) and reproduced here with permission from Elsevier.

S1PR1 and 3 were reported to promote tumor cell survival and proliferation in several cancer entities (Ogretmen, 2018). To test this in MCC cells, we abrogated the activity of S1PR1 and 3 in MKL-1 and WaGa cells using its pharmacological inhibitor VPC23019. MKL-1 and WaGa cells were either left untreated or treated with VPC23019 (1 and 5 µM) for 1 hour and then both cell lines were incubated in the presence of HDL and HDL-S1P (**Figure 16A** and **16B**). Cell viability was measured using the CellTiter-Glo 3D Cell viability assay. HDL and HDL-S1P treated MCC cells did show an increase in

proliferation in comparison to untreated cells. However, the presence of VPC23019 was without effect on chemiluminescence indicating that S1PR1/3 are not responsible for signal transmission (**Figure 16A and 16B**).

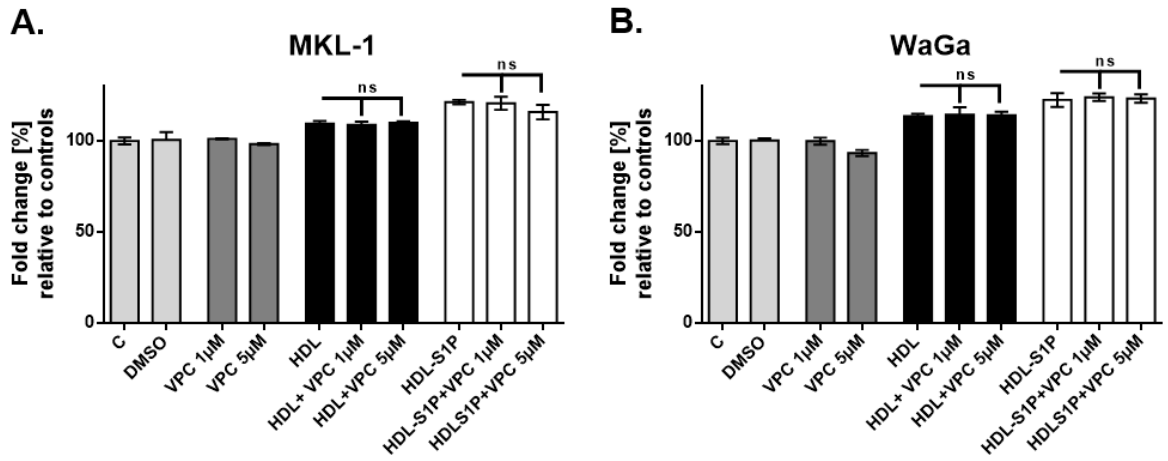

Figure 16: VPC23019, an S1P1/3 antagonist, does not affect proliferation induced by native HDL and S1P enriched HDL of MCPyV^{+} cells.

(**A** and **B**) MKL-1 and WaGa cells were either untreated ('C') or treated with DMSO (vehicle), VPC23019 (1 µM or 5 µM), HDL (20 µg/ml) and S1P enriched HDL (20 µg/ml) alone or in combination with VPC23019. After 48 h of treatment cell viability was assessed by CellTiter-Glo 3D Cell viability assay. The results were analyzed between native HDL and in combination with VPC23019 and S1P enriched HDL alone with a combination of VPC23019 using one-way ANOVA with Bonferroni's multiple comparison tests (ns., non-significant).

4.6.3 SPTLC1-3 and SK1/2 inhibitors induce apoptosis and/or necrosis in MCC cells

Since myriocin and SKI-II decreased cell viability of MKL-1 and WaGa MCC cells we aimed to determine whether the antagonists induce apoptosis or necrosis. MCC cells were incubated with DMSO, myriocin, or SKI-II for the indicated time periods and stained with Annexin V-FITC and propidium iodide. Stained samples were then analyzed using flow cytometry. These analyses revealed a decrease in viable cells and an increase in apoptotic and necrotic cells in response to myriocin and SKI-II treatment at 24 h (**Figure 17A** and **17B**), 36 h (**Figure 17C** and **17D**) and 48 h (**Figure 17E** and **17F**). Statistical analysis of the different cell populations (viable, apoptotic and necrotic) revealed a significant increase of apoptotic and necrotic cells at 15 µM myriocin and SKI-II treated MKL-1 (**Figure 18A** and **18B**) and WaGa cells (**Figure 19A** and **19B**). Forty-eight h post myriocin (15µM) incubation, MKL-1 cells show ≈ 25% cells in late apoptotic and ≈ 40% in necrotic stage and WaGa cells show ≈ 25% and ≈ 30% in late apoptotic and necrotic stage respectively. SKI-II treatment (48 h, 15 µM) resulted in ≈ 15% MKL-1 cells in late

apoptosis, and more than 80% cells were necrotic. In WaGa cells ≈ 20% and ≈ 75% were present as late apoptotic and necrotic cells respectively. Conversely, NHDF did not show an increase in apoptotic or necrotic cell counts in response to myriocin or SKI-II treatment (**Figure 17G** and **20**).

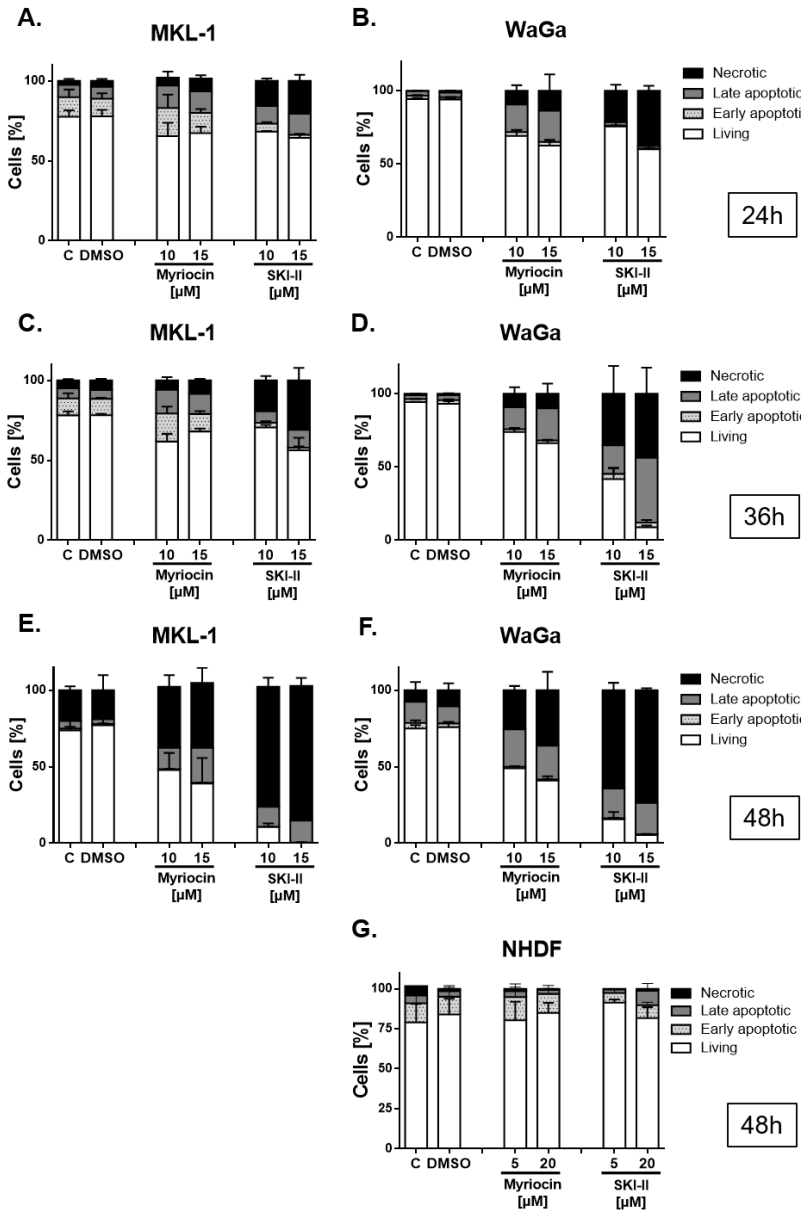

Figure 17: Myriocin and SKI-II treatment promote late apoptosis and necrosis in MKL-1 and WaGa cells.

MCC and NHDF cells were treated with myriocin and SKI-II for 24 h (**A-B**), 36 h (**C-D**), and 48 h (**E-G**) at the concentrations indicated. The cells were then harvested and stained with Annexin V-FITC and propidium iodide and analyzed by flow cytometry. The percentage of living, early apoptotic, late apoptotic, and necrotic cells is displayed in the bar graph. The experiment was performed in triplicates and results are shown as mean±sd. Representative scatter plots, and statistical evaluation of the different cell populations are shown in Figures 12,13 and 14. The data shown above are from my published article (Bhat et al., 2018a) and reproduced here with permission from Elsevier.

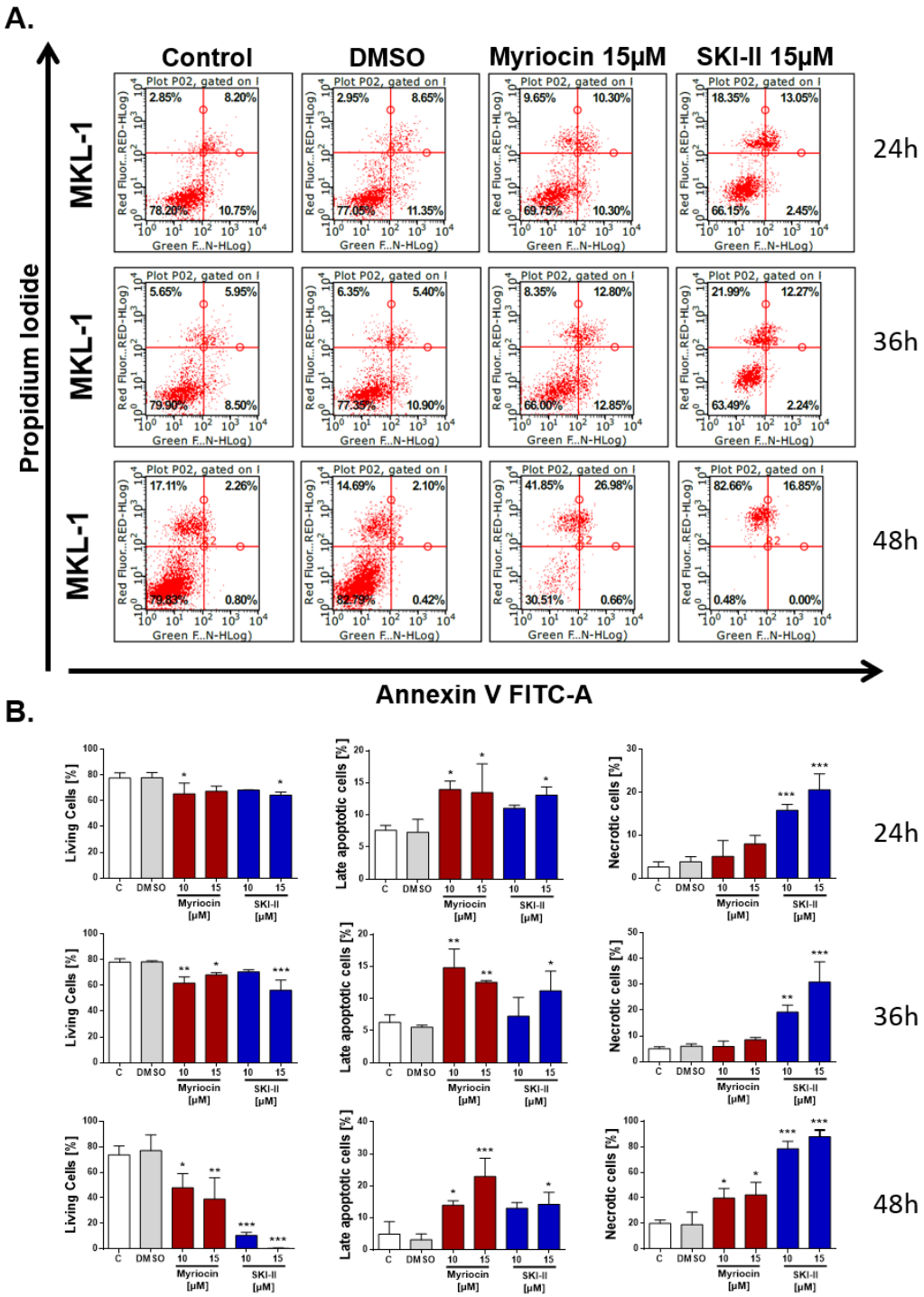

Figure 18: Myriocin and SKI-II treatment increase apoptosis and necrosis in MKL-1 cells.

(**A**) Scatter plots of annexin V-FITC (A) and propidium iodide (PI) stained untreated ('C'), DMSO, myriocin or SKI-II treated MKL-1 cells are shown after flow cytometry. In the scatter plots, the lower left quadrant represents living cells (A-/PI-). Cells present in the lower right quadrant signify early apoptotic (A+/PI-), those in the upper right quadrant show late apoptotic (A+/PI+) and the upper left necrotic cells (A-/PI+). (**B**) Bar graphs were plotted for a living, late apoptotic and necrotic cells separately. Mean±sd was plotted from the triplicate experiments, and statistical analysis was performed by comparing DMSO-treated to inhibitor-treated cells (one-way ANOVA, *p ≤ 0.05, **p ≤ 0.01, ***p ≤0.001). The data shown above are from my published article (Bhat et al., 2018a) and reproduced here with permission from Elsevier.

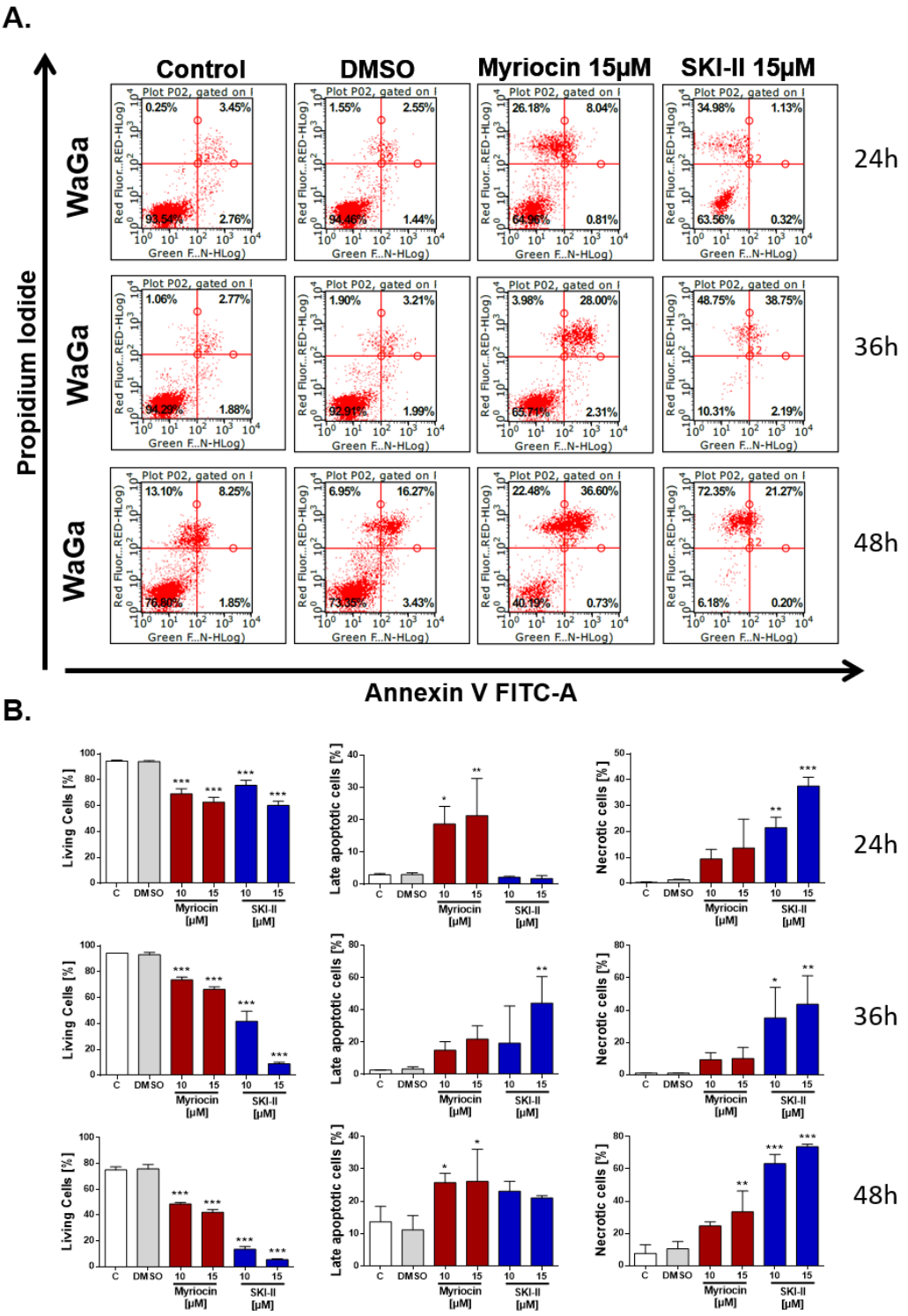

Figure 19: Myriocin and SKI-II treatment elevates apoptosis and necrosis in WaGa cells.

(**A**) Scatter plots of annexin V-FITC (A) and propidium iodide (PI) stained untreated ('C'), DMSO, myriocin or SKI-II treated WaGa cells are shown after flow cytometry. (**B**) Bar graphs were plotted for a living, late apoptotic and necrotic cells separately. Mean±sd was plotted from the triplicate experiments, and statistical analysis was performed by comparing DMSO-treated to inhibitor-treated cells (one-way ANOVA, *p ≤ 0.05, **p ≤ 0.01, ***p ≤0.001). The data shown above are from my published article (Bhat et al., 2018a) and reproduced here with permission from Elsevier.

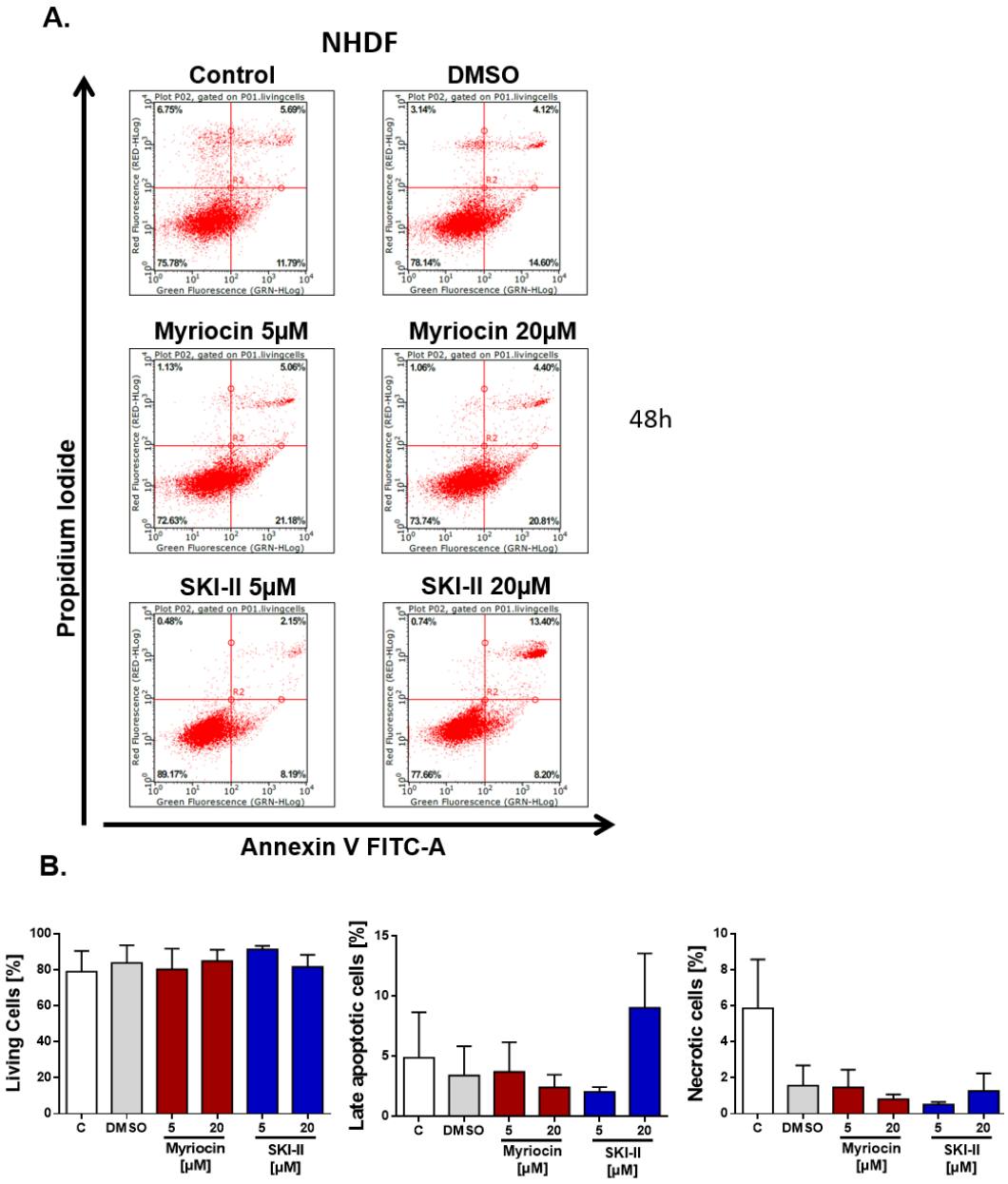

Figure 20: NHDF cell viability was not affected by myriocin and SKI-II treatment.

(**A**) Representative scattergrams of untreated control ('C'), DMSO and myriocin or SKI-II treated NHDF cells. (**B**) Bar graphs for untreated and treated cells were plotted separately for a living, late apoptotic and necrotic NHDF cells. Statistical analysis was performed by comparing inhibitor-treated to DMSO-treated cells (n=3, mean ± SD, one-way ANOVA, *p ≤ 0.05, **p ≤ 0.01, ***p ≤0.001). The data shown above are from my published article (Bhat et al., 2018a) and reproduced here with permission from Elsevier.

4.7 SPTLC1-3 and SK1/2 inhibitors induce caspase3 mediated apoptosis in MCC cell lines with a decrease in pAKT

Flow cytometry revealed an increase in apoptotic and necrotic MKL-1 and WaGa cells after treatment with myriocin and SKI-II. This prompted us to investigate the mechanism of apoptotic cell death induced by pharmacological inhibition of SL homeostasis. Western blot experiments revealed prominent expression of SPT and SK1/2 protein in MKL-1 and WaGa cells (**Figure 21A-D**). The treatment with myriocin did not alter the expression of SPT but induced pro-caspase3 and PARP cleavage in both cell lines (**Figure 21A** and **21B**). Further, SKI-II treatment did not affect the expression of SK1 but reduced the expression of SK2 and promoted the cleavage of caspase3 and PARP in both cell lines (**Figure 21C** and **21D**). Densitometric analysis of western blots revealed that myriocin and SKI-II induced significantly higher caspase3 and PARP activation in comparison to DMSO treated or untreated cells (**Figure 22** and **Figure 23**). The immunoblotting experiments showed that myriocin and SKI-II induced apoptotic pathway is mediated by active caspase3 and PARP in MKL-1 and WaGa MCC cells.

AKT is reported to be hyperphosphorylated in MCC cell lines and tumor tissues, and targeting the PI3K/AKT pathway with pharmacological inhibitors was shown to decrease cell viability (Lin et al., 2014, Hafner et al., 2012). Western blotting showed prominent expression of $pAKT^{S473}$ in both cell lines (**Figure 21A-D**). Treatment with myriocin decreased AKT phosphorylation without affecting pan-AKT (**Figure 21A** and **21B**). SKI-II treatment reduced expression of $pAKT^{S473}$ and showed a tendency towards a reduction in total AKT expression (**Figure 21C** and **21D**) in both cell lines. In line with this observation, densitometric analysis of western blots showed a significant reduction in $pAKT^{S473}$ without affecting total AKT in comparison to vehicle treatment (**Figure 22** and **Figure 23**).

Analysis of caspase3 activity (using the EnzChek Caspase-3 Assay) also showed caspase3 activation in myriocin and SKI-II treated MKL-1 and WaGa cells (**Figure 24A** and **24B**). Taken together, these data indicate that pharmacological interference with SPT and SK1/2 activity downregulates AKT activation and promotes apoptosis and induces a necrotic phenotype.

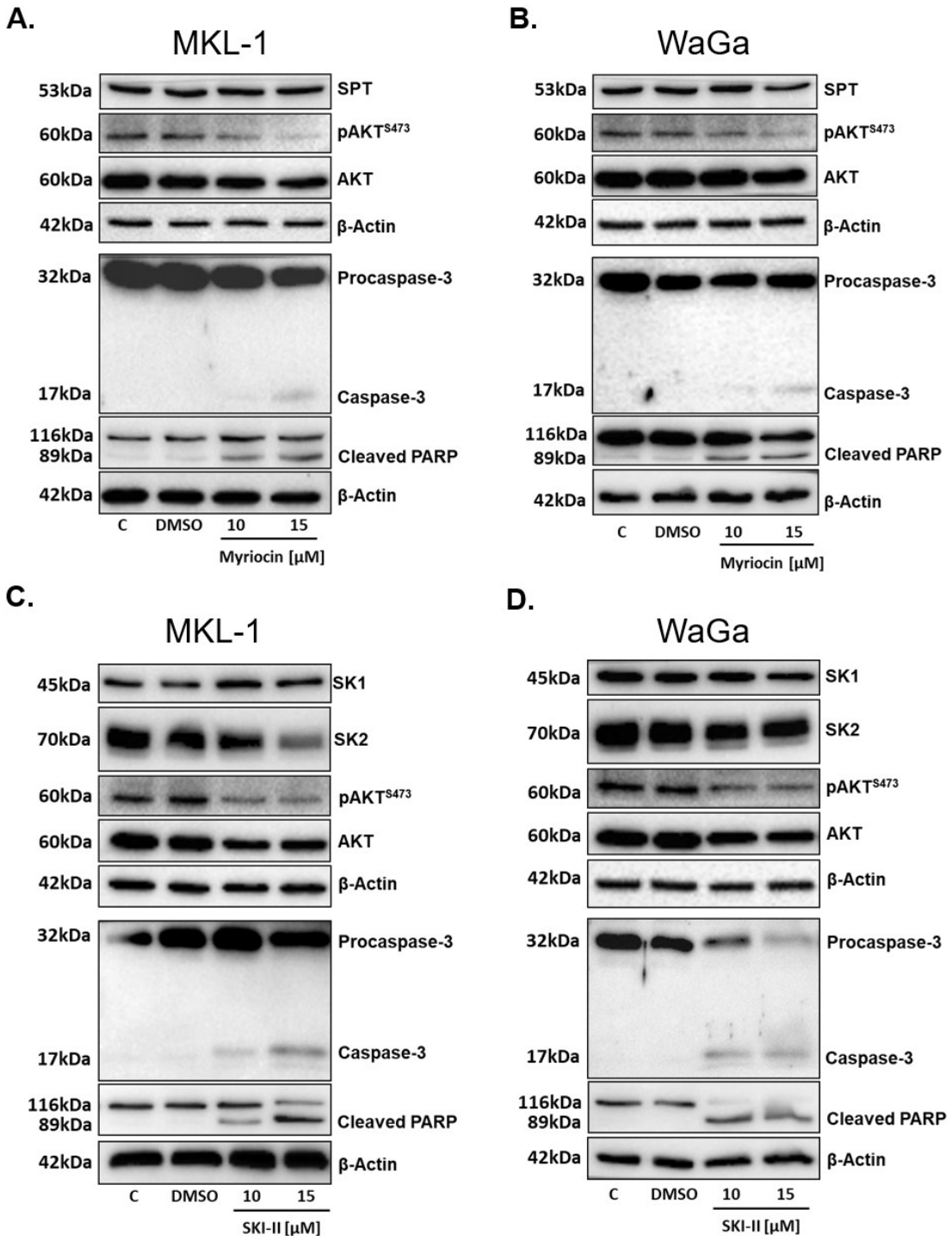

Figure 21: Myriocin and SKI-II treatment reduces AKT phosphorylation and promotes procaspase-3 and PARP cleavage.

MKL-1 and WaGa cells ($1x10^6$) were either untreated ('C') or treated with DMSO (vehicle) and myriocin (**A** and **B**) or SKI-II (**C** and **D**) at the indicated concentrations. Cells were then harvested for western blotting post 36 h of the treatment. Respective primary and secondary antibodies were used to detect SPTLC1, SK1, SK2, $pAKT^{S473}$, total AKT, as well as procaspase-3, and PARP and the respective cleavage products. β-Actin was used as a loading control. The data shown above are from my published article (Bhat et al., 2018a) and reproduced here with permission from Elsevier.

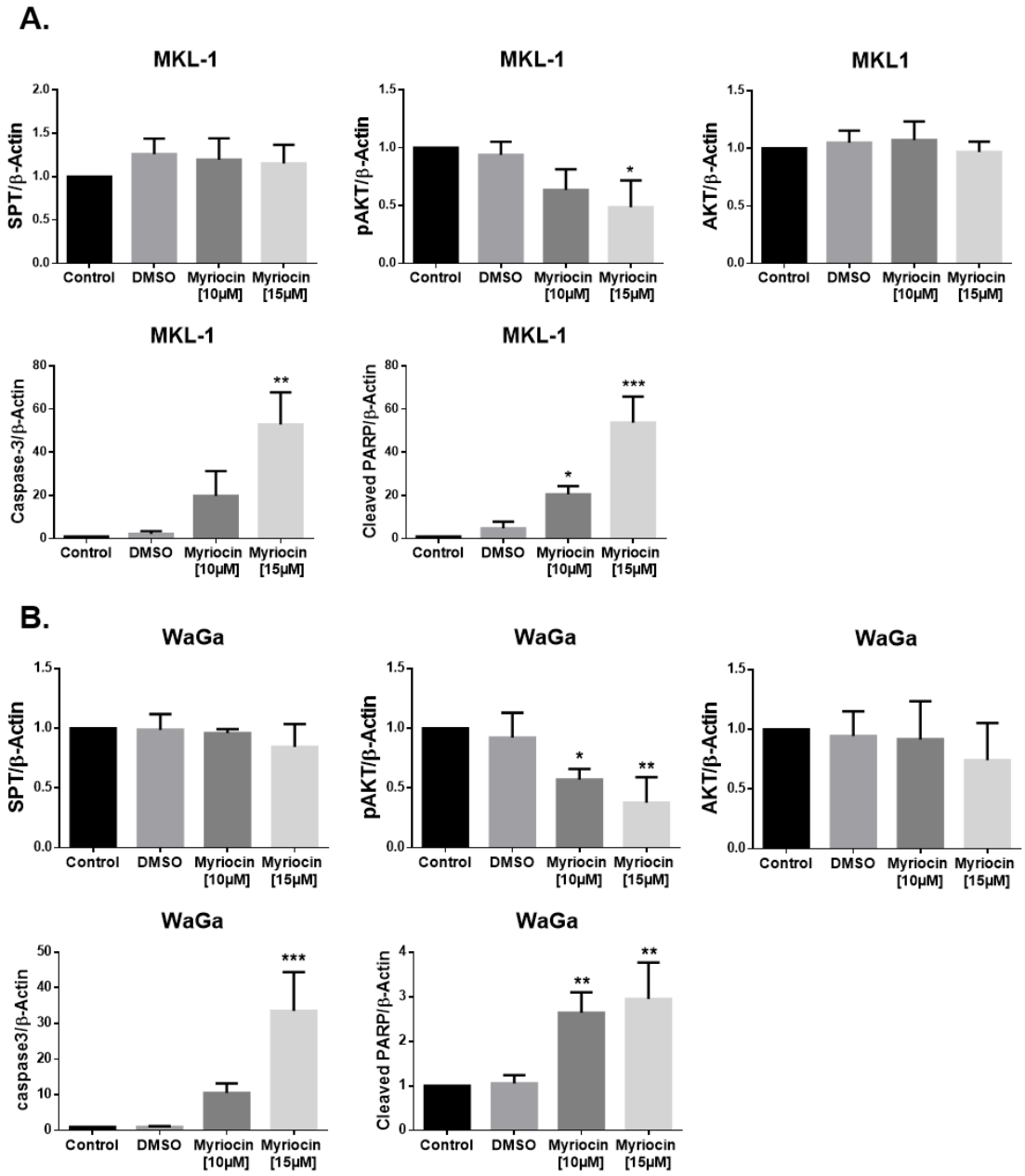

Figure 22: Densitometric immunoblot analysis of myriocin-treated cells

Western blots displayed in Figure 15 were subjected to densitometric evaluation for statistical analysis. MKL-1 (**A**) and WaGa (**B**) cells were treated with myriocin as indicated in Figure 15, and cellular lysates were immunoblotted for SPT, pAKT and total AKT, cleaved procaspase-3 and PARP. Densitometric analysis of three experiments was done using ImageJ software. Immunoreactive bands were normalized to β-actin and calculated relative to control. The bar graphs were plotted (mean ±SD) and analyzed using one-way ANOVA by comparing inhibitor-treated cells to control. (*$p \leq 0.05$, **$p \leq 0.01$, ***$p \leq 0.001$). The data shown above are from my published article (Bhat et al., 2018a) and reproduced here with permission from Elsevier.

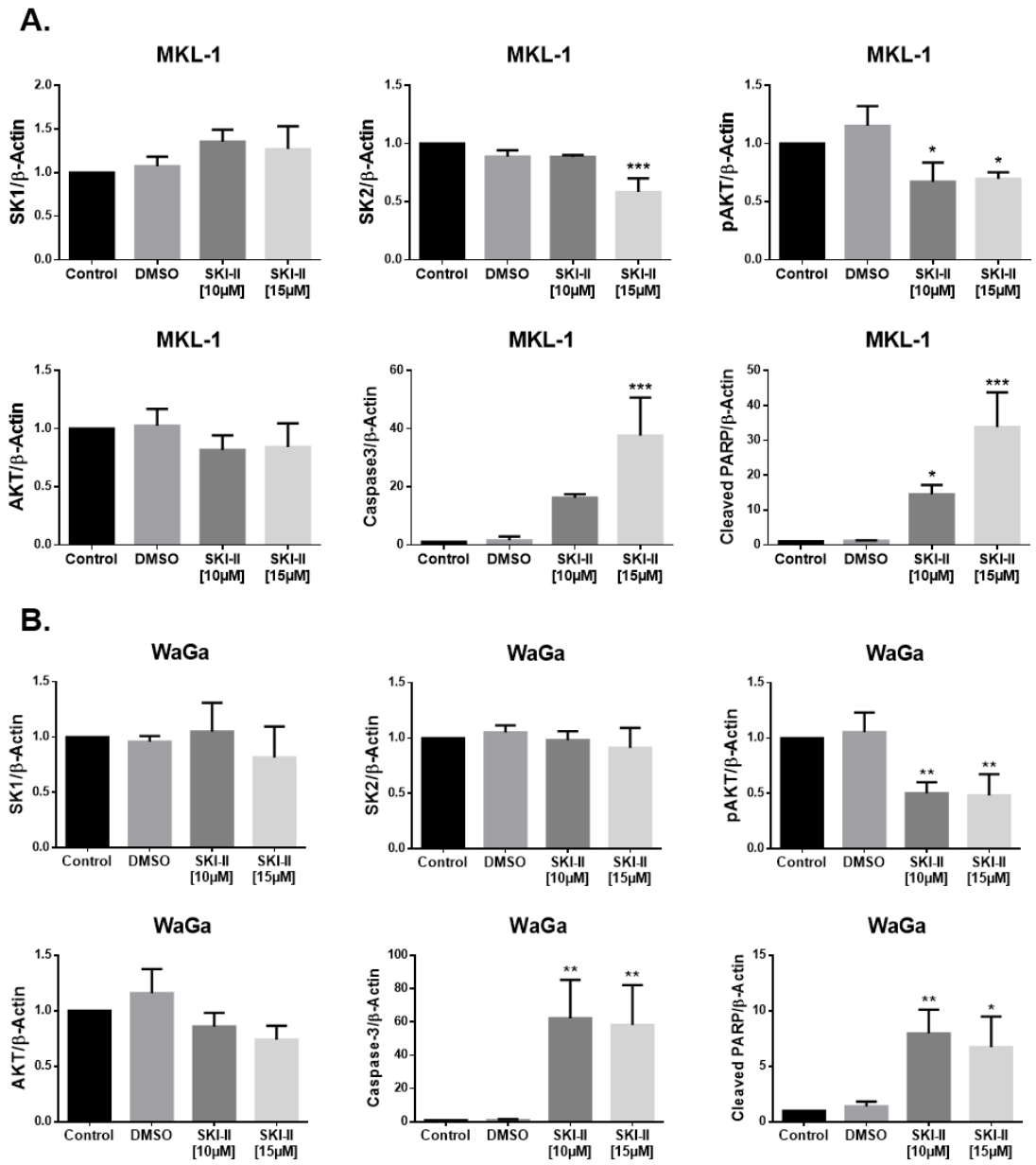

Figure 23: Densitometric immunoblot analysis of SKI-II-treated cells

Western blots displayed in Figure 15 were subjected to densitometric evaluation for statistical analysis. MKL-1 (**A**) and WaGa (**B**) cells were treated with SKI-II as indicated in Figure 15, and cellular lysates were immunoblotted for SK1/2, pAKT and total AKT, cleaved procaspase-3 and PARP. Densitometric analysis of three experiments was done using ImageJ software. Immunoreactive bands were normalized to β-actin and calculated relative to control. The bar graphs were plotted (mean ±SD) and analyzed using one-way ANOVA by comparing inhibitor-treated cells to control. (*$p \leq 0.05$, **$p \leq 0.01$, ***$p \leq 0.001$). The data shown above are from my published article (Bhat et al., 2018a) and reproduced here with permission from Elsevier.

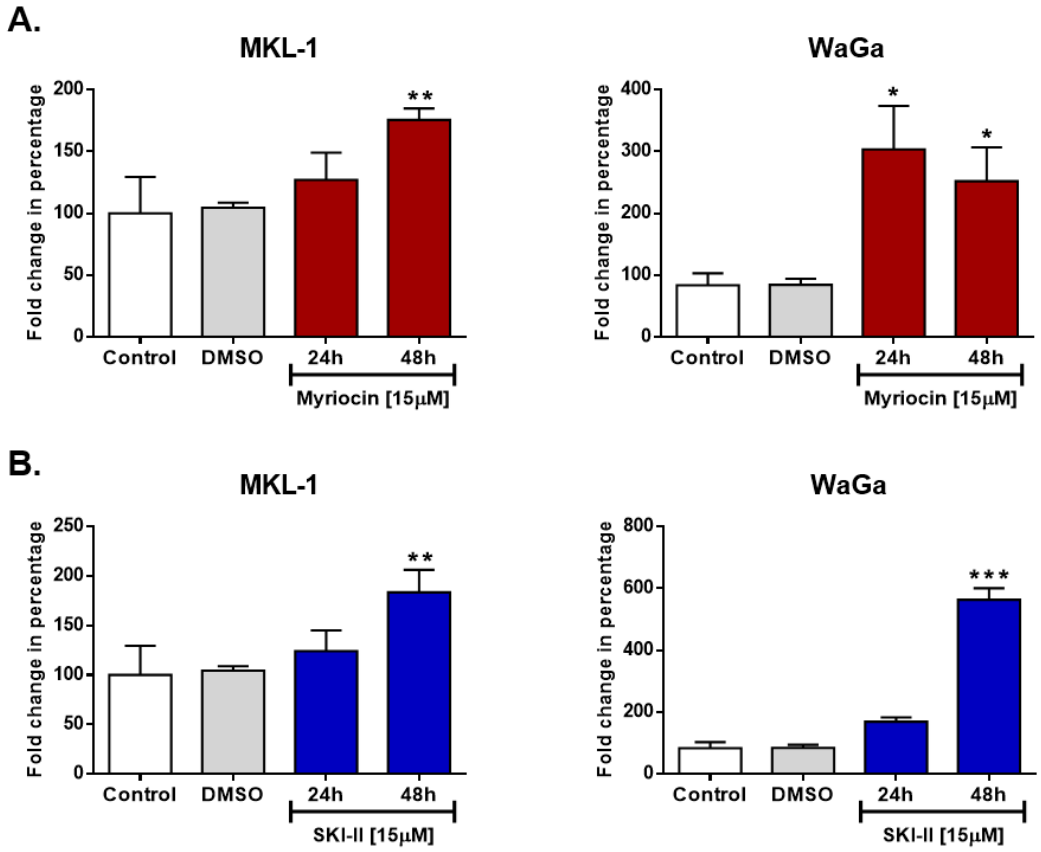

Figure 24: Myriocin and SKI-II treatment increase the enzymatic activity of caspase-3.
MKL-1 and WaGa cells were either left untreated (control) or treated with DMSO, myriocin (**A**) or SKI-II (**B**) for the indicated time period. Cells were then harvested, and caspase-3 activity was measured using a colorimetric kit. The results were plotted relative to untreated controls. Statistical analysis was done using unpaired t-test (n=3, mean ±SD, *p ≤ 0.05, **p ≤ 0.01, ***p≤ 0.001). The data shown above are from my published article (Bhat et al., 2018a) and reproduced here with permission from Elsevier.

4.8 Triciribine a pAKT inhibitor decreases MCC cell viability and induce apoptosis

Western blot experiments shown above revealed a significant decrease in the pAKT level and an increase in apoptosis. In order to identify the significance of AKT in MCC cell viability, MKL-1 and WaGa cells were targeted with triciribine (**Figure 25**), an inhibitor of AKT1-3 phosphorylation. CellTiter-Glo 3D Cell viability assay revealed that triciribine induced a dose-dependent decrease in MKL-1 and WaGa cell viability in comparison to vehicle control DMSO (**Figure 25A**). To verify the type of cell death, MKL-1 and WaGa cells were stained with Annexin V-FITC and propidium iodide and then flow cytometry was performed. FACS analysis showed that triciribine treatment significantly promotes apoptosis in both MCC cells in a dose-dependent manner with a decrease in viable cells

(**Figure 25B**). Triciribine impact at 15 µM was ≈4 fold higher in WaGa as compared to MKL-1 cells (**Figure 25B**).

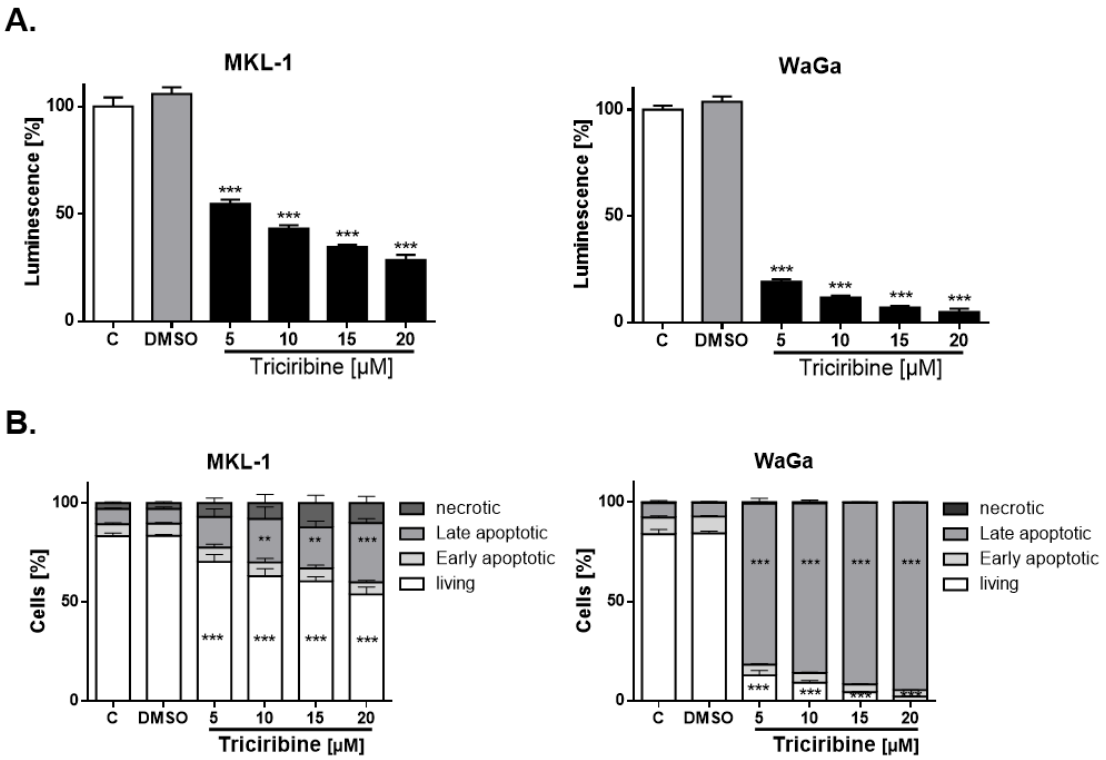

Figure 25: Triciribine treatment reduces cell viability and increases apoptosis in MKL-1 and WaGa cells.

Untreated ('C'), DMSO (vehicle), or triciribine-treated MKL-1 and WaGa cells were analyzed by (**A**) CellTiter-Glo 3D Cell viability assay and, (**B**) Annexin V-FITC and propidium iodide (PI) flow cytometry. Experiments were done in triplicates, and results are plotted as mean ± SD. Inhibitor-treated cells were compared to DMSO treated cells and analyzed by one-way ANOVA (*p≤ 0.05, **p ≤ 0.01, ***p ≤0.001). In flow cytometry, living, late apoptotic and necrotic cells were compared to the corresponding cell population of vehicle-treated cells. The data shown above are from my published article (Bhat et al., 2018a) and reproduced here with permission from Elsevier.

4.9 ABC294640 and FTY720 affect MCPyV$^+$ MCC cell proliferation

4.9.1 ABC294640 reduces cell viability and induces apoptosis in MCPyV$^+$ MCC cells

ABC294640 is a selective inhibitor of SK2 and currently in phase I/II clinical trial for myeloma (NCT02757326), cholangiocarcinoma (NCT03377179, NCT03414489), and hepatocellular carcinoma (NCT02939807). In order to study the efficacy of ABC294640 and its effect of SK2 inhibition in MCC in-vitro, we treated MKL-1 and WaGa cells with ABC294640 for 48 h (**Figure 26**). NHDF cells were taken as non-transformed controls and treated similarly as MCC cells (**Figure 26A**). After treatment, the CellTiter-Glo 3D

assay was performed to analyse cell viability. The results showed a dose-dependent decrease in viability in both MCC lines in comparison to vehicle treatment (**Figure 26A**). Viability was reduced by ≈50% when cells were treated with 30 µM ABC294640. In contrast, ABC294640 had less deleterious effects in NHDF cells (≈50% reduction observed at 50 µM) (**Figure 26A**).

Flow cytometry (Annexin V-FITC and propidium iodide staining) showed a significant decrease in viable cells and an increase in apoptotic and necrotic cells in ABC294640 treated MKL-1 and WaGa in comparison to DMSO (**Figure 26B**). At 40µM ABC294640 treatment, the percentage of apoptotic cells was higher in MKL-1 (≈70%) in comparison to WaGa which showed (**Figure 26B**) a surprisingly high number of necrotic cells (≈60%).

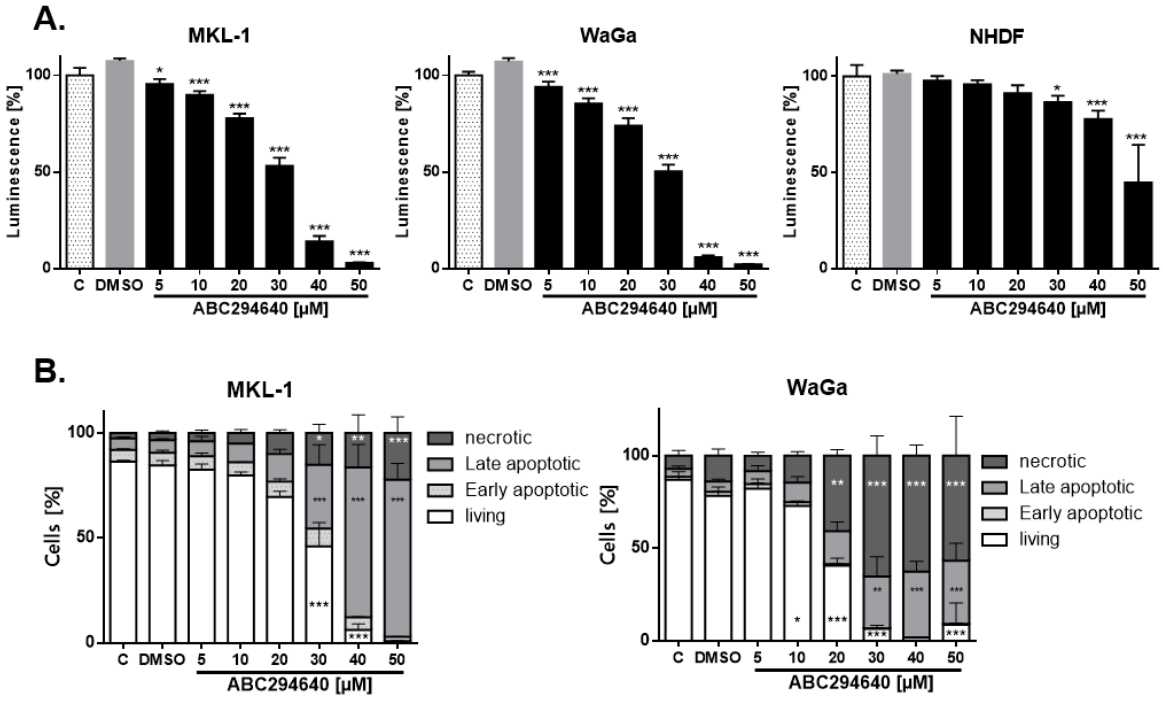

Figure 26: ABC294640 treatment reduces cell viability and promotes apoptosis and necrosis in MKL-1 and WaGa cells.

(**A**) MKL-1, WaGa, and non-transformed NHDF cells were left untreated ('C') or were treated with DMSO and ABC294640 at the indicated concentrations. After 48 h of treatment cell viability of MKL-1, WaGa and NHDF were determined with the CellTiter-Glo 3D assay. (**B**) Cells (untreated, 'C'; vehicle; DMSO; ABC294640-treated) were stained with Annexin and propidium iodide after 48 h and examined by flow cytometry (n=3, mean ± SD). Results were analyzed using one-way ANOVA by comparing inhibitor-treated to DMSO treated cells (living, late apoptotic and necrotic cells; *p ≤ 0.05, **p ≤ 0.01, ***p ≤0.001; compared to the corresponding cell population in vehicle-treated cells). The data shown above are from my published article (Bhat et al., 2018a) and reproduced here with permission from Elsevier.

4.9.2 FTY720 reduce cell viability and induce apoptosis in MCPyV$^+$ MCC cells

FTY720 (Fingolimod) is an FDA approved drug against multiple sclerosis (Kunkel et al., 2013). In glioma, it has completed a Phase I (NCT02490930) study, but the results of the trial have not yet been reported. In-vitro and in-vivo studies in several cancer entities reported that FTY720 decrease SK1 and S1PR1 expression along with cell proliferation and migration (Kunkel et al., 2013).

MKL-1 and WaGa cells were treated with FTY720 (dissolved in H_2O) for 24 h to identify the effect on MCC cell viability in-vitro (**Figure 27**). FTY720-treatment of MKL-1 and WaGa cells showed a significant decrease in cell viability (**Figure 27A**). At 5µM, FTY720 induced a rapid decrease in cell viability (≈90%) an effect observed in both cell lines (**Figure 27A**).

Flow cytometry of FTY720 treated and Annexin V-FITC and propidium iodide stained MKL-1 and WaGa cells revealed a significant decrease in viable cells and an increase in apoptotic and necrotic cell populations in comparison to untreated conditions (**Figure 27B**). However, FTY720 also severely impacted the number of viable NHDF and we observed a significant increase in apoptotic and necrotic cells in comparison to untreated cells (**Figure 27B**).

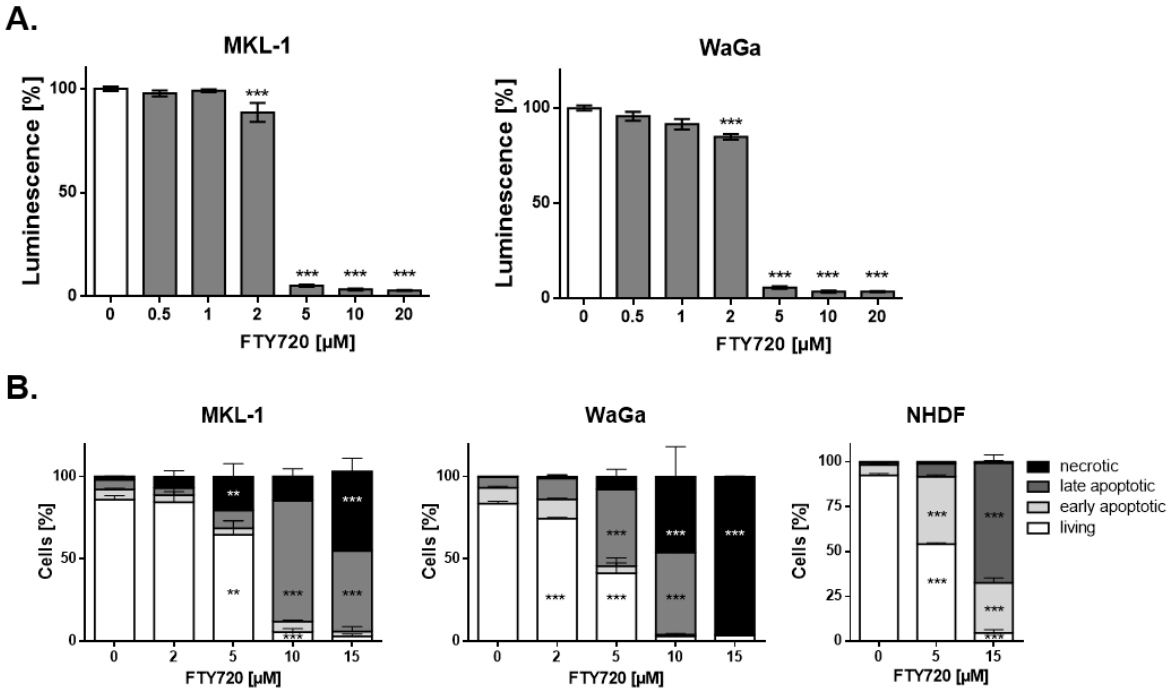

Figure 27: FTY720 affects cell viability and promotes apoptosis in MCPyV$^+$ cells.

(Figure 27: continued in the next page)

MKL-1, WaGa, and NHDF cells were untreated or treated with FTY720 with an indicated concentration above. Post 24 h, cell viability was assessed by (**A**) CellTiter-Glo 3D assay and (**B**) flow cytometry. Results were analyzed using one-way ANOVA (n=3, mean ± SD) by comparing inhibitor-treated to untreated cells (living, late apoptotic and necrotic cells; n=3, *p ≤ 0.05, **p ≤ 0.01, ***p ≤0.001; compared to the corresponding cell population in untreated cells).

4.10 MCC tumor chicken chorioallantoic membrane model

The chorioallantoic membrane (CAM) model is an attractive alternative to animal models to study tumor growth, proliferation, and metastasis as well as drug target effects (Bhat et al., 2018b). During my thesis, we developed an MCC tumor xenograft CAM model (MCC-CAM) and characterized this model in terms of MKL-1 and WaGa cell growth, angiogenesis, and proliferation (Bhat et al., 2018b).

A graphical summary of the general workflow of MCC-CAM is displayed in **Figure 28**. Three days post-fertilization the eggs were cracked and allowed the embryo to grow, at day 10 cancer cells were transplanted onto the CAM to induce tumor growth. Usually, the embryo is allowed to grow until day 17 (**Figure 28**).

Apart from MKL-1 and WaGa one more $MCPyV^+$ MCC cell line PeTa was used in MCC-CAM development experiment. MKL-1 (top panel), PeTa (middle panel) and WaGa (lower panel) cells formed solid tumors by day 15 of the embryo (**Figure 29A**). The development of the tumor xenografts was monitored on each day by photo documentation. There was a steady progression in tumor nodules, and a well-defined tumor vasculature was observed (**Figure 29A** and **Figure 30A-C**). On day 15 of the area of the tumor was calculated by Image J software (Bhat et al., 2018b). The macroscopic blood vessels surrounding the MCC xenograft were counted manually as described (Ribatti et al., 2006). We did not observe any significant differences between MKL-1, PeTa and WaGa xenografts concerning tumor area or a number of supplying blood vessels (**Figure 29B** and **29C**).

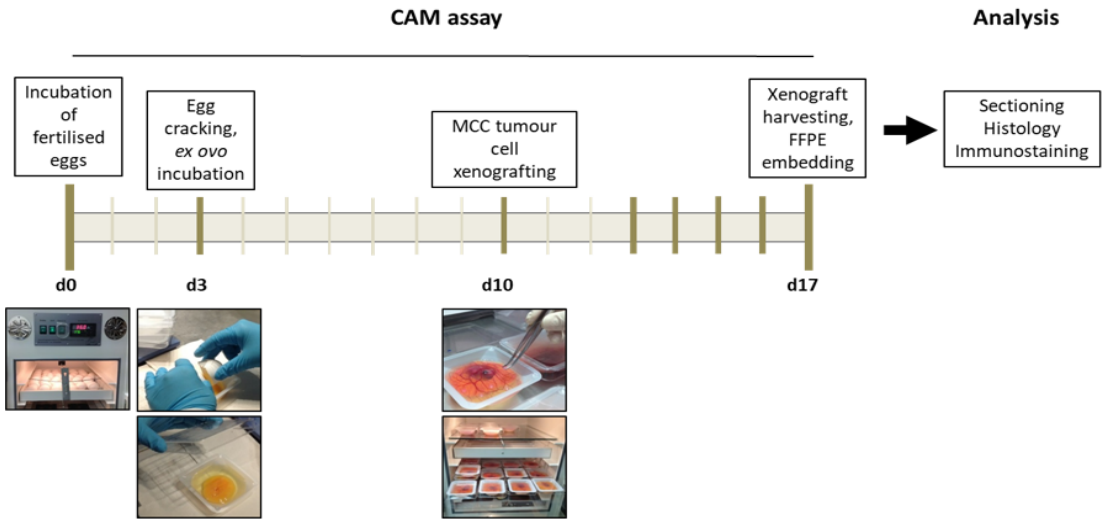

Figure 28: Schematic workflow of ex-ovo MCC -CAM establishment

Fertilized eggs were incubated for 3 days at 37^0 C; the eggshells were then cracked and incubated for 7 more days. MCC cells were applied on the CAM as shown above and incubated for 3-7 days. The CAM with the attached grafts was excised, followed by FFPE-tissue embedding and sectioning. The data shown above are from my published article Bhat KV et al. (Bhat et al., 2018b) and reproduced here with permission from Wiley publications.

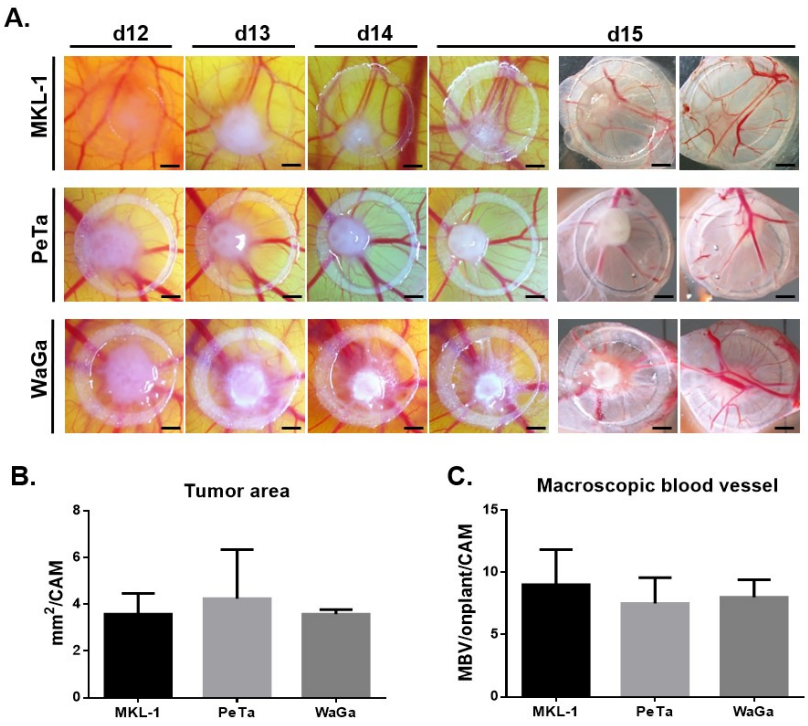

Figure 29: The CAM supports the growth of vascularized, three-dimensional MCC xenografts.

(**A**) MKL-1, PeTa (middle panel) and WaGa cells (10^6 cells/onplant) were monitored for 5 days upon engraftment. (scale bar = 1 mm). (**B**) Image J software was used to measure tumor area of xenografts. (**C**) Macroscopic blood vessels (MBV) were counted manually to measure angiogenesis. Results were plotted as mean±SD (N=6 tumors). One-way ANOVA was used for statistical analysis. The data shown above are from my published article (Bhat et al., 2018b) and reproduced here with permission from Wiley publications.

After photo documentation on day 15 of the CAM the MCC tumor xenografts were excised, fixed, paraffin embedded and stained with HE. The HE-stained samples showed robust interaction of MKL-1, PeTa and WaGa cells with the CAM mesenchyme and disruption of CAM epithelium by invading MCC tumor cells (**Figure 30D-F**). Histologically, the CAM tumor cell patterns were similar to that of MCC cells with chain-like or grouped small round cells having marginal cytoplasm and round nuclei (**Figure 30G-I**).

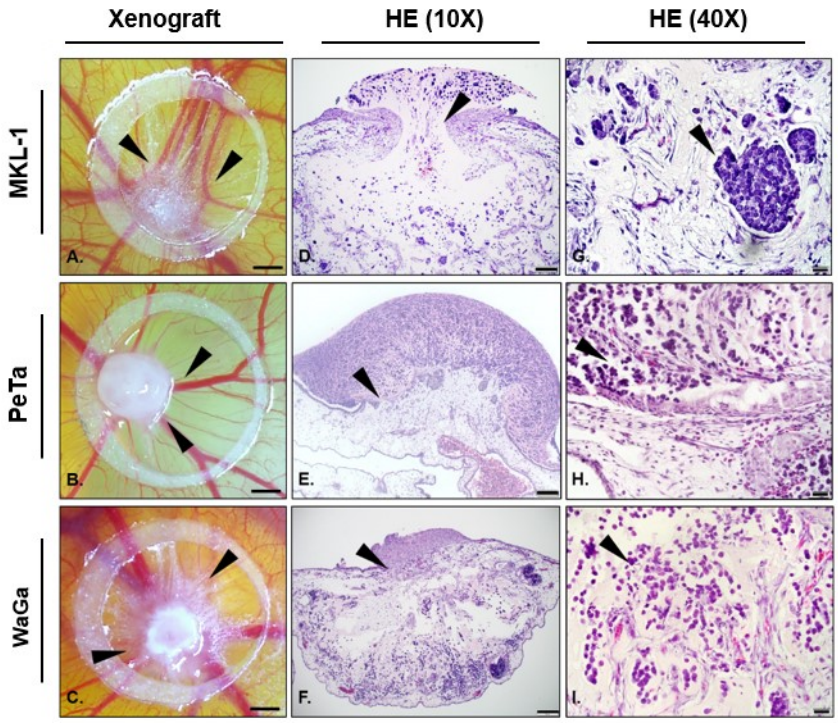

Figure 30: Morphological and histological evaluation of grafted MCC tumors on the CAM.
Solid tumors established with MKL-1 (**A**), PeTa (**B**) and WaGa (**C**) cells were seen upon 5 days of transplantation on the CAM surface, avian vessels developed radially towards onplants (indicated in arrows, scale bar = 1 mm). HE stained sections of MKL-1 (**D**), PeTa (**E**) and WaGa (**F**) xenograft showing tumor cell outgrowth from the primary onplant site into the surrounding of CAM tissue by disrupting the CAM upper epithelium (arrows, 10x Magnification, scale bar = 100 µm). MCC tumors are detected in the nest- or strand-like morphologies depending on tumor-initiating cells MKL-1 (**G**), PeTa (**H**), WaGa (**I**) MCC cells in the xenograft. (40x magnification, scale bar = 20 µm). The data shown above are from my published article (Bhat et al., 2018b) and reproduced here with permission from Wiley publications.

Furthermore, immunohistochemical analysis of MKL-1, PeTa, and WaGa xenografts confirmed the presence of cytokeratin 20 (**Figure 31A-C**) and MCPyV-LT antigen (**Figure 31D-F**). Ki-67 staining showed the presence of actively proliferating cells in the xenograft (**Figure 31G-I**).

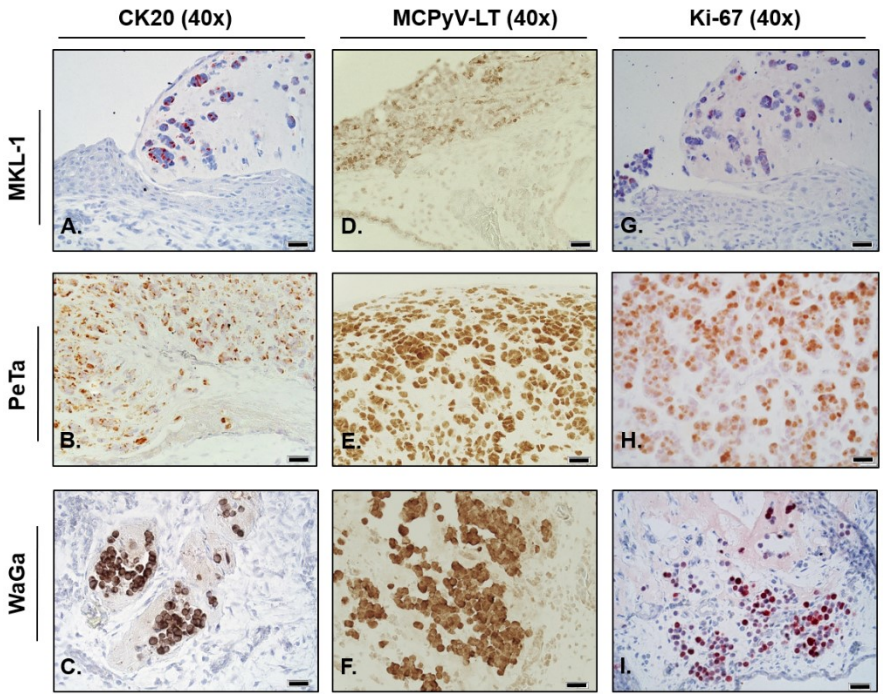

Figure 31: Immunohistochemical characterization of MCC xenografts.

(**A-C**) MKL-1, PeTa, and WaGa MCC xenografts were stained with antibodies specific to cytokeratin 20 and (**D-F**) MCPyV-LT. (**G-I**) Sections are showing proliferation marker Ki-67. (40x magnification, bars equal to 20 µm). The data shown above are from my published article (Bhat et al., 2018b) and reproduced here with permission from Wiley publications.

4.11 Myriocin and SKI-II abrogates tumor cell growth and proliferation in MCC-CAM ex-ovo tumor model

To study the effect of myriocin and SKI-II the MKL-1 and WaGa MCC-CAM model was used. There was a solid growth of MCC tumor within the CAM with a well-defined avian vasculature developed towards the tumor (**Figure 32A** and **32C**). Treatment with myriocin and SKI-II effectively inhibited MKL-1 xenograft size by ≈30% and ≈40% respectively in comparison to DMSO treated in CAM (**Figure 32A**). In WaGa-CAM the tumor size was reduced by ≈45% in response to myriocin and SKI-II treatment (**Figure 32C**).

The DMSO and inhibitor-treated tumors were excised, formalin fixed, paraffin embedded and then sectioned and subjected to HE staining. Immunohistochemistry was done to identify the tumor by staining CK20. Proliferating tumor cells were identified by Ki-67 staining. HE staining showed a robust interaction between MCC xenografts and the CAM which was partially ruptured by invading tumor cells that were incubated with the vehicle.

This was not less prominent in myriocin, and SKI-II treated tumors (**Figure 32B** and **32D**). CK20 and Ki-67 staining were lower in inhibitor-treated tumors in comparison to DMSO treatment (**Figure 32B** and **32D**). The Ki-67 index, a measure for tumor cell proliferation, was calculated with ImageJ. Statistical analysis of Ki-67 index showed a ≈50% reduction in myriocin-treated, and ≈40% reduction in SKI-II treated MKL-1 tumors in comparison to DMSO (**Figure 32B**). In WaGa xenografts, myriocin or SKI-II treatment reduced the Ki-67 index by ≈43% and ≈50% (**Figure 32D**).

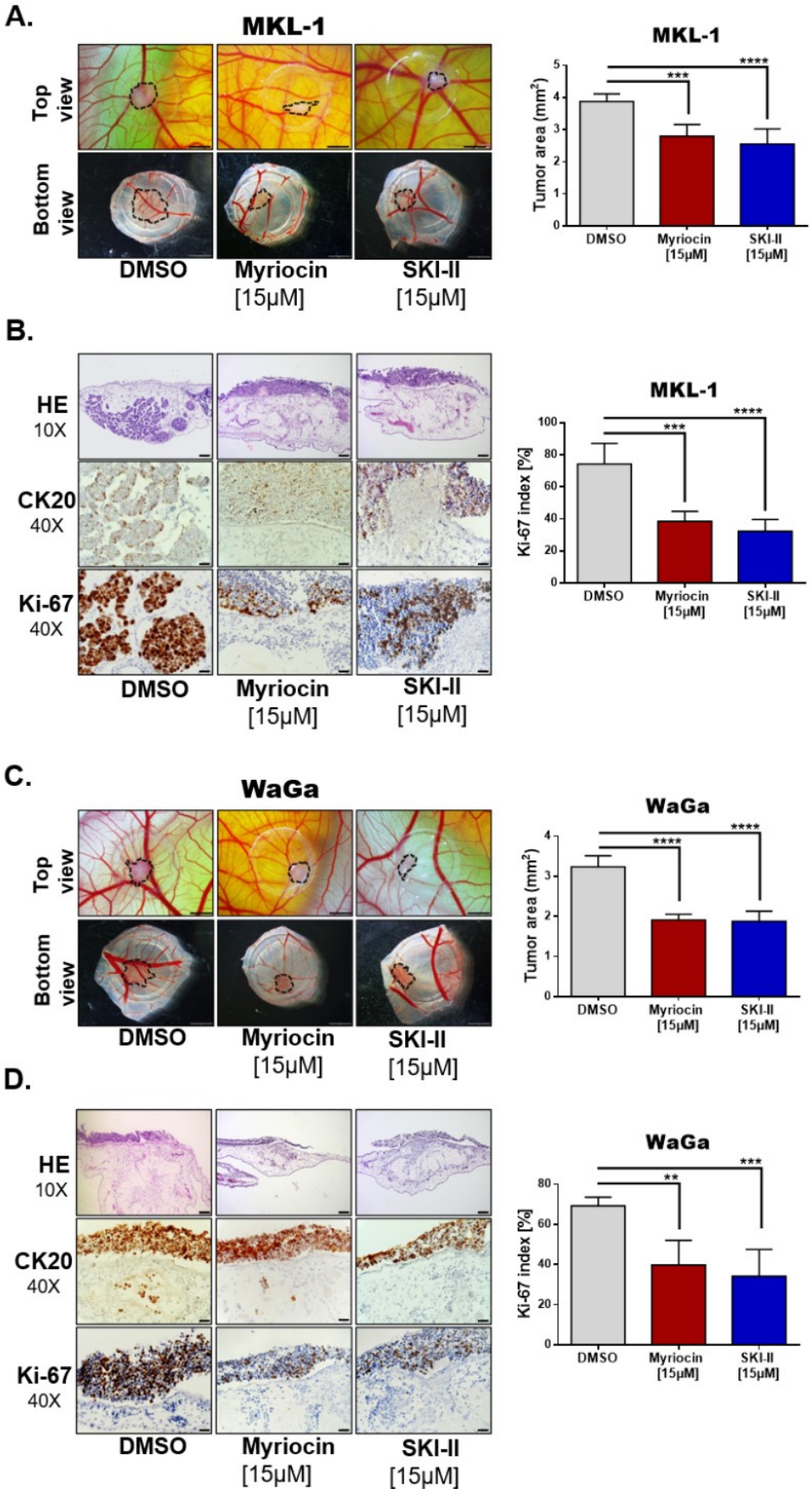

Figure 32: Myriocin and SKI-II inhibit tumor growth and proliferation in an MCC-CAM tumor model.

(Figure 32: continued in the next page)

10^6 cells/onplant in 1:3 mixture with Matrigel were applied within silicone rings placed on vascular branches of the CAM. The day after inhibitor treatment was started and continued every 24 h.

Images depicted (top and bottom view) of DMSO-, myriocin-, or SKI-II-treated (**A**) MKL-1 and (**C**) WaGa tumors formed on the CAM (Scale bar = 2mm). The tumor area (as indicated by broken lines) was calculated using ImageJ software (n = 5-6 tumors each) and is presented in the bar graph in the right panel.

Immunohistochemical analysis of (**B**) MKL-1 and (**D**) WaGa MCC-CAM tumors post-treatment with DMSO, myriocin or SKI-II. The tumor sections were stained with hematoxylin and eosin (HE, 10X magnification), cytokeratin 20 (CK20, 40X magnification) and Ki-67 proliferation marker (Ki-67, 40X magnification) as represented in the image (Scale bar = 100μm). Area of Ki-67 positive cells was calculated from 3 different tumor hotspots using ImageJ (mean ±SD, n=5 tumors each). Statistical analysis was performed using one-way ANOVA with Bonferroni's multiple comparison tests (**$p \leq 0.01$, ***$p \leq 0.001$). n = 5-6. The data shown above are from my published article (Bhat et al., 2018a) and reproduced here with permission from Elsevier.

5. Discussion

Part of the discussion section may resemble discussion section from my PhD published work (Bhat et al., 2018a).

Bioactive SLs have emerged as extremely potent regulators of several if not most of the cancer hallmarks including apoptosis/survival, tumorigenesis, tumor cell growth, proliferation, migration, metastasis, and resistance to chemotherapy and radiotherapy (Sedic et al., 2019, Ogretmen, 2018, Hannun and Obeid, 2018). S1P and SM promote tumor cell proliferation, survival, migration, and invasion whereas Cer species and sphingosine were shown to induce cell death, cell cycle arrest, and necrosis (Gault et al., 2010, Hannun and Obeid, 2018). In addition to these unique species-specific biological properties GSLs (which are produced from its precursor Cer), in particular, gangliosides, are essential structural constituents of specialized plasma membrane domains termed 'rafts' (Alves et al., 2018). Among other functions, these raft domains facilitate the invasion of bacteria, microbial toxins, and viruses (Suzuki et al., 2017). Examples for SL-mediated virus entry include measles virus, HIV, hepatitis C virus, and polyomaviridae (Schneider-Schaulies and Schneider-Schaulies, 2015, Taube et al., 2010). In terms of MCPyV, the capsid protein VP1 interacts with sialic acid residues on both branches of the GT1b carbohydrate chain (Erickson et al., 2009). Whether or not MCPyV modulates the SL environment for own survival advantages as reported for influenza A virus that upregulates SK-1 activity or rhinovirus which enhances the formation of Cer-enriched membrane domains for endocytosis (Schneider-Schaulies and Schneider-Schaulies, 2015) is currently unclear.

In MCC, clonally integrated MCPyV expresses the LT and sT antigens (Shuda et al., 2009). A number of studies have reported proto-oncogenic properties of MCPyV-LT and sT antigen in MCC (Houben et al., 2010, Gonzalez-Vela et al., 2017, Shuda et al., 2011, Verhaegen et al., 2017). In line, expression of sT can transform normal cells into cancer-like phenotype, yet the mechanism of LT and sT induced oncogenic transformation in MCC is not entirely understood (Berrios et al., 2016). However, sequestration and inactivation of RB1 by LT and inactivation of 4E-BP1 are thought to increase proliferation rates and confer transforming potential (Liu et al., 2016a). In terms of MCPyV infection, Moshiri and colleagues have demonstrated that $MCPyV^-$ MCC patients have decreased progression-free survival, decreased MCC-specific survival and a non-significant trend for

poorer overall survival (Moshiri et al., 2017). Furthermore, the mortality rate and recurrence risk in MCC are very high, and the FDA approved immune checkpoint inhibitor avelumab is effective in only 50% of the MCC patients (Colunga et al., 2018).

To further understand the mechanism that regulates MCC proliferation and survival, we pharmacologically targeted the SL synthesis pathway using myriocin and SKI-II. Myriocin is an inhibitor of SPTLC1-3 that governs the initial and rate-limiting step of de-novo sphingolipid synthesis pathway (Bernhart et al., 2015). SKI-II is an inhibitor of SK1 and 2 the two enzymes that synthesize pro-tumorigenic S1P (French et al., 2006). Mammalian SPT consists of two large subunits (SPTLC1/2 and SPTLC1/3) and a small regulatory (activating) subunit (ssSPTA or ssSPTB). Subunit composition of SPT determines acyl-CoA specificity (Kihara, 2016). SPTLC2 and -3 are pyridoxal-5'-phosphate (PALP)-dependent catalytic subunits and the actual myriocin targets: SPT inhibition by myriocin is a two-step process where the inhibitor first forms an aldimine with PALP and then undergoes retro-aldol-cleavage with the resulting aldehyde covalently modifying the essential lysine residue in the active center (Wadsworth et al., 2013). Further, SKI-II inhibits the activity of both SK1 and SK2 (Yang et al., 2015). It was reported that SKI-II shows a higher affinity towards SK2 (Madhunapantula et al., 2012). Additionally, inhibition of DES-1 (desaturase-1, the enzyme catalyzing Cer synthesis from the precursor dihydroceramide) was reported as a SKI-II off-target effect (Aurelio et al., 2016). Using these two inhibitors, we analyzed the impact of the pharmacological intervention on SL homeostasis in MCC in in-vitro and ex-ovo experimental approaches.

Initially, we analyzed the expression of the SPTLC1-3 and SK1/2 at mRNA level in MCC tissue samples (n =21) and 16 (10 $MCPyV^+$ and 6 $MCPyV^-$) MCC cell lines. In MCC tissues, SPTLC1 was significantly higher expressed as compared non-MCC tissues (**Figure 7A**), and in cell lines, SPTLC1 and 2 were highly expressed in most of them (**Figure 8A**). In line with our data, Carton and colleagues revealed high expression of SPTLC1 and SPTLC2 in seven different tumor types including thyroid carcinoma, pancreatic carcinoma, colon carcinoma, ovarian carcinoma, undifferentiated carcinoma, and two sarcomas. Additionally, intense expression was also observed in the three cancer cell lines Jurkat, HT-29, SH-SY 5Y during this immunohistochemical study (Carton et al., 2003).

On the other hand, SK1/2 showed a clear (though statistically not significant) trend towards high expression in MCC tissues (**Figure 7B**), and comparable observations were made in a smaller number of cell lines (**Figure 8A**). However, during re-analysis of already published microarray data from the GEO database (Harms et al., 2013) we observed statistically significant upregulation of SK1 and 2 in MCC tissues as compared to normal skin (**Figure 10A**). SK1 and 2 are reported to be upregulated in various cancer entities and overexpression is associated with resistance to tyrosine kinase inhibitors and lower overall survival (Wang et al., 2014). Furthermore, SK1 serves as a biomarker in pancreatic cancer (Nunes et al., 2012).

Importantly, we observed that SK1/2 expressions were higher in $MCPyV^+$ cell lines in comparison to the $MCPyV^-$ cell lines (**Figure 8B**). This prompted us to check the impact of MCPyV-LT antigen induction in the fibroblast cell line MRC5 on the expression of SPTLC1-3 and SK1/2. MCC cell line derived LT antigen-induced two morphologically distinct populations of this fibroblast cell line (growing adherent and non-adherent, free-floating) with significant upregulation of SK1 and 2 (**Figure 9C**). A transcriptome study performed by Berrios and colleagues revealed that MCPyV-sT expression in IMR90 cells (another fibroblast cell line) increased glycolytic gene expression and lactate concentrations in the cellular supernatant (Berrios et al., 2016). These findings are indicative of an increase in aerobic glycolysis (the 'Warburg effect'), which is considered a hallmark of cancer. We utilized this transcriptome data set (GSE79968) to clarify whether MCPyV-sT overexpression induces any changes within the regulators of the SL synthesis pathway that were analyzed during my thesis (i.e., SPTLC1-3 and SK1/2). In line with our results obtained during LT transduction experiments, re-analysis of the Berrios dataset showed that MCPyV-sT induction in IMR90 cells leads to a significant induction of SPTLC1/2 and SK1/2 expression on mRNA level (**Figure 10B**). In line with these results previous studies have reported upregulation of SK1 upon influenza infection and increased activity of SK1 in human cytomegalovirus and respiratory syncytial virus infections (Carr et al., 2013). Also, SK2 was upregulated in immortalized endothelial cells in response to infection with Kaposi sarcoma-associated herpesvirus (Dai et al., 2017).

Next, to study the effects of pharmacological inhibitors under in-vitro conditions two well-characterized $MCPyV^+$ cell lines, namely MKL-1 and WaGa, were used. Expression of SPT and SK1/2 enzymes were observed in both the cell lines. Treatment with myriocin

reduced pro-apoptotic Cer species, SM, and pro-proliferative S1P in both MCC cell lines (**Figure 12A-F**). In agreement with our data results from Yaguchi and colleagues also showed that inhibition of SPT with compound-2 reduced SM and Cer content in various cancer cell lines (Yaguchi et al., 2017). In addition, treatment with SKI-II reduced S1P and SM content and increased pro-apoptotic Cer concentrations (**Figure 12G-L**). Consequently, myriocin and SKI-II treatment decreased $MCPyV^+$ MCC cell viability and promoted apoptosis and necrosis in-vitro (**Figure 13 and Figure 17-19**). The fact that NHDF viability was unaffected by the treatment with myriocin, and SKI-II (confirmed by viability assay (**Figure 13**) and flow cytometry analysis (**Figure17 and 20**)) might be of potential importance for clinical translation of our data since the viability of non-transformed cells is not affected by these inhibitors.

S1P, Cer, and SM are synthesized during a condensation reaction of serine and palmitoyl CoA (Ogretmen, 2018). Pro-apoptotic Cer species are then subsequently converted to S1P and/or SM. SM forms an integral part of the lipid domains in the plasma membrane whereas Cer and S1P can interact with other intracellular proteins (Hannun and Obeid, 2018). Cer regulates PP2A and PKCζ activity (Fox et al., 2007) whereas S1P synthesized by SK2 binds to and regulates HDAC1/2 activity and protects telomeres by enhancing the activity of hTERT in cancer cells (Panneer Selvam et al., 2015).

Treatment with myriocin reduced S1P, ceramide, and SM content and SKI-II treatment induced ceramide accumulation and reduced S1P and SM concentration in $MCPyV^+$ MCC cells. It is possible that inhibition of the initial step of the SL synthesis pathway resulted in an overall reduction in the levels of Cer, S1P, and SM. Reduction in S1P might have affected the activity of hTERT leading it to proteasomal degradation thereby inducing a reduction in viable cells and an increase in apoptotic cells (Zhang et al., 1999). Further, SKI-II treatment inhibited S1P conversion from its precursor sphingosine which might induce a metabolic shift to increased ceramide synthesis. It is reasonable to assume that a higher ceramide content could increase the activity of tumor suppressor genes or contribute to caspase activation in a similar manner as reported for lymphoid cancer cell lines (Hetz, 2002).

S1P present in the cytosol is thought to be predominantly synthesized by SK1. The cytosolic S1P is then subject to cellular efflux, a process facilitated by transporters such as SPNS2 (Hisano and Hla, 2019). One of the HDL associated apolipoproteins, apoM, is

reported to be the primary physiological carrier of extracellular S1P. ApoM is a member of the lipocalin family with a hydrophobic binding pocket where S1P is transported (Zhang et al., 2016). After binding of HDL particles to SR-BI (Scavenger receptor class B, type 1) S1P is in the necessary spatial proximity to be able to interact with its specific G-protein coupled S1P-receptors (Lee et al., 2017). Downstream signaling cascades regulate tumor cell proliferation, migration, invasion, and metastasis (Blaho and Hla, 2014). We here demonstrated that all of the five receptors are expressed in MCC cell lines (**Figure 14**). Furthermore, treatment with S1P-enriched HDL increased cell viability in comparison to native HDL (**Figure 15A**) revealing the ability of HDL-bound S1P to positively regulate $MCPyV^+$ MCC cell proliferation in-vitro. In a reverse approach, we tried to reduce S1P level in human HDL applying a hydrolysis step with recombinant S1P lyase, an enzyme that catalyzes the irreversible hydrolysis of S1P. Incubation of MKL-1 and WaGa cells in the presence of S1P-lyase-treated HDL resulted in significantly lower proliferation rates. However, the relevance of these findings is currently unclear as treatment with S1P lyase alone also significantly decreased cell viability (**Figure 15B**).

The pro-oncogenic role of S1P receptors in cancer is accepted. In particular, S1PR1 and 3 are reported to promote cancer cell survival, proliferation, and migration (Blaho and Hla, 2014). To test such a possibility in MCC, we inhibited used S1PR1 and 3 using VPC23019 (Kennedy et al., 2011). However, using this pharmacological approach, we did not see any reduction in HDL or HDL-S1P induced cell viability in VPC23019 treated $MCPyV^+$ MCC cells (**Figure 16A** and **16B**). These results indicate that S1PR1 and 3 may not be essential for $MCPyV^+$ MCC cell viability. Altogether the results discussed above indicate a role of extracellular S1P in MCC cell viability under in-vitro conditions. However, further evidence is required to confirm these data as we did not see any difference in viability when we inhibited S1PR1 and 3.

Western blot analysis of myriocin and SKI-II treated MCC samples showed reduced phospho-AKT^{S473} and increased pro-caspase3 and PARP cleavage (**Figure 21**). Binding of S1P to S1PR leads to upregulation of a number of signaling pathways, including the PI3K-AKT pathway (Pchejetski et al., 2011). Dysregulation of the PI3K/Akt/mTOR pathway contributes to cancer cell survival, promotes resistance to chemotherapy and radiotherapy through the disruption of apoptosis, and initiates cell cycle progression, and cellular differentiation and growth (Ogretmen, 2018). During the present study, we observed

already basal AKT phosphorylation in MKL-1 and WaGa cells that was significantly diminished in response to myriocin and SKI-II treatment (**Figure 21-23**). Lin and colleagues reported phosphorylation of AKT at S473 in human MCC tissue where 19/22 samples stained positive indicating basal activation of this pro-proliferative axis (Lin et al., 2015). Since myriocin and SKI-II decreased the S1P content in MCC cells in-vitro (**Figure 12**), it is reasonable to hypothesize that diminished extracellular S1P concentrations resulted in reduced basal AKT phosphorylation. Moreover, an increase in the levels of intracellular Cer (Fig. 2) in response to SKI-II may have activated protein phosphatase 2A, leading to de-phosphorylation of active AKT (Kim et al., 2010). Induction of necrosis is upregulated by Cer, PARP, and low ATP levels (Vanden Berghe et al., 2014) as observed during the present study. In order to understand the role of AKT alone in MCC survival, we targeted it with the AKT1-3 inhibitor triciribine. Treatment of triciribine on MKL-1 and WaGa reduced cell viability and promoted apoptosis in-vitro (**Figure 25**) with a net effect that was comparable to that of SKI-II treatment (**Figure 13E and 13F**). Of note for the cancer field, triciribine is currently listed in 5 clinical trials. Two are in Phase I completed but results not declared that includes metastatic cancers (NCT00363454) and advanced hematologic cancers (NCT00642031). Three are in Phase I/II (recruitment stage) trail on ovarian cancer (NCT01690468), breast cancer (NCT01697293) and acute leukemia (NCT02930109). While to the best of my knowledge no AKT inhibitors are currently in clinical trials for MCC, a clinical phase I/II trial in MCC with the mTOR inhibitor MLN0128 is active (NCT02514824).

Currently, ABC294640 a selective inhibitor of SK2 is in phase I/II clinical trial for myeloma (NCT02757326 and NCT01410981) and cholangiocarcinoma (NCT03377179). Additionally, the immunomodulatory drug FTY720 (fingolimod, FDA approved the drug for MS treatment) an inhibitor of S1P receptor function has completed a Phase I clinical trial (NCT02490930) in glioma patients but results have not been published (Bhat et al., 2018a). We wanted to test the effect of these two FDA approved inhibitors in MKL-1 and WaGa MCC cells. Treatment with ABC294640 and FTY720 decreased cell viability and promoted apoptosis in both MCC cell lines (**Figure 26** and **Figure 27**). ABC294640 had a less pronounced effect on NHDF cell viability as compared to FTY720 that drastically reduced the viability of NHDF. Further preclinical studies are required to assess the efficacy of these two inhibitors. In MCC, expression of $CD4^+$ and $CD8^+$ $FOXP3^+$ regulatory T cells were frequently observed (Dowlatshahi et al., 2013) and $CD8^+$ $FOXP3^+$

T regs were shown to promote tumorigenesis in melanoma, colorectal, and prostate cancers (Dowlatshahi et al., 2013, Kiniwa et al., 2007). An immunomodulating drug such as FTY720 targeting the S1P/S1PR axis in MCC could be a promising anticancer strategy in future to modulate the tumor microenvironment.

We have recently developed a CAM model (**Figure 29-31**) that allows monitoring of grafted MCC tumors (Bhat et al., 2018b). Robust tumor growth was observed in the MKL-1, PeTa and WaGa MCC-CAM model. In the CAM model, all of the three MCC cell lines tested were equally effective in maintaining time-dependent xenograft growth and establishing of a functional tumor vasculature that originates from the chick embryo (**Figure 29**). Immunohistochemical analyses revealed that the tumor sections were positive for the CK20, MCPyV-LT antigen, and Ki-67, accepted markers in MCC histopathology. This model represents a valuable alternative to rodent tumor models to study growth, progression, tumor angiogenesis and invasion of MCC cells (**Figure 29-31**).

Here we demonstrate for the first time the pharmacological usefulness of this xenograft model in MCC research. In grafted MKL-1 and WaGa tumors, myriocin and SKI-II reduced tumor area and the Ki-67 index (**Figure 32**), however, in contrast to our in-vitro experiments (**Figure 13** and **17**) SKI-II did not display superior potency in the CAM assay as compared to myriocin. The reasons for these observations are currently unclear. Whether or not this model can be translated into clinical MCC settings for drug screening purposes to establish patient-derived xenograft models remains to be seen.

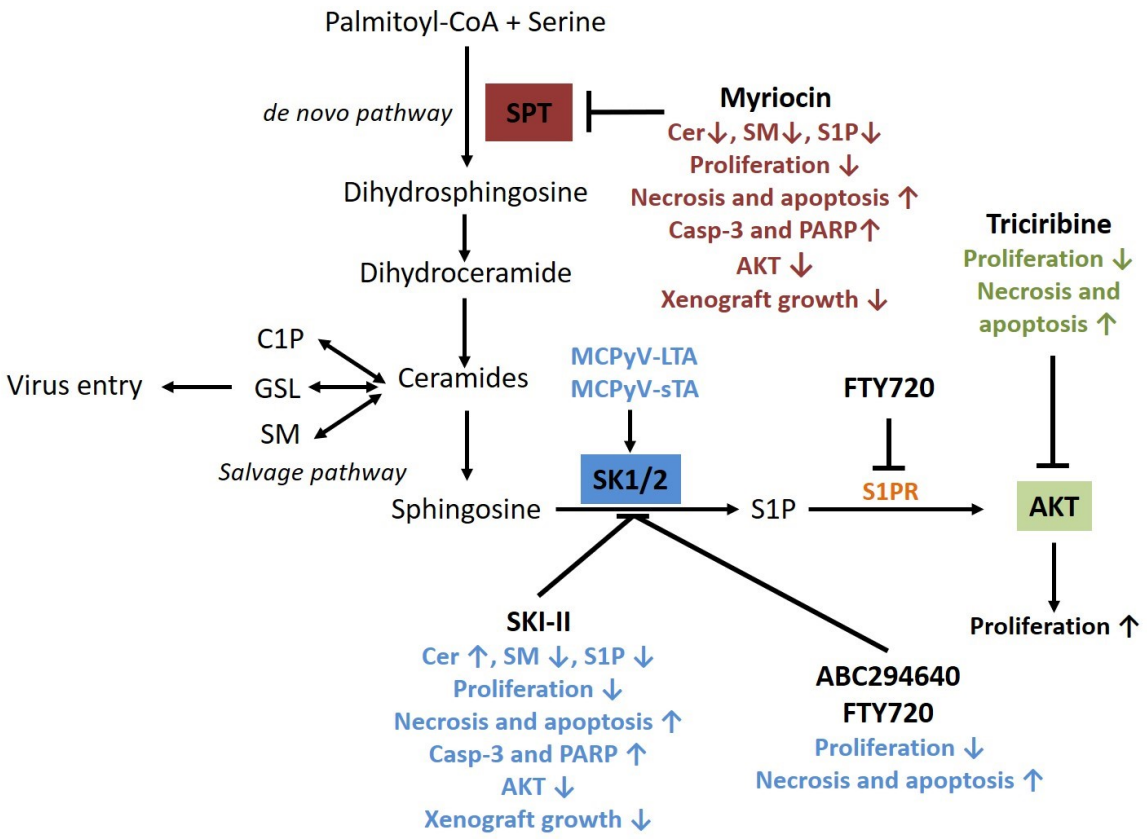

Figure 33: Graphical summary of findings obtained during this study.

De-novo sphingolipid (SL) synthesis starts from the condensation reaction of C16-CoA and serine catalyzed by serine-palmitoyltransferase (SPT) leading to the formation of bioactive ceramide (Cer) that can be converted to sphingomyelin (SM), ceramide-1-phosphate (C1P), and complex glycosphingolipids (GSL). In salvage pathway hydrolysis of SM, C1P, or GSL generates Cer. of Cer is converted to sphingosine by the de-acylation reaction. Sphingosine is phosphorylated by sphingosine kinase-1 or -2 (SK1/2) to form S1P.

Overexpression of MCPyV-LT or MCPyV-sT antigen (blue) increases gene expression of SK1/2. Inhibition of SPT by myriocin (red), SK1/2 by SKI-II (blue) induces changes in the cellular SL content and composition, decreases cell viability, induces apoptosis and necrosis, and decreases pAKT and xenograft growth in the CAM model. MCPyV+ MCC cells express all five S1P receptors and HDL-complexed S1P increases cell proliferation (orange).

The SK1/S1PR inhibitor FTY720, SK2 inhibitor ABC294640 (blue) and the AKT inhibitor Triciribine (green) inhibit proliferation and induce apoptosis and necrosis. All together obtained results summarizes bioactive SLs play a critical regulatory role in MCC cell survival and proliferation. The data shown above are from my published article Bhat KV and colleagues (Bhat et al., 2018a) and reproduced here with permission from Elsevier.

In conclusion, my thesis reports a critical role of SL homeostasis in MCC cell survival (**Figure 33**). We characterized the expression of SPTLC1-3 and SK1/2 in MCC tissues and cell lines. We demonstrated that SK1 and SK2 are upregulated in MCC tissues. In

addition, MCPyV LT and sT were shown to upregulate SK1/2 in transduced fibroblasts. Additionally, treatment of MKL-1 and WaGa cells (in-vitro or on the CAM) with myriocin or SKI-II resulted in subsequent disruption of SL homeostasis, significantly reduced MCC cell viability and tumor cell growth. Also, ABC294640, FTY720, and triciribine induced MCC cell death under in-vitro condition. Our findings indicate that exploration of inhibitors that interfere with SL metabolic/signaling pathways could provide a new approach for experimental drugs in MCC research.

6. Bibliography

ALVAREZ, S. E., HARIKUMAR, K. B., HAIT, N. C., ALLEGOOD, J., STRUB, G. M., KIM, E. Y., MACEYKA, M., JIANG, H., LUO, C., KORDULA, T., MILSTIEN, S. & SPIEGEL, S. 2010. Sphingosine-1-phosphate is a missing cofactor for the E3 ubiquitin ligase TRAF2. *Nature,* 465**,** 1084-8.

ALVES, A. C. S., DIAS, R. A., KAGAMI, L. P., DAS NEVES, G. M., TORRES, F. C., EIFLER-LIMA, V. L., CARVALHO, I., DE MIRANDA SILVA, C. & KAWANO, D. F. 2018. Beyond the "Lock and Key" Paradigm: Targeting Lipid Rafts to Induce the Selective Apoptosis of Cancer Cells. *Curr Med Chem,* 25**,** 2082-2104.

AMES, H. M., BICHAKJIAN, C. K., LIU, G. Y., ORAVECZ-WILSON, K. I., FULLEN, D. R., VERHAEGEN, M. E., JOHNSON, T. M., DLUGOSZ, A. A. & ROSS, T. S. 2011. Huntingtin-interacting protein 1: a Merkel cell carcinoma marker that interacts with c-Kit. *J Invest Dermatol,* 131**,** 2113-20.

ANCELLIN, N., COLMONT, C., SU, J., LI, Q., MITTEREDER, N., CHAE, S. S., STEFANSSON, S., LIAU, G. & HLA, T. 2002. Extracellular export of sphingosine kinase-1 enzyme. Sphingosine 1-phosphate generation and the induction of angiogenic vascular maturation. *J Biol Chem,* 277**,** 6667-75.

ANDREASEN, P. A., EGELUND, R. & PETERSEN, H. H. 2000. The plasminogen activation system in tumor growth, invasion, and metastasis. *Cell Mol Life Sci,* 57**,** 25-40.

ANDRES, C., BELLONI, B., JAEGER, T., PUCHTA, U., KONSTANTINOW, A., RING, J. & FLAIG, M. J. 2011. Immunohistochemical features of Merkel cell carcinoma in correlation with presence of Merkel cell polyomavirus DNA. *Acta Derm Venereol,* 91**,** 722-3.

ANELLI, V., GAULT, C. R., CHENG, A. B. & OBEID, L. M. 2008. Sphingosine kinase 1 is up-regulated during hypoxia in U87MG glioma cells. Role of hypoxia-inducible factors 1 and 2. *J Biol Chem,* 283**,** 3365-75.

ARIKAWA, K., TAKUWA, N., YAMAGUCHI, H., SUGIMOTO, N., KITAYAMA, J., NAGAWA, H., TAKEHARA, K. & TAKUWA, Y. 2003. Ligand-dependent inhibition of B16 melanoma cell migration and invasion via endogenous S1P2 G protein-coupled receptor. Requirement of inhibition of cellular RAC activity. *J Biol Chem,* 278**,** 32841-51.

AURELIO, L., SCULLINO, C. V., PITMAN, M. R., SEXTON, A., OLIVER, V., DAVIES, L., REBELLO, R. J., FURIC, L., CREEK, D. J., PITSON, S. M. & FLYNN, B. L. 2016. From Sphingosine Kinase to Dihydroceramide Desaturase: A Structure-Activity Relationship (SAR) Study of the Enzyme Inhibitory and Anticancer Activity of 4-((4-(4-Chlorophenyl)thiazol-2-yl)amino)phenol (SKI-II). *J Med Chem,* 59**,** 965-84.

AZOITEI, N., KLEGER, A., SCHOO, N., THAL, D. R., BRUNNER, C., PUSAPATI, G. V., FILATOVA, A., GENZE, F., MOLLER, P., ACKER, T., KUEFER, R., VAN LINT, J., BAUST, H., ADLER, G. & SEUFFERLEIN, T. 2011. Protein kinase D2 is a novel regulator of glioblastoma growth and tumor formation. *Neuro Oncol,* 13**,** 710-24.

BARAN, Y., SALAS, A., SENKAL, C. E., GUNDUZ, U., BIELAWSKI, J., OBEID, L. M. & OGRETMEN, B. 2007. Alterations of ceramide/sphingosine 1-phosphate rheostat involved in the regulation of resistance to imatinib-induced apoptosis in K562 human chronic myeloid leukemia cells. *J Biol Chem,* 282**,** 10922-34.

BARTKE, N. & HANNUN, Y. A. 2009. Bioactive sphingolipids: metabolism and function. *J Lipid Res,* 50 Suppl**,** S91-6.

BECHERT, C. J., SCHNADIG, V. & NAWGIRI, R. 2013. The Merkel cell carcinoma challenge: a review from the fine needle aspiration service. *Cancer Cytopathol,* 121**,** 179-88.

BECKER, J. C., HOUBEN, R., UGUREL, S., TREFZER, U., PFOHLER, C. & SCHRAMA, D. 2009. MC polyomavirus is frequently present in Merkel cell carcinoma of European patients. *J Invest Dermatol,* 129**,** 248-50.

BECKER, J. C., LORENZ, E., UGUREL, S., EIGENTLER, T. K., KIECKER, F., PFOHLER, C., KELLNER, I., MEIER, F., KAHLER, K., MOHR, P., BERKING, C., HAAS, G., HELWIG, C., OKSEN, D., SCHADENDORF, D., MAHNKE, L. & BHARMAL, M. 2017a. Evaluation of real-world treatment outcomes in patients with distant metastatic Merkel cell carcinoma following second-line chemotherapy in Europe. *Oncotarget,* 8**,** 79731-79741.

BECKER, J. C., STANG, A., DECAPRIO, J. A., CERRONI, L., LEBBE, C., VENESS, M. & NGHIEM, P. 2017b. Merkel cell carcinoma. *Nat Rev Dis Primers,* 3**,** 17077.

BECKER, J. C., STANG, A., HAUSEN, A. Z., FISCHER, N., DECAPRIO, J. A., TOTHILL, R. W., LYNGAA, R., HANSEN, U. K., RITTER, C., NGHIEM, P., BICHAKJIAN, C. K., UGUREL, S. & SCHRAMA, D. 2018. Epidemiology,

biology and therapy of Merkel cell carcinoma: conclusions from the EU project IMMOMEC. *Cancer Immunol Immunother,* 67**,** 341-351.

BERNHART, E., DAMM, S., WINTERSPERGER, A., NUSSHOLD, C., BRUNNER, A. M., PLASTIRA, I., RECHBERGER, G., REICHER, H., WADSACK, C., ZIMMER, A., MALLE, E. & SATTLER, W. 2015. Interference with distinct steps of sphingolipid synthesis and signaling attenuates proliferation of U87MG glioma cells. *Biochem Pharmacol,* 96**,** 119-30.

BERRIOS, C., PADI, M., KEIBLER, M. A., PARK, D. E., MOLLA, V., CHENG, J., LEE, S. M., STEPHANOPOULOS, G., QUACKENBUSH, J. & DECAPRIO, J. A. 2016. Merkel Cell Polyomavirus Small T Antigen Promotes Pro-Glycolytic Metabolic Perturbations Required for Transformation. *PLoS Pathog,* 12**,** e1006020.

BHAT, V. K., BERNHART, E., PLASTIRA, I., FAN, K., TABRIZI-WIZSY, N. G., WADSACK, C., RECHBERGER, G., EICHMANN, T., ASSLABER, M., SPASSOVA, I., VERHAEGEN, M. E., MALLE, E., BECKER, J. C. & SATTLER, W. 2018a. Pharmacological inhibition of serine palmitoyl transferase and sphingosine kinase-1/-2 inhibits Merkel Cell Carcinoma cell proliferation. *J Invest Dermatol,* 10.1016/j.jid.2018.10.024.

BHAT, V. K., KRUMP, C., BERNHART, E., BECKER, J. C., SATTLER, W. & GHAFFARI-TABRIZI-WIZSY, N. 2018b. A short-term in vivo model for Merkel Cell Carcinoma. *Exp Dermatol,* 27**,** 684-687.

BICHAKJIAN, C. K., OLENCKI, T., AASI, S. Z., ALAM, M., ANDERSEN, J. S., BLITZBLAU, R., BOWEN, G. M., CONTRERAS, C. M., DANIELS, G. A., DECKER, R., FARMA, J. M., FISHER, K., GASTMAN, B., GHOSH, K., GREKIN, R. C., GROSSMAN, K., HO, A. L., LEWIS, K. D., LOSS, M., LYDIATT, D. D., MESSINA, J., NEHAL, K. S., NGHIEM, P., PUZANOV, I., SCHMULTS, C. D., SHAHA, A. R., THOMAS, V., XU, Y. G., ZIC, J. A., HOFFMANN, K. G. & ENGH, A. M. 2018. Merkel Cell Carcinoma, Version 1.2018, NCCN Clinical Practice Guidelines in Oncology. *J Natl Compr Canc Netw,* 16**,** 742-774.

BLAHO, V. A. & HLA, T. 2014. An update on the biology of sphingosine 1-phosphate receptors. *J Lipid Res,* 55**,** 1596-608.

BOUCHARABA, A., GUILLET, B., MENAA, F., HNEINO, M., VAN WIJNEN, A. J., CLEZARDIN, P. & PEYRUCHAUD, O. 2009. Bioactive lipids lysophosphatidic

acid and sphingosine 1-phosphate mediate breast cancer cell biological functions through distinct mechanisms. *Oncol Res,* 18**,** 173-84.

BOURBON, N. A., SANDIRASEGARANE, L. & KESTER, M. 2002. Ceramide-induced inhibition of Akt is mediated through protein kinase Czeta: implications for growth arrest. *J Biol Chem,* 277**,** 3286-92.

BOUVARD, V., BAAN, R. A., GROSSE, Y., LAUBY-SECRETAN, B., EL GHISSASSI, F., BENBRAHIM-TALLAA, L., GUHA, N., STRAIF, K. & GROUP, W. H. O. I. A. F. R. O. C. M. W. 2012. Carcinogenicity of malaria and of some polyomaviruses. *Lancet Oncol,* 13**,** 339-40.

BRINKMANN, V., BILLICH, A., BAUMRUKER, T., HEINING, P., SCHMOUDER, R., FRANCIS, G., ARADHYE, S. & BURTIN, P. 2010. Fingolimod (FTY720): discovery and development of an oral drug to treat multiple sclerosis. *Nat Rev Drug Discov,* 9**,** 883-97.

BRYAN, L., PAUGH, B. S., KAPITONOV, D., WILCZYNSKA, K. M., ALVAREZ, S. M., SINGH, S. K., MILSTIEN, S., SPIEGEL, S. & KORDULA, T. 2008. Sphingosine-1-phosphate and interleukin-1 independently regulate plasminogen activator inhibitor-1 and urokinase-type plasminogen activator receptor expression in glioblastoma cells: implications for invasiveness. *Mol Cancer Res,* 6**,** 1469-77.

BUSAM, K. J., JUNGBLUTH, A. A., REKTHMAN, N., COIT, D., PULITZER, M., BINI, J., ARORA, R., HANSON, N. C., TASSELLO, J. A., FROSINA, D., MOORE, P. & CHANG, Y. 2009. Merkel cell polyomavirus expression in merkel cell carcinomas and its absence in combined tumors and pulmonary neuroendocrine carcinomas. *Am J Surg Pathol,* 33**,** 1378-85.

CALDER, K. B. & SMOLLER, B. R. 2010. New insights into merkel cell carcinoma. *Adv Anat Pathol,* 17**,** 155-61.

CARR, J. M., MAHALINGAM, S., BONDER, C. S. & PITSON, S. M. 2013. Sphingosine kinase 1 in viral infections. *Rev Med Virol,* 23**,** 73-84.

CARTON, J. M., UHLINGER, D. J., BATHEJA, A. D., DERIAN, C., HO, G., ARGENTERI, D. & D'ANDREA, M. R. 2003. Enhanced serine palmitoyltransferase expression in proliferating fibroblasts, transformed cell lines, and human tumors. *J Histochem Cytochem,* 51**,** 715-26.

CHAE, S. S., PAIK, J. H., FURNEAUX, H. & HLA, T. 2004. Requirement for sphingosine 1-phosphate receptor-1 in tumor angiogenesis demonstrated by in vivo RNA interference. *J Clin Invest,* 114**,** 1082-9.

CHENG, J., PARK, D. E., BERRIOS, C., WHITE, E. A., ARORA, R., YOON, R., BRANIGAN, T., XIAO, T., WESTERLING, T., FEDERATION, A., ZEID, R., STROBER, B., SWANSON, S. K., FLORENS, L., BRADNER, J. E., BROWN, M., HOWLEY, P. M., PADI, M., WASHBURN, M. P. & DECAPRIO, J. A. 2017. Merkel cell polyomavirus recruits MYCL to the EP400 complex to promote oncogenesis. *PLoS Pathog,* 13**,** e1006668.

CHENG, J., ROZENBLATT-ROSEN, O., PAULSON, K. G., NGHIEM, P. & DECAPRIO, J. A. 2013. Merkel cell polyomavirus large T antigen has growth-promoting and inhibitory activities. *J Virol,* 87**,** 6118-26.

CHI, H. 2011. Sphingosine-1-phosphate and immune regulation: trafficking and beyond. *Trends Pharmacol Sci,* 32**,** 16-24.

CHIPUK, J. E., MCSTAY, G. P., BHARTI, A., KUWANA, T., CLARKE, C. J., SISKIND, L. J., OBEID, L. M. & GREEN, D. R. 2012. Sphingolipid metabolism cooperates with BAK and BAX to promote the mitochondrial pathway of apoptosis. *Cell,* 148**,** 988-1000.

CIMINO, P. J., ROBIRDS, D. H., TRIPP, S. R., PFEIFER, J. D., ABEL, H. J. & DUNCAVAGE, E. J. 2014. Retinoblastoma gene mutations detected by whole exome sequencing of Merkel cell carcinoma. *Mod Pathol,* 27**,** 1073-87.

COLUNGA, A., PULLIAM, T. & NGHIEM, P. 2018. Merkel Cell Carcinoma in the Age of Immunotherapy: Facts and Hopes. *Clin Cancer Res,* 24**,** 2035-2043.

DAI, L., BAI, A., SMITH, C. D., RODRIGUEZ, P. C., YU, F. & QIN, Z. 2017. ABC294640, A Novel Sphingosine Kinase 2 Inhibitor, Induces Oncogenic Virus-Infected Cell Autophagic Death and Represses Tumor Growth. *Mol Cancer Ther,* 16**,** 2724-2734.

DAILY, K., COXON, A., WILLIAMS, J. S., LEE, C. R., COIT, D. G., BUSAM, K. J. & BROWNELL, I. 2015. Assessment of cancer cell line representativeness using microarrays for Merkel cell carcinoma. *J Invest Dermatol,* 135**,** 1138-1146.

DENG, X., GAO, F. & MAY, W. S. 2009. Protein phosphatase 2A inactivates Bcl2's antiapoptotic function by dephosphorylation and up-regulation of Bcl2-p53 binding. *Blood,* 113**,** 422-8.

DERYUGINA, E. I. & QUIGLEY, J. P. 2008. Chapter 2. Chick embryo chorioallantoic membrane models to quantify angiogenesis induced by inflammatory and tumor cells or purified effector molecules. *Methods Enzymol,* 444**,** 21-41.

DEVINE, K. M., SMICUN, Y., HOPE, J. M. & FISHMAN, D. A. 2008. S1P induced changes in epithelial ovarian cancer proteolysis, invasion, and attachment are mediated by Gi and Rac. *Gynecol Oncol,* 110**,** 237-45.

DILLEHAY, D. L., WEBB, S. K., SCHMELZ, E. M. & MERRILL, A. H., JR. 1994. Dietary sphingomyelin inhibits 1,2-dimethylhydrazine-induced colon cancer in CF1 mice. *J Nutr,* 124**,** 615-20.

DING, G., SONODA, H., YU, H., KAJIMOTO, T., GOPARAJU, S. K., JAHANGEER, S., OKADA, T. & NAKAMURA, S. 2007. Protein kinase D-mediated phosphorylation and nuclear export of sphingosine kinase 2. *J Biol Chem,* 282**,** 27493-502.

DOWLATSHAHI, M., HUANG, V., GEHAD, A. E., JIANG, Y., CALARESE, A., TEAGUE, J. E., DOROSARIO, A. A., CHENG, J., NGHIEM, P., SCHANBACHER, C. F., THAKURIA, M., SCHMULTS, C. D., WANG, L. C. & CLARK, R. A. 2013. Tumor-specific T cells in human Merkel cell carcinomas: a possible role for Tregs and T-cell exhaustion in reducing T-cell responses. *J Invest Dermatol,* 133**,** 1879-89.

EDGAR, R., DOMRACHEV, M. & LASH, A. E. 2002. Gene Expression Omnibus: NCBI gene expression and hybridization array data repository. *Nucleic Acids Res,* 30**,** 207-10.

EFTEKHARI, F., WALLACE, S., SILVA, E. G. & LENZI, R. 1996. Merkel cell carcinoma of the skin: imaging and clinical features in 93 cases. *Br J Radiol,* 69**,** 226-33.

ENGELS, E. A., FRISCH, M., GOEDERT, J. J., BIGGAR, R. J. & MILLER, R. W. 2002. Merkel cell carcinoma and HIV infection. *Lancet,* 359**,** 497-8.

ERICKSON, K. D., GARCEA, R. L. & TSAI, B. 2009. Ganglioside GT1b is a putative host cell receptor for the Merkel cell polyomavirus. *J Virol,* 83**,** 10275-9.

FAN, K., RITTER, C., NGHIEM, P., BLOM, A., VERHAEGEN, M. E., DLUGOSZ, A., ODUM, N., WOETMANN, A., TOTHILL, R. W., HICKS, R. J., SAND, M., SCHRAMA, D., SCHADENDORF, D., UGUREL, S. & BECKER, J. C. 2018. Circulating cell-free miR-375 as surrogate marker of tumor burden in Merkel cell carcinoma. *Clin Cancer Res,* doi:10.1158/1078-0432.CCR-18-1184.

FENG, H., SHUDA, M., CHANG, Y. & MOORE, P. S. 2008. Clonal integration of a polyomavirus in human Merkel cell carcinoma. *Science,* 319**,** 1096-100.

FENIG, E., BRENNER, B., KATZ, A., RAKOVSKY, E., HANA, M. B. & SULKES, A. 1997. The role of radiation therapy and chemotherapy in the treatment of Merkel cell carcinoma. *Cancer,* 80**,** 881-5.

FLEMING, K. E., LY, T. Y., PASTERNAK, S., GODLEWSKI, M., DOUCETTE, S. & WALSH, N. M. 2014. Support for p63 expression as an adverse prognostic marker in Merkel cell carcinoma: report on a Canadian cohort. *Hum Pathol,* 45**,** 952-60.

FOCHTMANN-FRANA, A., HAYMERLE, G., SCHACHNER, H., PAMMER, J., LOEWE, R., KERJASCHKI, D., PERISANIDIS, C. & EROVIC, B. M. 2018. Expression of 15-lipoxygenase-1 in Merkel cell carcinoma is linked to advanced disease. *Clin Otolaryngol,* 43**,** 1335-1344.

FOX, T. E., HOUCK, K. L., O'NEILL, S. M., NAGARAJAN, M., STOVER, T. C., POMIANOWSKI, P. T., UNAL, O., YUN, J. K., NAIDES, S. J. & KESTER, M. 2007. Ceramide recruits and activates protein kinase C zeta (PKC zeta) within structured membrane microdomains. *J Biol Chem,* 282**,** 12450-7.

FRENCH, K. J., UPSON, J. J., KELLER, S. N., ZHUANG, Y., YUN, J. K. & SMITH, C. D. 2006. Antitumor activity of sphingosine kinase inhibitors. *J Pharmacol Exp Ther,* 318**,** 596-603.

FUTERMAN, A. H. & RIEZMAN, H. 2005. The ins and outs of sphingolipid synthesis. *Trends Cell Biol,* 15**,** 312-8.

GAULT, C. R., OBEID, L. M. & HANNUN, Y. A. 2010. An overview of sphingolipid metabolism: from synthesis to breakdown. *Adv Exp Med Biol,* 688**,** 1-23.

GOH, G., WALRADT, T., MARKAROV, V., BLOM, A., RIAZ, N., DOUMANI, R., STAFSTROM, K., MOSHIRI, A., YELISTRATOVA, L., LEVINSOHN, J., CHAN, T. A., NGHIEM, P., LIFTON, R. P. & CHOI, J. 2016. Mutational landscape of MCPyV-positive and MCPyV-negative Merkel cell carcinomas with implications for immunotherapy. *Oncotarget,* 7**,** 3403-15.

GONZALEZ-VELA, M. D., CURIEL-OLMO, S., DERDAK, S., BELTRAN, S., SANTIBANEZ, M., MARTINEZ, N., CASTILLO-TRUJILLO, A., GUT, M., SANCHEZ-PACHECO, R., ALMARAZ, C., CERECEDA, L., LLOMBART, B., AGRAZ-DOBLAS, A., REVERT-ARCE, J., LOPEZ GUERRERO, J. A., MOLLEJO, M., MARRON, P. I., ORTIZ-ROMERO, P., FERNANDEZ-CUESTA, L., VARELA, I., GUT, I., CERRONI, L., PIRIS, M. A. & VAQUE, J. P. 2017. Shared Oncogenic Pathways Implicated in Both Virus-Positive and UV-Induced Merkel Cell Carcinomas. *J Invest Dermatol,* 137**,** 197-206.

GRASSME, H., RIEHLE, A., WILKER, B. & GULBINS, E. 2005. Rhinoviruses infect human epithelial cells via ceramide-enriched membrane platforms. *J Biol Chem,* 280**,** 26256-62.

GUILLERMET-GUIBERT, J., DAVENNE, L., PCHEJETSKI, D., SAINT-LAURENT, N., BRIZUELA, L., GUILBEAU-FRUGIER, C., DELISLE, M. B., CUVILLIER, O., SUSINI, C. & BOUSQUET, C. 2009. Targeting the sphingolipid metabolism to defeat pancreatic cancer cell resistance to the chemotherapeutic gemcitabine drug. *Mol Cancer Ther,* 8**,** 809-20.

HAFNER, C., HOUBEN, R., BAEURLE, A., RITTER, C., SCHRAMA, D., LANDTHALER, M. & BECKER, J. C. 2012. Activation of the PI3K/AKT pathway in Merkel cell carcinoma. *PLoS One,* 7**,** e31255.

HAIT, N. C., ALLEGOOD, J., MACEYKA, M., STRUB, G. M., HARIKUMAR, K. B., SINGH, S. K., LUO, C., MARMORSTEIN, R., KORDULA, T., MILSTIEN, S. & SPIEGEL, S. 2009. Regulation of histone acetylation in the nucleus by sphingosine-1-phosphate. *Science,* 325**,** 1254-7.

HAIT, N. C., BELLAMY, A., MILSTIEN, S., KORDULA, T. & SPIEGEL, S. 2007. Sphingosine kinase type 2 activation by ERK-mediated phosphorylation. *J Biol Chem,* 282**,** 12058-65.

HAKOMORI, S. 2003. Structure, organization, and function of glycosphingolipids in membrane. *Curr Opin Hematol,* 10**,** 16-24.

HANADA, K. 2010. Intracellular trafficking of ceramide by ceramide transfer protein. *Proc Jpn Acad Ser B Phys Biol Sci,* 86**,** 426-37.

HANEL, P., ANDREANI, P. & GRALER, M. H. 2007. Erythrocytes store and release sphingosine 1-phosphate in blood. *FASEB J,* 21**,** 1202-9.

HANNUN, Y. A. & OBEID, L. M. 2018. Sphingolipids and their metabolism in physiology and disease. *Nat Rev Mol Cell Biol,* 19**,** 175-191.

HARMS, K. L., HEALY, M. A., NGHIEM, P., SOBER, A. J., JOHNSON, T. M., BICHAKJIAN, C. K. & WONG, S. L. 2016a. Analysis of Prognostic Factors from 9387 Merkel Cell Carcinoma Cases Forms the Basis for the New 8th Edition AJCC Staging System. *Ann Surg Oncol,* 23**,** 3564-3571.

HARMS, P. W., COLLIE, A. M., HOVELSON, D. H., CANI, A. K., VERHAEGEN, M. E., PATEL, R. M., FULLEN, D. R., OMATA, K., DLUGOSZ, A. A., TOMLINS, S. A. & BILLINGS, S. D. 2016b. Next generation sequencing of Cytokeratin 20-

negative Merkel cell carcinoma reveals ultraviolet-signature mutations and recurrent TP53 and RB1 inactivation. *Mod Pathol,* 29**,** 240-8.

HARMS, P. W., PATEL, R. M., VERHAEGEN, M. E., GIORDANO, T. J., NASH, K. T., JOHNSON, C. N., DAIGNAULT, S., THOMAS, D. G., GUDJONSSON, J. E., ELDER, J. T., DLUGOSZ, A. A., JOHNSON, T. M., FULLEN, D. R. & BICHAKJIAN, C. K. 2013. Distinct gene expression profiles of viral- and nonviral-associated merkel cell carcinoma revealed by transcriptome analysis. *J Invest Dermatol,* 133**,** 936-45.

HARMS, P. W., VATS, P., VERHAEGEN, M. E., ROBINSON, D. R., WU, Y. M., DHANASEKARAN, S. M., PALANISAMY, N., SIDDIQUI, J., CAO, X., SU, F., WANG, R., XIAO, H., KUNJU, L. P., MEHRA, R., TOMLINS, S. A., FULLEN, D. R., BICHAKJIAN, C. K., JOHNSON, T. M., DLUGOSZ, A. A. & CHINNAIYAN, A. M. 2015. The Distinctive Mutational Spectra of Polyomavirus-Negative Merkel Cell Carcinoma. *Cancer Res,* 75**,** 3720-3727.

HARTLER, J., TROTZMULLER, M., CHITRAJU, C., SPENER, F., KOFELER, H. C. & THALLINGER, G. G. 2011. Lipid Data Analyzer: unattended identification and quantitation of lipids in LC-MS data. *Bioinformatics,* 27**,** 572-7.

HARTMANN, D., LUCKS, J., FUCHS, S., SCHIFFMANN, S., SCHREIBER, Y., FERREIROS, N., MERKENS, J., MARSCHALEK, R., GEISSLINGER, G. & GROSCH, S. 2012. Long chain ceramides and very long chain ceramides have opposite effects on human breast and colon cancer cell growth. *Int J Biochem Cell Biol,* 44**,** 620-8.

HEATH, M., JAIMES, N., LEMOS, B., MOSTAGHIMI, A., WANG, L. C., PENAS, P. F. & NGHIEM, P. 2008. Clinical characteristics of Merkel cell carcinoma at diagnosis in 195 patients: the AEIOU features. *J Am Acad Dermatol,* 58**,** 375-81.

HESBACHER, S., PFITZER, L., WIEDORFER, K., ANGERMEYER, S., BORST, A., HAFERKAMP, S., SCHOLZ, C. J., WOBSER, M., SCHRAMA, D. & HOUBEN, R. 2016. RB1 is the crucial target of the Merkel cell polyomavirus Large T antigen in Merkel cell carcinoma cells. *Oncotarget,* 7**,** 32956-68.

HETZ, C. A. 2002. Caspase-dependent initiation of apoptosis and necrosis by the Fas receptor in lymphoid cells: onset of necrosis is associated with delayed ceramide increase. *Journal of Cell Science,* 115**,** 4671-4683.

HISANO, Y. & HLA, T. 2019. Bioactive lysolipids in cancer and angiogenesis. *Pharmacol Ther,* 193**,** 91-98.

HOUBEN, R., DREHER, C., ANGERMEYER, S., BORST, A., UTIKAL, J., HAFERKAMP, S., PEITSCH, W. K., SCHRAMA, D. & HESBACHER, S. 2013. Mechanisms of p53 restriction in Merkel cell carcinoma cells are independent of the Merkel cell polyoma virus T antigens. *J Invest Dermatol,* 133**,** 2453-2460.

HOUBEN, R., SCHRAMA, D. & BECKER, J. C. 2009. Molecular pathogenesis of Merkel cell carcinoma. *Exp Dermatol,* 18**,** 193-8.

HOUBEN, R., SHUDA, M., WEINKAM, R., SCHRAMA, D., FENG, H., CHANG, Y., MOORE, P. S. & BECKER, J. C. 2010. Merkel cell polyomavirus-infected Merkel cell carcinoma cells require expression of viral T antigens. *J Virol,* 84**,** 7064-72.

HUGHES, M. P., HARDEE, M. E., CORNELIUS, L. A., HUTCHINS, L. F., BECKER, J. C. & GAO, L. 2014. Merkel Cell Carcinoma: Epidemiology, Target, and Therapy. *Curr Dermatol Rep,* 3**,** 46-53.

ITOH, M., KITANO, T., WATANABE, M., KONDO, T., YABU, T., TAGUCHI, Y., IWAI, K., TASHIMA, M., UCHIYAMA, T. & OKAZAKI, T. 2003. Possible role of ceramide as an indicator of chemoresistance: decrease of the ceramide content via activation of glucosylceramide synthase and sphingomyelin synthase in chemoresistant leukemia. *Clin Cancer Res,* 9**,** 415-23.

KAPITONOV, D., ALLEGOOD, J. C., MITCHELL, C., HAIT, N. C., ALMENARA, J. A., ADAMS, J. K., ZIPKIN, R. E., DENT, P., KORDULA, T., MILSTIEN, S. & SPIEGEL, S. 2009. Targeting sphingosine kinase 1 inhibits Akt signaling, induces apoptosis, and suppresses growth of human glioblastoma cells and xenografts. *Cancer Res,* 69**,** 6915-23.

KASSEM, A., SCHOPFLIN, A., DIAZ, C., WEYERS, W., STICKELER, E., WERNER, M. & ZUR HAUSEN, A. 2008. Frequent detection of Merkel cell polyomavirus in human Merkel cell carcinomas and identification of a unique deletion in the VP1 gene. *Cancer Res,* 68**,** 5009-13.

KAUFMAN, H. L., RUSSELL, J., HAMID, O., BHATIA, S., TERHEYDEN, P., D'ANGELO, S. P., SHIH, K. C., LEBBE, C., LINETTE, G. P., MILELLA, M., BROWNELL, I., LEWIS, K. D., LORCH, J. H., CHIN, K., MAHNKE, L., VON HEYDEBRECK, A., CUILLEROT, J. M. & NGHIEM, P. 2016. Avelumab in patients with chemotherapy-refractory metastatic Merkel cell carcinoma: a multicentre, single-group, open-label, phase 2 trial. *Lancet Oncol,* 17**,** 1374-1385.

KAUFMAN, H. L., RUSSELL, J. S., HAMID, O., BHATIA, S., TERHEYDEN, P., D'ANGELO, S. P., SHIH, K. C., LEBBE, C., MILELLA, M., BROWNELL, I.,

LEWIS, K. D., LORCH, J. H., VON HEYDEBRECK, A., HENNESSY, M. & NGHIEM, P. 2018. Updated efficacy of avelumab in patients with previously treated metastatic Merkel cell carcinoma after >/=1 year of follow-up: JAVELIN Merkel 200, a phase 2 clinical trial. *J Immunother Cancer,* 6**,** 7.

KENNEDY, P. C., ZHU, R., HUANG, T., TOMSIG, J. L., MATHEWS, T. P., DAVID, M., PEYRUCHAUD, O., MACDONALD, T. L. & LYNCH, K. R. 2011. Characterization of a sphingosine 1-phosphate receptor antagonist prodrug. *J Pharmacol Exp Ther,* 338**,** 879-89.

KIHARA, A. 2016. Synthesis and degradation pathways, functions, and pathology of ceramides and epidermal acylceramides. *Prog Lipid Res,* 63**,** 50-69.

KIM, C. W., LEE, H. M., LEE, T. H., KANG, C., KLEINMAN, H. K. & GHO, Y. S. 2002. Extracellular membrane vesicles from tumor cells promote angiogenesis via sphingomyelin. *Cancer Res,* 62**,** 6312-7.

KIM, S. W., KIM, H. J., CHUN, Y. J. & KIM, M. Y. 2010. Ceramide produces apoptosis through induction of p27(kip1) by protein phosphatase 2A-dependent Akt dephosphorylation in PC-3 prostate cancer cells. *J Toxicol Environ Health A,* 73**,** 1465-76.

KINIWA, Y., MIYAHARA, Y., WANG, H. Y., PENG, W., PENG, G., WHEELER, T. M., THOMPSON, T. C., OLD, L. J. & WANG, R. F. 2007. CD8+ Foxp3+ regulatory T cells mediate immunosuppression in prostate cancer. *Clin Cancer Res,* 13**,** 6947-58.

KITATANI, K., IDKOWIAK-BALDYS, J. & HANNUN, Y. A. 2008. The sphingolipid salvage pathway in ceramide metabolism and signaling. *Cell Signal,* 20**,** 1010-8.

KNITTELFELDER, O. L., WEBERHOFER, B. P., EICHMANN, T. O., KOHLWEIN, S. D. & RECHBERGER, G. N. 2014. A versatile ultra-high performance LC-MS method for lipid profiling. *J Chromatogr B Analyt Technol Biomed Life Sci,* 951-952**,** 119-28.

KOLHE, R., REID, M. D., LEE, J. R., COHEN, C. & RAMALINGAM, P. 2013. Immunohistochemical expression of PAX5 and TdT by Merkel cell carcinoma and pulmonary small cell carcinoma: a potential diagnostic pitfall but useful discriminatory marker. *Int J Clin Exp Pathol,* 6**,** 142-7.

KOLJONEN, V., HAGLUND, C., TUKIAINEN, E. & BOHLING, T. 2005. Neuroendocrine differentiation in primary Merkel cell carcinoma--possible prognostic significance. *Anticancer Res,* 25**,** 853-8.

KOUZMINA, M., KOLJONEN, V., LEIKOLA, J., BOHLING, T. & LANTTO, E. 2017. Frequency and locations of systemic metastases in Merkel cell carcinoma by imaging. *Acta Radiol Open,* 6**,** 2058460117700449.

KREITZBURG, K. M., FEHLING, S. C., LANDEN, C. N., GAMBLIN, T. L., VANCE, R. B., AREND, R. C., KATRE, A. A., OLIVER, P. G., VAN WAARDENBURG, R., ALVAREZ, R. D. & YOON, K. J. 2018. FTY720 enhances the anti-tumor activity of carboplatin and tamoxifen in a patient-derived xenograft model of ovarian cancer. *Cancer Lett,* 436**,** 75-86.

KSIAZEK, M., CHACINSKA, M., CHABOWSKI, A. & BARANOWSKI, M. 2015. Sources, metabolism, and regulation of circulating sphingosine-1-phosphate. *J Lipid Res,* 56**,** 1271-81.

KUNKEL, G. T., MACEYKA, M., MILSTIEN, S. & SPIEGEL, S. 2013. Targeting the sphingosine-1-phosphate axis in cancer, inflammation and beyond. *Nat Rev Drug Discov,* 12**,** 688-702.

KWUN, H. J., SHUDA, M., FENG, H., CAMACHO, C. J., MOORE, P. S. & CHANG, Y. 2013. Merkel cell polyomavirus small T antigen controls viral replication and oncoprotein expression by targeting the cellular ubiquitin ligase SCFFbw7. *Cell Host Microbe,* 14**,** 125-35.

LEE, H., DENG, J., KUJAWSKI, M., YANG, C., LIU, Y., HERRMANN, A., KORTYLEWSKI, M., HORNE, D., SOMLO, G., FORMAN, S., JOVE, R. & YU, H. 2010. STAT3-induced S1PR1 expression is crucial for persistent STAT3 activation in tumors. *Nat Med,* 16**,** 1421-8.

LEE, M. H., APPLETON, K. M., EL-SHEWY, H. M., SORCI-THOMAS, M. G., THOMAS, M. J., LOPES-VIRELLA, M. F., LUTTRELL, L. M., HAMMAD, S. M. & KLEIN, R. L. 2017. S1P in HDL promotes interaction between SR-BI and S1PR1 and activates S1PR1-mediated biological functions: calcium flux and S1PR1 internalization. *J Lipid Res,* 58**,** 325-338.

LEE, Y. M., VENKATARAMAN, K., HWANG, S. I., HAN, D. K. & HLA, T. 2007. A novel method to quantify sphingosine 1-phosphate by immobilized metal affinity chromatography (IMAC). *Prostaglandins Other Lipid Mediat,* 84**,** 154-62.

LEMOS, B. & NGHIEM, P. 2007. Merkel cell carcinoma: more deaths but still no pathway to blame. *J Invest Dermatol,* 127**,** 2100-3.

LEMOS, B. D., STORER, B. E., IYER, J. G., PHILLIPS, J. L., BICHAKJIAN, C. K., FANG, L. C., JOHNSON, T. M., LIEGEOIS-KWON, N. J., OTLEY, C. C.,

PAULSON, K. G., ROSS, M. I., YU, S. S., ZEITOUNI, N. C., BYRD, D. R., SONDAK, V. K., GERSHENWALD, J. E., SOBER, A. J. & NGHIEM, P. 2010. Pathologic nodal evaluation improves prognostic accuracy in Merkel cell carcinoma: analysis of 5823 cases as the basis of the first consensus staging system. *J Am Acad Dermatol,* 63**,** 751-61.

LEWIS, C. S., VOELKEL-JOHNSON, C. & SMITH, C. D. 2016. Suppression of c-Myc and RRM2 expression in pancreatic cancer cells by the sphingosine kinase-2 inhibitor ABC294640. *Oncotarget,* 7**,** 60181-60192.

LI, M. H., SWENSON, R., HAREL, M., JANA, S., STOLARZEWICZ, E., HLA, T., SHAPIRO, L. H. & FERRER, F. 2015. Antitumor Activity of a Novel Sphingosine-1-Phosphate 2 Antagonist, AB1, in Neuroblastoma. *J Pharmacol Exp Ther,* 354**,** 261-8.

LIANG, J., NAGAHASHI, M., KIM, E. Y., HARIKUMAR, K. B., YAMADA, A., HUANG, W. C., HAIT, N. C., ALLEGOOD, J. C., PRICE, M. M., AVNI, D., TAKABE, K., KORDULA, T., MILSTIEN, S. & SPIEGEL, S. 2013. Sphingosine-1-phosphate links persistent STAT3 activation, chronic intestinal inflammation, and development of colitis-associated cancer. *Cancer Cell,* 23**,** 107-20.

LIN, Z., MCDERMOTT, A., SHAO, L., KANNAN, A., MORGAN, M., STACK, B. C., JR., MORENO, M., DAVIS, D. A., CORNELIUS, L. A. & GAO, L. 2014. Chronic mTOR activation promotes cell survival in Merkel cell carcinoma. *Cancer Lett,* 344**,** 272-281.

LIN, Z., MEI, H., FAN, J., YIN, Z. & WU, G. 2015. Effect of the dual phosphatidylinositol 3-kinase/mammalian target of rapamycin inhibitor NVP-BEZ235 against human Merkel cell carcinoma MKL-1 cells. *Oncol Lett,* 10**,** 3663-3667.

LIPSON, E. J., VINCENT, J. G., LOYO, M., KAGOHARA, L. T., LUBER, B. S., WANG, H., XU, H., NAYAR, S. K., WANG, T. S., SIDRANSKY, D., ANDERS, R. A., TOPALIAN, S. L. & TAUBE, J. M. 2013. PD-L1 expression in the Merkel cell carcinoma microenvironment: association with inflammation, Merkel cell polyomavirus and overall survival. *Cancer Immunol Res,* 1**,** 54-63.

LIU, H., TOMAN, R. E., GOPARAJU, S. K., MACEYKA, M., NAVA, V. E., SANKALA, H., PAYNE, S. G., BEKTAS, M., ISHII, I., CHUN, J., MILSTIEN, S. & SPIEGEL, S. 2003. Sphingosine kinase type 2 is a putative BH3-only protein that induces apoptosis. *J Biol Chem,* 278**,** 40330-6.

LIU, W., MACDONALD, M. & YOU, J. 2016a. Merkel cell polyomavirus infection and Merkel cell carcinoma. *Curr Opin Virol,* 20**,** 20-27.

LIU, W., YANG, R., PAYNE, A. S., SCHOWALTER, R. M., SPURGEON, M. E., LAMBERT, P. F., XU, X., BUCK, C. B. & YOU, J. 2016b. Identifying the Target Cells and Mechanisms of Merkel Cell Polyomavirus Infection. *Cell Host Microbe,* 19**,** 775-87.

LIU, Y., WADA, R., YAMASHITA, T., MI, Y., DENG, C. X., HOBSON, J. P., ROSENFELDT, H. M., NAVA, V. E., CHAE, S. S., LEE, M. J., LIU, C. H., HLA, T., SPIEGEL, S. & PROIA, R. L. 2000. Edg-1, the G protein-coupled receptor for sphingosine-1-phosphate, is essential for vascular maturation. *J Clin Invest,* 106**,** 951-61.

LLOMBART, B., KINDEM, S. & CHUST, M. 2017. Merkel Cell Carcinoma: An Update of Key Imaging Techniques, Prognostic Factors, Treatment, and Follow-up. *Actas Dermosifiliogr,* 108**,** 98-107.

MACEYKA, M., HARIKUMAR, K. B., MILSTIEN, S. & SPIEGEL, S. 2012. Sphingosine-1-phosphate signaling and its role in disease. *Trends Cell Biol,* 22**,** 50-60.

MACEYKA, M., SANKALA, H., HAIT, N. C., LE STUNFF, H., LIU, H., TOMAN, R., COLLIER, C., ZHANG, M., SATIN, L. S., MERRILL, A. H., JR., MILSTIEN, S. & SPIEGEL, S. 2005. SphK1 and SphK2, sphingosine kinase isoenzymes with opposing functions in sphingolipid metabolism. *J Biol Chem,* 280**,** 37118-29.

MADHUNAPANTULA, S. V., HENGST, J., GOWDA, R., FOX, T. E., YUN, J. K. & ROBERTSON, G. P. 2012. Targeting sphingosine kinase-1 to inhibit melanoma. *Pigment Cell Melanoma Res,* 25**,** 259-74.

MARICICH, S. M., WELLNITZ, S. A., NELSON, A. M., LESNIAK, D. R., GERLING, G. J., LUMPKIN, E. A. & ZOGHBI, H. Y. 2009. Merkel cells are essential for light-touch responses. *Science,* 324**,** 1580-2.

MARTIN, J. D., FUKUMURA, D., DUDA, D. G., BOUCHER, Y. & JAIN, R. K. 2016. Reengineering the Tumor Microenvironment to Alleviate Hypoxia and Overcome Cancer Heterogeneity. *Cold Spring Harb Perspect Med,* 6.

MAUZO, S. H., FERRAROTTO, R., BELL, D., TORRES-CABALA, C. A., TETZLAFF, M. T., PRIETO, V. G. & AUNG, P. P. 2016. Molecular characteristics and potential therapeutic targets in Merkel cell carcinoma. *J Clin Pathol,* 69**,** 382-90.

MENDOZA, A., BREART, B., RAMOS-PEREZ, W. D., PITT, L. A., GOBERT, M., SUNKARA, M., LAFAILLE, J. J., MORRIS, A. J. & SCHWAB, S. R. 2012. The transporter Spns2 is required for secretion of lymph but not plasma sphingosine-1-phosphate. *Cell Rep,* 2**,** 1104-10.

MODRAK, D. E., CARDILLO, T. M., NEWSOME, G. A., GOLDENBERG, D. M. & GOLD, D. V. 2004. Synergistic interaction between sphingomyelin and gemcitabine potentiates ceramide-mediated apoptosis in pancreatic cancer. *Cancer Res,* 64**,** 8405-10.

MORTIER, L., MIRABEL, X., FOURNIER, C., PIETTE, F. & LARTIGAU, E. 2003. Radiotherapy alone for primary Merkel cell carcinoma. *Arch Dermatol,* 139**,** 1587-90.

MOSHIRI, A. S., DOUMANI, R., YELISTRATOVA, L., BLOM, A., LACHANCE, K., SHINOHARA, M. M., DELANEY, M., CHANG, O., MCARDLE, S., THOMAS, H., ASGARI, M. M., HUANG, M. L., SCHWARTZ, S. M. & NGHIEM, P. 2017. Polyomavirus-Negative Merkel Cell Carcinoma: A More Aggressive Subtype Based on Analysis of 282 Cases Using Multimodal Tumor Virus Detection. *J Invest Dermatol,* 137**,** 819-827.

MUKHOPADHYAY, P., RAMANATHAN, R. & TAKABE, K. 2015. S1P promotes breast cancer progression by angiogenesis and lymphangiogenesis. *Breast Cancer Manag,* 4**,** 241-244.

NAGAHASHI, M., TAKABE, K., TERRACINA, K. P., SOMA, D., HIROSE, Y., KOBAYASHI, T., MATSUDA, Y. & WAKAI, T. 2014. Sphingosine-1-phosphate transporters as targets for cancer therapy. *Biomed Res Int,* 2014**,** 651727.

NEHETE, P. N., VELA, E. M., HOSSAIN, M. M., SARKAR, A. K., YAHI, N., FANTINI, J. & SASTRY, K. J. 2002. A post-CD4-binding step involving interaction of the V3 region of viral gp120 with host cell surface glycosphingolipids is common to entry and infection by diverse HIV-1 strains. *Antiviral Res,* 56**,** 233-51.

NEU, U., HENGEL, H., BLAUM, B. S., SCHOWALTER, R. M., MACEJAK, D., GILBERT, M., WAKARCHUK, W. W., IMAMURA, A., ANDO, H., KISO, M., ARNBERG, N., GARCEA, R. L., PETERS, T., BUCK, C. B. & STEHLE, T. 2012. Structures of Merkel cell polyomavirus VP1 complexes define a sialic acid binding site required for infection. *PLoS Pathog,* 8**,** e1002738.

NUNES, J., NAYMARK, M., SAUER, L., MUHAMMAD, A., KEUN, H., STURGE, J., STEBBING, J., WAXMAN, J. & PCHEJETSKI, D. 2012. Circulating sphingosine-1-phosphate and erythrocyte sphingosine kinase-1 activity as novel biomarkers for early prostate cancer detection. *Br J Cancer,* 106**,** 909-15.

O'CONNOR, W. J., ROENIGK, R. K. & BRODLAND, D. G. 1997. Merkel cell carcinoma. Comparison of Mohs micrographic surgery and wide excision in eighty-six patients. *Dermatol Surg,* 23**,** 929-33.

OGRETMEN, B. 2018. Sphingolipid metabolism in cancer signalling and therapy. *Nat Rev Cancer,* 18**,** 33-50.

OKAMOTO, Y., WANG, F., YOSHIOKA, K., TAKUWA, N. & TAKUWA, Y. 2011. Sphingosine-1-Phosphate-Specific G Protein-Coupled Receptors as Novel Therapeutic Targets for Atherosclerosis. *Pharmaceuticals,* 4**,** 117-137.

OLESCH, C., RINGEL, C., BRUNE, B. & WEIGERT, A. 2017. Beyond Immune Cell Migration: The Emerging Role of the Sphingosine-1-phosphate Receptor S1PR4 as a Modulator of Innate Immune Cell Activation. *Mediators Inflamm,* 2017**,** 6059203.

OLIVERA, A., MIZUGISHI, K., TIKHONOVA, A., CIACCIA, L., ODOM, S., PROIA, R. L. & RIVERA, J. 2007. The sphingosine kinase-sphingosine-1-phosphate axis is a determinant of mast cell function and anaphylaxis. *Immunity,* 26**,** 287-97.

PANNEER SELVAM, S., DE PALMA, R. M., OAKS, J. J., OLEINIK, N., PETERSON, Y. K., STAHELIN, R. V., SKORDALAKES, E., PONNUSAMY, S., GARRETT-MAYER, E., SMITH, C. D. & OGRETMEN, B. 2015. Binding of the sphingolipid S1P to hTERT stabilizes telomerase at the nuclear periphery by allosterically mimicking protein phosphorylation. *Sci Signal,* 8**,** ra58.

PAULSON, K. G., IYER, J. G., TEGEDER, A. R., THIBODEAU, R., SCHELTER, J., KOBA, S., SCHRAMA, D., SIMONSON, W. T., LEMOS, B. D., BYRD, D. R., KOELLE, D. M., GALLOWAY, D. A., LEONARD, J. H., MADELEINE, M. M., ARGENYI, Z. B., DISIS, M. L., BECKER, J. C., CLEARY, M. A. & NGHIEM, P. 2011. Transcriptome-wide studies of merkel cell carcinoma and validation of intratumoral CD8+ lymphocyte invasion as an independent predictor of survival. *J Clin Oncol,* 29**,** 1539-46.

PCHEJETSKI, D., BOHLER, T., STEBBING, J. & WAXMAN, J. 2011. Therapeutic potential of targeting sphingosine kinase 1 in prostate cancer. *Nat Rev Urol,* 8**,** 569-678.

PCHEJETSKI, D., GOLZIO, M., BONHOURE, E., CALVET, C., DOUMERC, N., GARCIA, V., MAZEROLLES, C., RISCHMANN, P., TEISSIE, J., MALAVAUD, B. & CUVILLIER, O. 2005. Sphingosine kinase-1 as a chemotherapy sensor in prostate adenocarcinoma cell and mouse models. *Cancer Res,* 65**,** 11667-75.

PELOSCHEK, P., NOVOTNY, C., MUELLER-MANG, C., WEBER, M., SAILER, J., DAWID, M., CZERNY, C., DUDCZAK, R., KLETTER, K. & BECHERER, A. 2010. Diagnostic imaging in Merkel cell carcinoma: lessons to learn from 16 cases with correlation of sonography, CT, MRI and PET. *Eur J Radiol,* 73**,** 317-23.

PEULEN, O., GONZALEZ, A., PEIXOTO, P., TURTOI, A., MOTTET, D., DELVENNE, P. & CASTRONOVO, V. 2013. The anti-tumor effect of HDAC inhibition in a human pancreas cancer model is significantly improved by the simultaneous inhibition of cyclooxygenase 2. *PLoS One,* 8**,** e75102.

PHAM, T. H., BALUK, P., XU, Y., GRIGOROVA, I., BANKOVICH, A. J., PAPPU, R., COUGHLIN, S. R., MCDONALD, D. M., SCHWAB, S. R. & CYSTER, J. G. 2010. Lymphatic endothelial cell sphingosine kinase activity is required for lymphocyte egress and lymphatic patterning. *J Exp Med,* 207**,** 17-27.

PITSON, S. M., MORETTI, P. A., ZEBOL, J. R., LYNN, H. E., XIA, P., VADAS, M. A. & WATTENBERG, B. W. 2003. Activation of sphingosine kinase 1 by ERK1/2-mediated phosphorylation. *EMBO J,* 22**,** 5491-500.

PROIA, R. L. & HLA, T. 2015. Emerging biology of sphingosine-1-phosphate: its role in pathogenesis and therapy. *J Clin Invest,* 125**,** 1379-87.

PYNE, N. J. & PYNE, S. 2010. Sphingosine 1-phosphate and cancer. *Nat Rev Cancer,* 10**,** 489-503.

RIBATTI, D., NICO, B., VACCA, A. & PRESTA, M. 2006. The gelatin sponge-chorioallantoic membrane assay. *Nat Protoc,* 1**,** 85-91.

RIDLEY, A. J. 2015. Rho GTPase signalling in cell migration. *Curr Opin Cell Biol,* 36**,** 103-12.

RODIG, S. J., CHENG, J., WARDZALA, J., DOROSARIO, A., SCANLON, J. J., LAGA, A. C., MARTINEZ-FERNANDEZ, A., BARLETTA, J. A., BELLIZZI, A. M., SADASIVAM, S., HOLLOWAY, D. T., COOPER, D. J., KUPPER, T. S., WANG, L. C. & DECAPRIO, J. A. 2012. Improved detection suggests all Merkel cell carcinomas harbor Merkel polyomavirus. *J Clin Invest,* 122**,** 4645-53.

RYLAND, L. K., FOX, T. E., LIU, X., LOUGHRAN, T. P. & KESTER, M. 2011. Dysregulation of sphingolipid metabolism in cancer. *Cancer Biol Ther,* 11**,** 138-49.

SADDOUGHI, S. A., GENCER, S., PETERSON, Y. K., WARD, K. E., MUKHOPADHYAY, A., OAKS, J., BIELAWSKI, J., SZULC, Z. M., THOMAS, R. J., SELVAM, S. P., SENKAL, C. E., GARRETT-MAYER, E., DE PALMA, R. M., FEDAROVICH, D., LIU, A., HABIB, A. A., STAHELIN, R. V., PERROTTI, D. & OGRETMEN, B. 2013. Sphingosine analogue drug FTY720 targets I2PP2A/SET and mediates lung tumour suppression via activation of PP2A-RIPK1-dependent necroptosis. *EMBO Mol Med,* 5**,** 105-21.

SADDOUGHI, S. A. & OGRETMEN, B. 2013. Diverse functions of ceramide in cancer cell death and proliferation. *Adv Cancer Res,* 117**,** 37-58.

SAHI, H., SIHTO, H., ARTAMA, M., KOLJONEN, V., BOHLING, T. & PUKKALA, E. 2017. History of chronic inflammatory disorders increases the risk of Merkel cell carcinoma, but does not correlate with Merkel cell polyomavirus infection. *Br J Cancer,* 116**,** 260-264.

SANKALA, H. M., HAIT, N. C., PAUGH, S. W., SHIDA, D., LEPINE, S., ELMORE, L. W., DENT, P., MILSTIEN, S. & SPIEGEL, S. 2007. Involvement of sphingosine kinase 2 in p53-independent induction of p21 by the chemotherapeutic drug doxorubicin. *Cancer Res,* 67**,** 10466-74.

SASTRE-GARAU, X., PETER, M., AVRIL, M. F., LAUDE, H., COUTURIER, J., ROZENBERG, F., ALMEIDA, A., BOITIER, F., CARLOTTI, A., COUTURAUD, B. & DUPIN, N. 2009. Merkel cell carcinoma of the skin: pathological and molecular evidence for a causative role of MCV in oncogenesis. *J Pathol,* 218**,** 48-56.

SATTLER, W., MOHR, D. & STOCKER, R. 1994. Rapid isolation of lipoproteins and assessment of their peroxidation by high-performance liquid chromatography postcolumn chemiluminescence. *Methods Enzymol,* 233**,** 469-89.

SAUER, C. M., HAUGG, A. M., CHTEINBERG, E., RENNSPIESS, D., WINNEPENNINCKX, V., SPEEL, E. J., BECKER, J. C., KURZ, A. K. & ZUR HAUSEN, A. 2017. Reviewing the current evidence supporting early B-cells as the cellular origin of Merkel cell carcinoma. *Crit Rev Oncol Hematol,* 116**,** 99-105.

SCHADENDORF, D., LEBBE, C., ZUR HAUSEN, A., AVRIL, M. F., HARIHARAN, S., BHARMAL, M. & BECKER, J. C. 2017. Merkel cell carcinoma: Epidemiology, prognosis, therapy and unmet medical needs. *Eur J Cancer,* 71**,** 53-69.

SCHNEIDER-SCHAULIES, J. & SCHNEIDER-SCHAULIES, S. 2015. Sphingolipids in viral infection. *Biol Chem,* 396**,** 585-95.

SCHNITZER, S. E., WEIGERT, A., ZHOU, J. & BRUNE, B. 2009. Hypoxia enhances sphingosine kinase 2 activity and provokes sphingosine-1-phosphate-mediated chemoresistance in A549 lung cancer cells. *Mol Cancer Res,* 7**,** 393-401.

SCHOWALTER, R. M., PASTRANA, D. V. & BUCK, C. B. 2011. Glycosaminoglycans and sialylated glycans sequentially facilitate Merkel cell polyomavirus infectious entry. *PLoS Pathog,* 7**,** e1002161.

SCHRAMA, D., UGUREL, S. & BECKER, J. C. 2012. Merkel cell carcinoma: recent insights and new treatment options. *Curr Opin Oncol,* 24**,** 141-9.

SCHWARTZ, B. M., HONG, G., MORRISON, B. H., WU, W., BAUDHUIN, L. M., XIAO, Y. J., MOK, S. C. & XU, Y. 2001. Lysophospholipids increase interleukin-8 expression in ovarian cancer cells. *Gynecol Oncol,* 81**,** 291-300.

SEDIC, M., GRBCIC, P. & PAVELIC, S. K. 2019. Bioactive Sphingolipids as Biomarkers Predictive of Disease Severity and Treatment Response in Cancer: Current Status and Translational Challenges. *Anticancer Res,* 39**,** 41-56.

SEIDEL, J. A., OTSUKA, A. & KABASHIMA, K. 2018. Anti-PD-1 and Anti-CTLA-4 Therapies in Cancer: Mechanisms of Action, Efficacy, and Limitations. *Front Oncol,* 8**,** 86.

SENTELLE, R. D., SENKAL, C. E., JIANG, W., PONNUSAMY, S., GENCER, S., SELVAM, S. P., RAMSHESH, V. K., PETERSON, Y. K., LEMASTERS, J. J., SZULC, Z. M., BIELAWSKI, J. & OGRETMEN, B. 2012. Ceramide targets autophagosomes to mitochondria and induces lethal mitophagy. *Nat Chem Biol,* 8**,** 831-8.

SHAKOR, A. B., TANIGUCHI, M., KITATANI, K., HASHIMOTO, M., ASANO, S., HAYASHI, A., NOMURA, K., BIELAWSKI, J., BIELAWSKA, A., WATANABE, K., KOBAYASHI, T., IGARASHI, Y., UMEHARA, H., TAKEYA, H. & OKAZAKI, T. 2011. Sphingomyelin synthase 1-generated sphingomyelin plays an important role in transferrin trafficking and cell proliferation. *J Biol Chem,* 286**,** 36053-62.

SHAROV, A. A., SCHLESSINGER, D. & KO, M. S. 2015. ExAtlas: An interactive online tool for meta-analysis of gene expression data. *J Bioinform Comput Biol,* 13**,** 1550019.

SHI, J. & WEI, P. K. 2016. Interleukin-8: A potent promoter of angiogenesis in gastric cancer. *Oncol Lett,* 11**,** 1043-1050.

SHIDA, D., TAKABE, K., KAPITONOV, D., MILSTIEN, S. & SPIEGEL, S. 2008. Targeting SphK1 as a New Strategy against Cancer. *Current Drug Targets,* 9**,** 662-673.

SHUDA, M., ARORA, R., KWUN, H. J., FENG, H., SARID, R., FERNANDEZ-FIGUERAS, M. T., TOLSTOV, Y., GJOERUP, O., MANSUKHANI, M. M., SWERDLOW, S. H., CHAUDHARY, P. M., KIRKWOOD, J. M., NALESNIK, M. A., KANT, J. A., WEISS, L. M., MOORE, P. S. & CHANG, Y. 2009. Human Merkel cell polyomavirus infection I. MCV T antigen expression in Merkel cell carcinoma, lymphoid tissues and lymphoid tumors. *Int J Cancer,* 125**,** 1243-9.

SHUDA, M., FENG, H., KWUN, H. J., ROSEN, S. T., GJOERUP, O., MOORE, P. S. & CHANG, Y. 2008. T antigen mutations are a human tumor-specific signature for Merkel cell polyomavirus. *Proc Natl Acad Sci U S A,* 105**,** 16272-7.

SHUDA, M., KWUN, H. J., FENG, H., CHANG, Y. & MOORE, P. S. 2011. Human Merkel cell polyomavirus small T antigen is an oncoprotein targeting the 4E-BP1 translation regulator. *J Clin Invest,* 121**,** 3623-34.

SHUDA, M., VELASQUEZ, C., CHENG, E., CORDEK, D. G., KWUN, H. J., CHANG, Y. & MOORE, P. S. 2015. CDK1 substitutes for mTOR kinase to activate mitotic cap-dependent protein translation. *Proc Natl Acad Sci U S A,* 112**,** 5875-82.

SINHA, U. K., SCHORN, V. J., HOCHSTIM, C., CHINN, S. B., ZHU, S. & MASOOD, R. 2011. Increased radiation sensitivity of head and neck squamous cell carcinoma with sphingosine kinase 1 inhibition. *Head Neck,* 33**,** 178-88.

SOBUE, S., NEMOTO, S., MURAKAMI, M., ITO, H., KIMURA, A., GAO, S., FURUHATA, A., TAKAGI, A., KOJIMA, T., NAKAMURA, M., ITO, Y., SUZUKI, M., BANNO, Y., NOZAWA, Y. & MURATE, T. 2008. Implications of sphingosine kinase 1 expression level for the cellular sphingolipid rheostat: relevance as a marker for daunorubicin sensitivity of leukemia cells. *Int J Hematol,* 87**,** 266-75.

SPIEGEL, S. & MILSTIEN, S. 2003. Sphingosine-1-phosphate: an enigmatic signalling lipid. *Nat Rev Mol Cell Biol,* 4**,** 397-407.

SPURGEON, M. E. & LAMBERT, P. F. 2013. Merkel cell polyomavirus: a newly discovered human virus with oncogenic potential. *Virology,* 435**,** 118-30.

STRUB, G. M., MACEYKA, M., HAIT, N. C., MILSTIEN, S. & SPIEGEL, S. 2010. Extracellular and intracellular actions of sphingosine-1-phosphate. *Adv Exp Med Biol,* 688**,** 141-55.

STRUB, G. M., PAILLARD, M., LIANG, J., GOMEZ, L., ALLEGOOD, J. C., HAIT, N. C., MACEYKA, M., PRICE, M. M., CHEN, Q., SIMPSON, D. C., KORDULA, T., MILSTIEN, S., LESNEFSKY, E. J. & SPIEGEL, S. 2011. Sphingosine-1-phosphate produced by sphingosine kinase 2 in mitochondria interacts with prohibitin 2 to regulate complex IV assembly and respiration. *FASEB J,* 25**,** 600-12.

SUAREZ, A. L., LOUIS, P., KITTS, J., BUSAM, K., MYSKOWSKI, P. L., WONG, R. J., CHEN, C. S., SPENCER, P., LACOUTURE, M. & PULITZER, M. P. 2015. Clinical and dermoscopic features of combined cutaneous squamous cell carcinoma (SCC)/neuroendocrine [Merkel cell] carcinoma (MCC). *J Am Acad Dermatol,* 73**,** 968-75.

SUNSHINE, J. C., JAHCHAN, N. S., SAGE, J. & CHOI, J. 2018. Are there multiple cells of origin of Merkel cell carcinoma? *Oncogene,* 37**,** 1409-1416.

SUZUKI, K. G. N., ANDO, H., KOMURA, N., FUJIWARA, T. K., KISO, M. & KUSUMI, A. 2017. Development of new ganglioside probes and unraveling of raft domain structure by single-molecule imaging. *Biochim Biophys Acta Gen Subj,* 1861**,** 2494-2506.

TAFESSE, F. G., HUITEMA, K., HERMANSSON, M., VAN DER POEL, S., VAN DEN DIKKENBERG, J., UPHOFF, A., SOMERHARJU, P. & HOLTHUIS, J. C. 2007. Both sphingomyelin synthases SMS1 and SMS2 are required for sphingomyelin homeostasis and growth in human HeLa cells. *J Biol Chem,* 282**,** 17537-47.

TAI, P. T., YU, E., WINQUIST, E., HAMMOND, A., STITT, L., TONITA, J. & GILCHRIST, J. 2000. Chemotherapy in neuroendocrine/Merkel cell carcinoma of the skin: case series and review of 204 cases. *J Clin Oncol,* 18**,** 2493-9.

TAKABE, K., KIM, R. H., ALLEGOOD, J. C., MITRA, P., RAMACHANDRAN, S., NAGAHASHI, M., HARIKUMAR, K. B., HAIT, N. C., MILSTIEN, S. & SPIEGEL, S. 2010. Estradiol induces export of sphingosine 1-phosphate from breast cancer cells via ABCC1 and ABCG2. *J Biol Chem,* 285**,** 10477-86.

TAKABE, K., PAUGH, S. W., MILSTIEN, S. & SPIEGEL, S. 2008. "Inside-out" signaling of sphingosine-1-phosphate: therapeutic targets. *Pharmacol Rev,* 60**,** 181-95.

TAKASUGI, N., SASAKI, T., SUZUKI, K., OSAWA, S., ISSHIKI, H., HORI, Y., SHIMADA, N., HIGO, T., YOKOSHIMA, S., FUKUYAMA, T., LEE, V. M., TROJANOWSKI, J. Q., TOMITA, T. & IWATSUBO, T. 2011. BACE1 activity is modulated by cell-associated sphingosine-1-phosphate. *J Neurosci,* 31**,** 6850-7.

TANIGUCHI, M. & OKAZAKI, T. 2014. The role of sphingomyelin and sphingomyelin synthases in cell death, proliferation and migration-from cell and animal models to human disorders. *Biochim Biophys Acta,* 1841**,** 692-703.

TAUBE, S., JIANG, M. & WOBUS, C. E. 2010. Glycosphingolipids as receptors for non-enveloped viruses. *Viruses,* 2**,** 1011-49.

TOKER, C. 1972. Trabecular carcinoma of the skin. *Arch Dermatol,* 105**,** 107-10.

UCHI, H. 2018. Merkel Cell Carcinoma: An Update and Immunotherapy. *Front Oncol,* 8**,** 48.

VAN BROCKLYN, J. R., JACKSON, C. A., PEARL, D. K., KOTUR, M. S., SNYDER, P. J. & PRIOR, T. W. 2005. Sphingosine kinase-1 expression correlates with poor survival of patients with glioblastoma multiforme: roles of sphingosine kinase isoforms in growth of glioblastoma cell lines. *J Neuropathol Exp Neurol,* 64**,** 695-705.

VAN DER WEYDEN, L., ARENDS, M. J., CAMPBELL, A. D., BALD, T., WARDLE-JONES, H., GRIGGS, N., VELASCO-HERRERA, M. D., TUTING, T., SANSOM, O. J., KARP, N. A., CLARE, S., GLEESON, D., RYDER, E., GALLI, A., TUCK, E., CAMBRIDGE, E. L., VOET, T., MACAULAY, I. C., WONG, K., SANGER MOUSE GENETICS, P., SPIEGEL, S., SPEAK, A. O. & ADAMS, D. J. 2017. Genome-wide in vivo screen identifies novel host regulators of metastatic colonization. *Nature,* 541**,** 233-236.

VAN DOORN, R., LOPES PINHEIRO, M. A., KOOIJ, G., LAKEMAN, K., VAN HET HOF, B., VAN DER POL, S. M., GEERTS, D., VAN HORSSEN, J., VAN DER VALK, P., VAN DER KAM, E., RONKEN, E., REIJERKERK, A. & DE VRIES, H. E. 2012. Sphingosine 1-phosphate receptor 5 mediates the immune quiescence of the human brain endothelial barrier. *J Neuroinflammation,* 9**,** 133.

VANDEN BERGHE, T., LINKERMANN, A., JOUAN-LANHOUET, S., WALCZAK, H. & VANDENABEELE, P. 2014. Regulated necrosis: the expanding network of non-apoptotic cell death pathways. *Nat Rev Mol Cell Biol,* 15**,** 135-47.

VENESS, M., FOOTE, M., GEBSKI, V. & POULSEN, M. 2010. The role of radiotherapy alone in patients with merkel cell carcinoma: reporting the Australian experience of 43 patients. *Int J Radiat Oncol Biol Phys,* 78**,** 703-9.

VENKATARAMAN, K., THANGADA, S., MICHAUD, J., OO, M. L., AI, Y., LEE, Y. M., WU, M., PARIKH, N. S., KHAN, F., PROIA, R. L. & HLA, T. 2006. Extracellular export of sphingosine kinase-1a contributes to the vascular S1P gradient. *Biochem J,* 397**,** 461-71.

VERHAEGEN, M. E., MANGELBERGER, D., HARMS, P. W., EBERL, M., WILBERT, D. M., MEIRELES, J., BICHAKJIAN, C. K., SAUNDERS, T. L., WONG, S. Y. & DLUGOSZ, A. A. 2017. Merkel Cell Polyomavirus Small T Antigen Initiates Merkel Cell Carcinoma-like Tumor Development in Mice. *Cancer Res,* 77**,** 3151-3157.

VERHAEGEN, M. E., MANGELBERGER, D., HARMS, P. W., VOZHEIKO, T. D., WEICK, J. W., WILBERT, D. M., SAUNDERS, T. L., ERMILOV, A. N., BICHAKJIAN, C. K., JOHNSON, T. M., IMPERIALE, M. J. & DLUGOSZ, A. A. 2015. Merkel cell polyomavirus small T antigen is oncogenic in transgenic mice. *J Invest Dermatol,* 135**,** 1415-1424.

VERHAEGEN, M. E., MANGELBERGER, D., WEICK, J. W., VOZHEIKO, T. D., HARMS, P. W., NASH, K. T., QUINTANA, E., BACIU, P., JOHNSON, T. M., BICHAKJIAN, C. K. & DLUGOSZ, A. A. 2014. Merkel cell carcinoma dependence on bcl-2 family members for survival. *J Invest Dermatol,* 134**,** 2241-2250.

VILLANI, M., SUBATHRA, M., IM, Y. B., CHOI, Y., SIGNORELLI, P., DEL POETA, M. & LUBERTO, C. 2008. Sphingomyelin synthases regulate production of diacylglycerol at the Golgi. *Biochem J,* 414**,** 31-41.

WADSWORTH, J. M., CLARKE, D. J., MCMAHON, S. A., LOWTHER, J. P., BEATTIE, A. E., LANGRIDGE-SMITH, P. R., BROUGHTON, H. B., DUNN, T. M., NAISMITH, J. H. & CAMPOPIANO, D. J. 2013. The chemical basis of serine palmitoyltransferase inhibition by myriocin. *J Am Chem Soc,* 135**,** 14276-85.

WANG, Q., LI, J., LI, G., LI, Y., XU, C., LI, M., XU, G. & FU, S. 2014. Prognostic significance of sphingosine kinase 2 expression in non-small cell lung cancer. *Tumour Biol,* 35**,** 363-8.

WANG, T. S., BYRNE, P. J., JACOBS, L. K. & TAUBE, J. M. 2011. Merkel cell carcinoma: update and review. *Semin Cutan Med Surg,* 30**,** 48-56.

XIA, P., GAMBLE, J. R., WANG, L., PITSON, S. M., MORETTI, P. A., WATTENBERG, B. W., D'ANDREA, R. J. & VADAS, M. A. 2000. An oncogenic role of sphingosine kinase. *Curr Biol,* 10**,** 1527-30.

YAGUCHI, M., SHIBATA, S., SATOMI, Y., HIRAYAMA, M., ADACHI, R., ASANO, Y., KOJIMA, T., HIRATA, Y., MIZUTANI, A., KIBA, A. & SAGIYA, Y. 2017. Antitumor activity of a novel and orally available inhibitor of serine palmitoyltransferase. *Biochem Biophys Res Commun,* 484**,** 493-500.

YAMANAKA, M., SHEGOGUE, D., PEI, H., BU, S., BIELAWSKA, A., BIELAWSKI, J., PETTUS, B., HANNUN, Y. A., OBEID, L. & TROJANOWSKA, M. 2004. Sphingosine kinase 1 (SPHK1) is induced by transforming growth factor-beta and mediates TIMP-1 up-regulation. *J Biol Chem,* 279**,** 53994-4001.

YANG, L., WENG, W., SUN, Z. X., FU, X. J., MA, J. & ZHUANG, W. F. 2015. SphK1 inhibitor II (SKI-II) inhibits acute myelogenous leukemia cell growth in vitro and in vivo. *Biochem Biophys Res Commun,* 460**,** 903-8.

YATOMI, Y., IGARASHI, Y., YANG, L., HISANO, N., QI, R., ASAZUMA, N., SATOH, K., OZAKI, Y. & KUME, S. 1997. Sphingosine 1-phosphate, a bioactive sphingolipid abundantly stored in platelets, is a normal constituent of human plasma and serum. *J Biochem,* 121**,** 969-73.

YOULDEN, D. R., SOYER, H. P., YOUL, P. H., FRITSCHI, L. & BAADE, P. D. 2014. Incidence and survival for Merkel cell carcinoma in Queensland, Australia, 1993-2010. *JAMA Dermatol,* 150**,** 864-72.

YOUNG, N. & VAN BROCKLYN, J. R. 2006. Signal transduction of sphingosine-1-phosphate G protein-coupled receptors. *ScientificWorldJournal,* 6**,** 946-66.

ZAAR, O., GILLSTEDT, M., LINDELOF, B., WENNBERG-LARKO, A. M. & PAOLI, J. 2016. Merkel cell carcinoma incidence is increasing in Sweden. *J Eur Acad Dermatol Venereol,* 30**,** 1708-1713.

ZACHARIAH, M. A. & CYSTER, J. G. 2010. Neural crest-derived pericytes promote egress of mature thymocytes at the corticomedullary junction. *Science,* 328**,** 1129-35.

ZHANG, H., PLUHACKOVA, K., JIANG, Z. & BOCKMANN, R. A. 2016. Binding Characteristics of Sphingosine-1-Phosphate to ApoM hints to Assisted Release Mechanism via the ApoM Calyx-Opening. *Sci Rep,* 6**,** 30655.

ZHANG, X., MAR, V., ZHOU, W., HARRINGTON, L. & ROBINSON, M. O. 1999. Telomere shortening and apoptosis in telomerase-inhibited human tumor cells. *Genes Dev,* 13**,** 2388-99.

ZHANG, Y., WANG, Y., WAN, Z., LIU, S., CAO, Y. & ZENG, Z. 2014. Sphingosine kinase 1 and cancer: a systematic review and meta-analysis. *PLoS One,* 9**,** e90362.

ZHOU, H., SUMMERS, S. A., BIRNBAUM, M. J. & PITTMAN, R. N. 1998. Inhibition of Akt kinase by cell-permeable ceramide and its implications for ceramide-induced apoptosis. *J Biol Chem,* 273**,** 16568-75.

7. Appendix

Table 1. Primer list

SPTLC1	Hs_SPTLC1_1_SG	Qiagen, Hilden, Germany
SPTLC2	Hs_SPTLC2_1_SG	Qiagen, Hilden, Germany
SPTLC3	Hs_SPTLC3_1_SG	Qiagen, Hilden, Germany
SPHK1	Hs_SPHK1_1_SG	Qiagen, Hilden, Germany
SPHK2	Hs_SPHK2_1_SG	Qiagen, Hilden, Germany
S1PR1	Hs_S1PR1_1_SG	Qiagen, Hilden, Germany
S1PR2	Hs_S1PR2_1_SG	Qiagen, Hilden, Germany
S1PR3	Hs_S1PR3_1_SG	Qiagen, Hilden, Germany
S1PR4	Hs_S1PR4_1_SG	Qiagen, Hilden, Germany
S1PR5	Hs_S1PR5_1_SG	Qiagen, Hilden, Germany
HPRT	Hs_HPRT_1_SG	Qiagen, Hilden, Germany
RPLP0 Forward	5'-CCATCAGCACCACAGCCTTA-3'	IDT, Coralville, IA, USA
RPLP0 Reverse	5'-GGCGACCTGGAAGTCCAACT-3'	IDT, Coralville, IA, USA
RPLP0 Probe	5'-ATCTGCTGCATCTGCTTGGAGCCCA-3'	IDT, Coralville, IA, USA

Table 2. Antibodies used

Antibody	Company
β-actin (mouse)	Sigma Aldrich, St. Louis, MO, USA
SPT (rabbit)	Santa Cruz Biotechnology Dallas, TX, USA
SK1 (SPHK1) (rabbit)	Cell Signaling, Beverly, MA, USA
SK2 (SPHK2) (goat)	Santa Cruz Biotechnology Dallas, TX, USA
phospho-Akt (Ser473) (rabbit)	Cell Signaling, Beverly, MA, USA
Akt (rabbit)	Cell Signaling, Beverly, MA, USA
Caspase-3 (rabbit)	Santa Cruz Biotechnology Dallas, TX, USA
PARP (rabbit)	Cell Signaling, Beverly, MA, USA
CK-20 (mouse)	Agilent Technologies, Santa Clara, CA, USA
Ki-67 (mouse)	Agilent Technologies, Santa Clara, CA, USA
MCPyV-LT (mouse)	Santa Cruz Biotechnology Dallas, TX, USA

Table 3. List of reagents and Kits

Reagents and Kits	Company
Accutase	Sigma Aldrich, St. Louis, MO, USA
ABC294640	Cayman, Ann Arbor, MI, USA
Acrylamide	Thermo Fisher Scientific, Waltham, USA
Ammoniumpersulfate (APS)	Sigma Aldrich, St. Louis, MO, USA
Aprotinin	Sigma Aldrich, St. Louis, MO, USA
CellTiter-Glo 3D cell viability assay kit	Promega, Madison, WI, USA
Dimethyl sulfoxide (DMSO)	Sigma Aldrich, St. Louis, MO, USA
EnzChek Caspase-3 Assay Kit #2	Invitrogen, Waltham, MA, USA
Ethylenediaminetetraacetic Acid (EDTA)	Sigma Aldrich, St. Louis, MO, USA
Fetal Calf Serum (FCS)	Sigma Aldrich, St. Louis, MO, USA
Fibroblast Cell Medium BulletKit	Lonza, Walkersville, MD, USA
FITC Annexin V Apoptosis Detection Kit 1	BD Biosciences, San Jose, CA, USA
FTY720	Sigma Aldrich, St. Louis, MO, USA
KH_2PO_4	Sigma Aldrich, St. Louis, MO, USA
Leupeptin	Sigma Aldrich, St. Louis, MO, USA
Mercaptoethanol	Sigma Aldrich, St. Louis, MO, USA

Methanol	New England Biolabs, Ipswich, USA
Myriocin	Sigma Aldrich, St. Louis, MO, USA
Na_2HPO_4	Sigma Aldrich, St. Louis, MO, USA
Pepstatin	Sigma Aldrich, St. Louis, MO, USA
PeqGOLD total RNA Kit	Peqlab, Erlangen, Germany
Phenylmethylsulfonylfluoride (PMSF)	Sigma Aldrich, St. Louis, MO, USA
Phosphate Buffered Saline (PBS)	Sigma Aldrich, St. Louis, MO, USA
Pierce BCA Protein Assay Kit	Thermo Fisher Scientific, Waltham, USA
RPMI 1640 Cell Culture Medium	Thermo Fisher Scientific, Waltham, USA
S1P	Santa Cruz, Dallas, TX, USA
S1P ELISA kit	Echelon, Salt Lake City, UT, USA
S1P lyase	Sigma Aldrich, St. Louis, MO, USA
SKI-II	Sigma Aldrich, St. Louis, MO, USA
Sodium Chloride (NaCl)	Sigma Aldrich, St. Louis, MO, USA
Sodium Dodecyl Sulfate (SDS)	Sigma Aldrich, St. Louis, MO, USA
Sodium Fluoride (NaF)	Sigma Aldrich, St. Louis, MO, USA
Sodium Orthovanadate (Na_3VO_4)	Sigma Aldrich, St. Louis, MO, USA
SuperSignal Western blot detection kit	Pierce, Thermo Scientific, MA, USA
Transcriptor First Strand cDNA Synthesis Kit	Roche Life Science, IN, USA
Triciribine	Cayman, Ann Arbor, MI, USA
Tris-HCl	Sigma Aldrich, St. Louis, MO, USA
TritonX	Sigma Aldrich, St. Louis, MO, USA
Tween 20	Sigma Aldrich, St. Louis, MO, USA